UNIVERSITY OF OKLAHOMA

GRADUATE COLLEGE

THE BIOCHEMICAL CHARACTERIZATION OF TWO PHOSPHORELAY SIGNALING PROTEINS: YPD1 HOMOLOGS FROM *SACCHAROMYCES CEREVISIAE* AND *CRYPTOCOCCUS NEOFORMANS*

A DISSERTATION

SUBMITTED TO THE GRADUATE FACULTY

in partial fulfillment of the requirements for the

Degree of

DOCTOR OF PHILOSOPHY

By

EMILY N. KENNEDY
Norman, Oklahoma
2016

Downloaded from SHAREOK. Persistent Handle URL: https://hdl.handle.net/11244/44880

THE BIOCHEMICAL CHARACTERIZATION OF TWO PHOSPHORELAY SIGNALING PROTEINS: YPD1 HOMOLOGS FROM *SACCHAROMYCES CEREVISIAE* AND *CRYPTOCOCCUS NEOFORMANS*

A DISSERTATION APPROVED FOR THE
DEPARTMENT OF CHEMISTRY AND BIOCHEMISTRY

BY

_____
Dr. Ann West, Chair

_____
Dr. Elizabeth Karr

_____
Dr. Robert Cichewicz

_____
Dr. Christina Bourne

_____
Dr. Elena Zgurskaya

© Copyright by EMILY N. KENNEDY 2016
All Rights Reserved.

Acknowledgements

I would first like to give my greatest appreciation to my major professor, Dr. Ann West. She has been a wonderful mentor and guide through all of the time that I have spent at the University of Oklahoma. Her continuous support inside and outside of the laboratory have enabled me to complete the work presented in this dissertation. I would like to especially thank her for sharing her knowledge and for passing down her deep love of science to me. I would also like to acknowledge Dr. Paul Cook. He was always happy and willing to answer any questions and he spent a lot of time making sure that I truly understood the answers, even after his official retirement.

Many thanks to the members of my Graduate Advisory Committee, Dr. Elizabeth Karr, Dr. Robert Cichewicz, Dr. Christina Bourne, and Dr. Elena Zgurskaya. Their feedback has been greatly appreciated and helped to further my knowledge.

Fellow graduate students Dr. Katie Branscum, Clay Foster, Skyler Hebdon, Jamie Sykes, and all of the undergraduate students made the lab such a pleasant place to work and I enjoyed having all of them as friends and colleagues. Very special thanks to Dr. Smita Menon for all of her help.

I also cannot thank enough my husband, Peter. He has been there every step of the way to celebrate with me when things go well, to encourage me, or just to be a shoulder to cry on during challenging times as a graduate student, wife, and mother of two. Without him being there to help me to juggle all of the challenges as a Ph.D. student, all of this would not have been possible.

Table of Contents

Acknowledgements iv

Table of Contents v

List of Tables ix

List of Figures xi

Abstract xiv

Introduction 1

1.1 Signal transduction through histidine-to-aspartate pathways 1

1.2 Histidine-to-aspartate systems in prokaryotes 2

1.3 Expanded two-component systems in bacteria 7

1.4 Histidine-to-aspartate two-component systems in eukaryotes 8

1.5 Research focus 11

1.6 Significance 12

References 13

Role of the highly conserved G68 residue in the yeast phosphorelay protein Ypd1: implications for interactions between histidine phosphotransfer and response regulator proteins 21

1.1 Introduction 21

1.2 Materials and Methods 26

1.2.1 Cloning 26

1.2.2 Protein purification 27

1.2.3 Sequence alignment 28

1.2.4 *In vitro* phosphorylation assay 28

1.2.5 Fluorescence-based affinity assay (assay performed by Skyler Hebdon) 29
1.2.6 Crystallization (structure determination completed by Dr. Smita Menon) 31
1.2.7 X-ray data collection and processing 31
1.2.8 Structure solution and refinement 31
1.2.9 Molecular dynamics simulations (simulations performed by Clay Foster) 32
1.2.10 Molecular graphics 33
1.3 Results 33
1.3.1 A glycine in the *H+4* position of HPt domains and stand-alone HPt proteins is highly conserved 33
1.3.2 Non-conservative mutations at ScYpd1 G68 disrupt phosphotransfer .. 35
1.3.3 Substitutions at the G68 position cause only modest changes in affinity of ScYpd1 for ScSln1-R1 (Experiments performed by Skyler Hebdon) 36
1.3.4 Crystal structure of ScYpd1-G68Q (Structure solution determined by Dr. Smita Menon.) 37
1.3.5 Mutations at the G68 position lead to changes in active site residues involved in catalysis (Molecular dynamics simulation performed by Clay Foster. Analysis of data completed in collaboration) 40
1.4 Discussion 41
References 47

Extended N-terminal region of the essential phosphorelay signaling protein Ypd1 from *Cryptococcus neoformans* contributes to structural stability, phospho-stability, and binding of calcium ions 54

2.1 Introduction 54

2.2 Material and Methods 59

2.2.1 Materials 59

2.2.2 Cloning 60

2.2.3 Protein expression and purification 62

2.2.4 Determination of oligomeric state of CnYpd1 64

2.2.5 Pull down assay with receiver domain of CnSkn7 (CnSkn7-R3) 65

2.2.6 Solubility studies of CnYpd1 N-terminal deletion constructs 65

2.2.7 *In vitro* phosphorylation assay 66

2.2.8 Size exclusion chromatography analysis for metal binding studies 67

2.2.9 Inductively coupled plasma atomic emission spectroscopy (ICP-MS) analysis 68

2.3 Results 69

2.3.1 CnYpd1 functions as a histidine phosphotransfer protein 69

2.3.2 CnYpd1 interactions with downstream RR proteins 72

2.3.3 N-terminal region of CnYpd1 important for structural integrity 74

2.3.4 CnYpd1 functions a monomer in solution 78

2.3.5 CnYpd1 exhibits an extended phosphorylated lifetime in comparison to other HPt proteins 85

2.3.6 N-terminal region stabilizes phosphoryl group on CnYpd1 86

2.3.7 CnYpd1 binds calcium ions in a 2:1 molar ratio 87
2.3.8 Calcium is not required for phosphorylation of CnYpd1 92
2.3.9 Crystallization attempts for CnYpd1 94
2.3.10 Discussion 96
References 100
Appendix A: Table of West Lab plasmids, cell strains, and primers 105
Appendix B: Crystallography attempts for CnYpd1 110
Appendix C: Table of Abbreviations 123

List of Tables

Table 1. His-to-Asp phosphorelay systems 2

Table 2. Quantification of residues found in the *H+4* position of HPt proteins and HPt domains..... 34

Table 3. Ability of ScYpd1-G68X mutants to function as a phosphorelay protein 35

Table 4. Binding constants for ScYpd1 with ScSln1-R1 37

Table 5. Calculated molecular weight, extinction coefficient and pI information for CnYpd1 constructs 63

Table 6. Approximate percentage of CnYpd1 ΔN protein found in supernatant and pellet after lysis..... 77

Table 7. Predicted and apparent molecular weights of ScYpd1 and CnYpd1 80

Table 8. Predicted and apparent molecular weights of ScYpd1, full length CnYpd1 and CnYpd1 ΔN constructs..... 81

Table 9. Micromolar concentrations of metal ions determined by ICP-MS 90

Table 10. Calculated molar ratio of metal ions per protein based on ICP-MS 91

Table 11. OU Construct Summary 105

Table 12. Oligo names, OU numbers, and Sequences 107

Table 13. Crystallography attempts for CnYpd1 constructs 110

Table 14. ScYpd1 Optimization Screen 115

Table 15. MSCG II B1 Optimization Screen 1 116

Table 16. MSCG II B1 Optimization Screen 2 117

Table 17. MCSG III E5 Optimization Screen 1 118

Table 18. CnYpd1-H138Q Optimization 1 + 0.5 M 1,2,3-octanetriol isomer H 118

Table 19. Octanetriol Optimization 1 119

Table 20. Octanetriol Optimization 2 119

Table 21. CSHT D3 Optimization 120

Table 22. CSHT H5 Optimization 120

Table 23. JCSG D7 Optimization 121

Table 24. MCSG I C5 Optimization 121

Table 25. MCSG I C5 Optimization 122

List of Figures

Figure 1. Histidine-to-Aspartate phosphorelay systems 3

Figure 2. Crystal structure of the cytoplasmic portion of HK853 from *T. maritima* 5

Figure 3. Crystal structure of the response regulator CheY 6

Figure 4. Crystal structure of histidine containing phosphotransfer protein ScYpd1 from *Saccharomyces cerevisiae* 9

Figure 5. Sln1-Ypd1-Ssk1/Skn7 pathway in *S. cerevisiae* 22

Figure 6. ScSln1 domain architecture 23

Figure 7. Crystal structure of complex between ScSln1-R1 and ScYpd1 24

Figure 8. Representative sequence alignment of HPt proteins or domains from fungi, plants and bacteria 33

Figure 9. Phosphoryl transfer from phosopho~ScSln1-R1 to ScYpd1 35

Figure 10. Phosphoryl transfer from phosopho~Ypd1 to Ssk1-R2 36

Figure 11. Representative titration of ScYpd1-T12C with ScSln1-R1 37

Figure 12. Shift in I18 residue of ScYpd1-G68Q 39

Figure 13. Overlay and surface representations of wild-type ScYpd1 (cyan) (PDB ID: 1QSP) and the ScYpd1-G68Q mutant (magenta) 39

Figure 14. Overlay of the ScYpd1-G68Q mutant (magenta)(PDB ID: 5JH4) with the ScYpd1•Sln1-R1•Mg^{2+}•BeF_3^- complex (cyan) (PDB ID: 2R25) 44

Figure 15. Multi-step histidine-to-aspartate pathway in *C. neoformans* 55

Figure 16. Proposed domain architecture of Tco1 and Tco2 HHK proteins found in *C. neoformans* 56

Figure 17. Plasmid map of pTrcHis-TOPO vector 60

Figure 18. Schematic for phosphorylation of CnYpd1 67
Figure 19. Purification summary for CnYpd1 69
Figure 20. Representative sequence alignment of HPt proteins 70
Figure 21. Phosphorylation of CnYpd1 from a heterologous phosphodonor 72
Figure 22. Expression and purification of CnSkn7-R3 73
Figure 23. Pull down assay and phosphotransfer between CnYpd1 and CnSkn7-R3 74
Figure 24. CnYpd1 N-terminal deletion mutants 75
Figure 25. Solubility studies of CnYpd1 deletion constructs 76
Figure 26. Phosphorylation of CnYpd1 ΔN constructs 77
Figure 27. CnYpd1 apparent molecular weight on a calibrate S00 column 79
Figure 28. SDS-PAGE gel of CnYpd1 protein 79
Figure 29. Elution profile of ScYpd1 with CnYpd1 on a S200 column 80
Figure 30. SEC elution profile of CnYpd1 in presence and absence of reducing agent 82
Figure 31. Native gel analysis of CnYpd1 constructs 83
Figure 32. SEC-MALS of CnYpd1 84
Figure 33. Extended phosphorylated life-time of CnYpd1 85
Figure 34. Phosphoryl stability of CnYpd1 after affinity tag removal 86
Figure 35. CnYpd1 ΔN70 dephosphorylation 87
Figure 36. CnYpd1 shows a shift in elution volume in the presence and absence of EDTA 88
Figure 37. Re-introduction of metal ions to CnYpd1 causes a change in the elution volume during SEC 89
Figure 38. CnYpd1 and CnYpd1 ΔN70 protein samples for ICP-MS 90

Figure 39. Highly homologous region of N-terminal sequence alignment. 92

Figure 40. Phosphorylation of CnYpd1, CnYpd1 E58A and CnYpd1 D60A-E67A 93

Figure 41. Analysis of oligomeric distribution of CnYpd1 by DLS 94

Figure 42. Analysis of oligomeric distribution of CnYpd1 by DLS 95

Figure 43. Analysis of oligomeric distribution of CnYpd1 by DLS 95

Figure 44. Phylogenetic tree of HPt proteins with extended N-terminal region 97

Abstract

Histidine-to-aspartate multi-step phosphorelay systems are used extensively by eukaryotes and bacteria to sense and respond to changes in their external environment and to control the regulation of crucial biological functions such as cell cycle, mating, and virulence. These pathways generally consists of a hybrid histidine kinase (HHK), a single histidine phosphotransfer protein (HPt), and one or more response regulator proteins (RR). The histidine phosphotransfer protein, Ypd1, is found at the branch point of these signal transduction pathways in several fungal organisms, and acts as an intermediate that is responsible for relaying messages between the HHK, which senses the signal, and the RR, which initiates a cellular response. This protein, or a homolog, is often the sole HPt in fungal organisms. In several fungal species it has been shown to be essential for viability. These organisms include the common baker's yeast *Saccharomyces cerevisiae* (Sc) and the human fungal pathogen *Cryptococcus neoformans* (Cn).

HPt proteins are genetically diverse, but share a common tertiary fold with conserved residues near the active site. A surface-exposed glycine at the *H+4* position, relative to the phosphorylatable histidine is found in a significant number of annotated HPts. Substitution of residues with larger side chains at this position typically disrupts signal transduction by altering the structure and/or enzymatic activity of the phosphotransfer-competent complex formed between HPts and their cognate partners.

Previous work using yeast two-hybrid assays has shown that the residue in the *H+4* position on the surface of ScYpd1 in the G68 position has an only slightly diminished activity in its ability to accept a phosphoryl group from the receiver domain

of ScSln1, but a highly diminished activity in its ability to transfer its phosphoryl group to the receiver domain of ScSsk1. Here we report a comprehensive analysis of a set of point mutants at position 68 of Ypd1 to gain insights into the evolutionary constraints leading to the exceptionally high conservation of glycine at position *H+4* in HPts. We combine bioinformatics, phosphoryl transfer assays, X-ray crystallography, fluorescence-based binding assay and molecular dynamics techniques to help explain the delicate balance of interatomic interactions required for phosphotransfer to occur between an HPt and its cognate RR. The conclusions that can be drawn clarify the importance of a small and/or hydrophilic residue in the *H+4* position.

Ypd1 from *C. neoformans* is distinct from Ypd1 from *S. cerevisiae.* Based on sequence alignments, CnYpd1 includes an extended N-terminal region that is not present in ScYpd1 of approximately 60 residues. This extended N-terminal region shares no close sequence homology with any other known protein domain. Organisms with stand-alone HPt proteins that include an extended N-terminal region are rare, and are found strictly in fungal species that have been shown to be pathogenic to plants or humans, or that live in extreme environments. Results from this study indicate that CnYpd1 exhibits unique characteristics in comparison to other histidine phosphotransfer proteins, such as an extended N-terminal amino acid sequence, which we find contributes to structural integrity, a longer phosphorylated life-time and the ability to bind calcium ions.

Introduction

1.1 Signal transduction through histidine-to-aspartate pathways

Sensing external environment and responding to changes detected is crucial to an organism's ability to survive and proliferate. Stimuli are sensed through a multitude of mechanisms, such as small molecule/hormone binding, or through structural changes of cellular components such as proteins. Frequently, the response to an external stimulus is an alteration in gene expression. This process of transmitting external stimuli to the interior of the cell is known as signal transduction. One of the most common signal transduction mechanisms is the reversible transfer of a phosphoryl group between proteins in signaling pathways [1, 2].

The most common form of phosphoryl group transfer involves the phosphorylation and dephosphorylation of serine, threonine, and tyrosine residues [3, 4]. However, in bacteria this type of phosphorylation is less common, and histidine-to-aspartate (His-to-Asp) phosphotransfer pathways dominate signal transduction mechanisms [5]. These pathways are called "two-component systems." According to the Prokaryotic 2-Component Systems (P2CS) Database (http://www.p2cs.org/), a comprehensive database of two-component systems from organisms with completely sequenced genomes, on average more than 50 two-component system proteins are encoded by a bacterial species, which accounts for as much as 1% of all the encoded proteins [6, 7]. Two-component systems are used in stress response and the regulation of other essential or beneficial biological functions such as cell proliferation, virulence, and antibiotic resistance [5, 8].

In lower eukaryotes such as fungi and plants the use of His-to-Asp signal

transduction systems are also quite abundant [9-11]. Activation of these pathways often results in the regulation of gene expression directly, or through regulation of other downstream pathways [12]. **Table 1** gives examples of histidine-to-aspartate phosphorelay systems in various organisms.

Table 1. His-to-Asp phosphorelay systems

Organism	Kinase	Histidine Phosphotransfer protein	Response Regulator	Function
Bacteria				
Escherichia coli	CpxA	---	CpxR	Regulation of protein trafficking factors
Escherichia coli	CheA	---	CheY	Chemotaxis
Bacillus subtilis	Spo0F	Spo0B	Spo0A	Sporulation
Pseudomonas aeruginosa	NarX	---	NarL	Nitrogen respiration
Vibrio harveyi	LuxN/LuxQ	---	LuxO	Luminescence
Salmonella typhimurium	PhoP	---	PhoQ	Virulence and macrophage survival
Caulobacter crescentus	Ccka	ChpT	CtrA	Cell cycle progression
Bordetella pertussis	BvgS	---	BvgA	Virulence
Myxococcus xanthus	RedC	RedE	RedF	Cell cycle/development
Streptococcus pneumoniae	CiaH	---	CiaR	Beta-lactam resistance
Eukaryotes				
Schizosaccharomyces pombe	Mak2/3	Mpr1	Msc4	Oxidative stress
Saccharomyces cerevisiae	Sln1	Ypd1	Ssk1	Osmotic stress
Candida albicans	Nik1/Chk1/Sln1	Ypd1	Ssk1	Stress repsonse
Arabidopsis thaliana	AHK5	AHP1,2,5	ARR4,ARR7	Regulation of stomatal closure
Cryptococcus neoformans	Tco1,Tco2	Ypd1	Ssk1	Drug sensitivity, sexual development, virulence
Archaea				
Halobacterium salinarum	VicK	---	VicR	Temperature sensing
Methanosaeta harundinacea	FilI	---	FilR	methanogenesis

1.2 Histidine-to-aspartate systems in prokaryotes

As the name implies, His-to-Asp two-component systems generally consist of two distinct protein components; an often membrane bound histidine kinase (HK) and a downstream response regulator (RR) (**Figure 1A**) [13, 14]. While bacteria often

contain numerous two-component systems, each individual system generally consists of a single HK and RR cognate pair clustered with in the same operon as proteins of similar function [8].

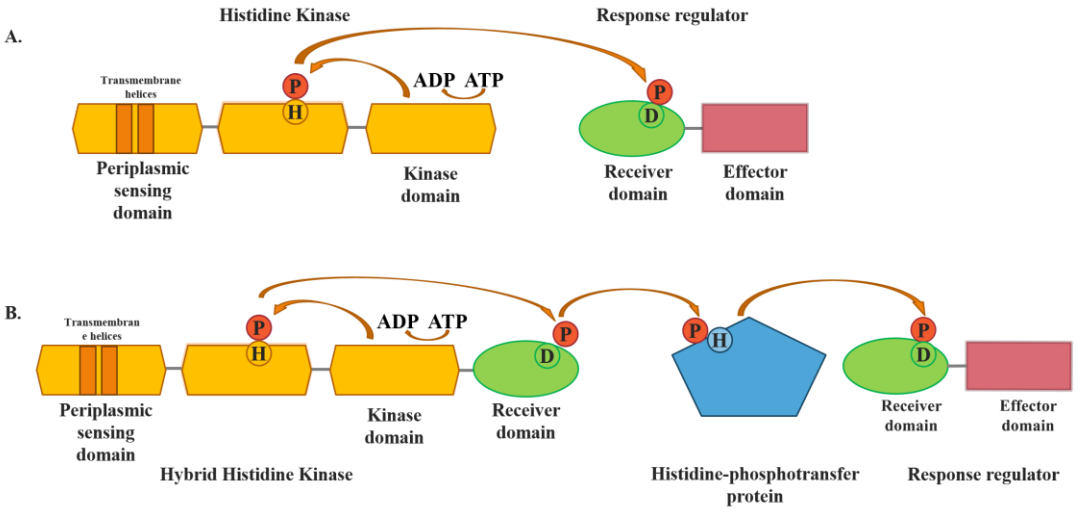


Figure 1. Histidine-to-Aspartate phosphorelay systems

A. Canonical two-component system. Consists of a membrane bound HK and cytoplasmic RR. ATP is used as a phosphoryl donor during HK autophosphorylation on a conserved histidine. The phosphoryl group is then transferred to an aspartate residue on a downstream RR. Phosphorylation of the RR leads to protein activation which results in a cellular response.

B. Multi-step His-to-Asp phosphorelay system. Consists of an HHK, an HPt and an RR. Autophosphorylation occurs in a conserved histidine of the HHK, the phosphoryl group and is then transferred to a conserved aspartate in the receiver domain of the HHK. The phosphoryl group is then transferred to a histidine in an HPt, and finally to an aspartate in an RR protein.

HKs are multi-domain proteins with a minimum of two domains, an input (or sensory) domain and a cytoplasmic catalytic kinase domain [15]. Sensory domains of HK proteins are highly variable in structure and function due to the necessity of sensing a wide variety of external stimuli [16-20]. For example, for the membrane bound HK from *Enterococcus faecalis* FsrC, binding of the small peptide ligand gelatinase biosynthesis-activating pheromone (GBAP) results in regulation of quorum sensing genes which are important for virulence [21]; for the HK CusS in *Escherichia coli*,

CusS directly binds silver ions and undergoes a conformational change which activates kinase activity and results in gene expression of the CusCFBA efflux pump [22]. Ligand binding, whether a small molecule or in the form of another protein, results in a structural rearrangement of the HK from an "inactive" to an "active" conformation, at which point nucleotide binding and autophosphorylation occur.

Because the sensory domain is highly variable, HK proteins are classified according to their cytoplasmic domain architecture. Currently there are three structural classes of HK proteins: Class 1 HKs contain an extra-cytoplasmic sensory domain that senses external stimuli and transmits the signal across the membrane; Class 2 HKs lack an apparent extra-cytoplasmic domain and the sensing region is thought to be the trans-membrane domains themselves; Class 3 HKs are characterized by a single cytoplasmic sensory domain [23].

Unifying structural features found in the cytoplasmic region of all HK proteins include a dimerization and histidine phosphotransfer (DHp) domain and a C-terminal catalytic and ATP binding domain (CA). There are five conserved "boxes" which contain characteristic amino acid sequences. In the DHp domain, the H-box contains the phospho-accepting histidine residue, while in the CA domain the Nl, Gl, G2 and F boxes are involved in ATP-dependent autophosphorylation and nucleotide binding [5, 24].

Generally, two monomeric subunits dimerize to form the DHp domain. Structural information available about the DHp domain demonstrates a conserved 4 α-helix bundle [25-28]. From the X-ray crystal structure of the entire cytoplasmic region of the class I HK, HK853 from *Thermotoga maritima* (PDB 2C2A), both the core four

α-helix bundle forming the DHp domain as well as the catalytic kinase domain are observed [29]. The phosphorylatable histidine residue (H260) found in the DHp domain is shown to be completely solvent exposed and bound to a sulfate ion which is believed to act as a phosphoryl mimic. The C-terminal CA domain shows a characteristic α/β sandwich fold composed of three α-helices packed against five antiparallel β-strands. The bound ADP molecule shows where nucleotide binding occurs (**Figure 2**) [29]. The structure of HK853 reveals that nucleotide binding occurs between 2 loops in the catalytic domain (**Figure 2).** Typically this nucleotide is held in place by a flexible "ATP lid" loop which was not observed in the X-ray crystal structure.

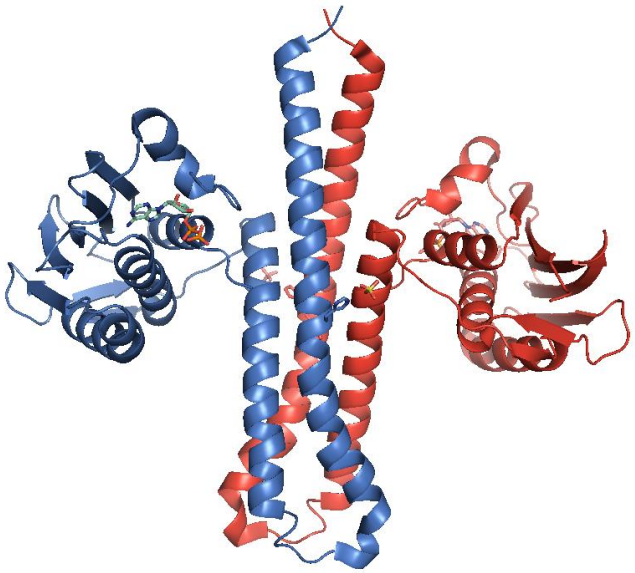


Figure 2. Crystal structure of the cytoplasmic portion of HK853 from *T. maritima*

Ribbon diagram of the homodimeric HK853 (PDB ID: 2C2A) shows how the monomers (one monomer colored blue and one monomer colored red) dimerize to for a DHp domain to form of a core four alpha-helix bundle. Phosphorylatable histidine residues are completely solvent exposed and with a bound sulfate ion which mimics a phosphoryl group (shown in stick representation). The CA domain shows a bound ADP molecule and a conserved α/β sandwich fold.

HK autophosphorylation involves transferring the γ-phosphate from ATP to the Nε atom of the catalytic histidine to form a high energy N~P bond [15]. Autophosphorylation can either occur in *cis* or *trans* fashion. *Cis* autophosphorylation occurs when the catalytic site on one monomer catalyzes the phosphorylation of the histidine residue on the same monomer, while in *trans* autophosphorylation the catalytic domain of one monomer catalyzes the phosphorylation of the histidine on the other monomer of the homodimer [15].

Once ATP-dependent autophosphorylation of the HK occurs, the phosphoryl group is transferred to a conserved aspartate residue found in the receiver domain of a downstream RR (**Figure 1A**). For phosphotransfer to occur between HK and RR, a divalent metal ion, most often magnesium, must be present in the active site of the RR. It is responsible for neutralization of charged acidic residues found in the active site [30-32]. The aspartate residue acts as a nucleophile and attacks the positively charged phosphorous on the phosphoryl group attached to the histidine. Phosphorylation of the RR often results in dimerization and the protein is in an "activated" form.

An overall conserved architecture has been observed from crystal structures of receiver domains from various RR proteins [33-40]. From the crystal structure of CheY from *E. coli* (PDB ID: 1A0O), a central five-stranded parallel β-sheet can be seen

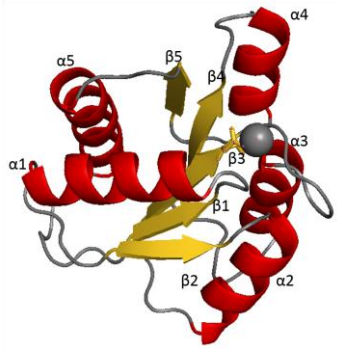


Figure 3. Crystal structure of the response regulator CheY
Ribbon diagram from crystal structure of the RR protein CheY from *E. coli* (PDB ID: 1A0O). Receiver domains from RR proteins have a conserved $(\alpha/\beta)_5$ topology. The phospho-accepting aspartate is shown in stick representation with a bound Mg^{2+} ion (grey sphere).

surrounded by five amphipathic α-helices (Figure 3**)**. The phospho-accepting aspartate residue is located on the end of the third beta strand [41].

RR proteins commonly contain two domains, a receiver domain, where the conserved aspartate residue is located, and an effector domain. The effector domain is variable in sequence and in structure, but frequently contains a DNA binding domain [42]. Function of RR proteins vary greatly depending not only on the stimulus from the HK, but also on the function of the effector domain. RR protein activation can result in activation of many functions, such as stress response [43-46] gene regulation involved in cell cycle progression [47-51], virulence [52-58] and biofilm formation [59-61].

1.3 Expanded two-component systems in bacteria

While the canonical two-component system model in bacteria shows that these phosphotransfer systems generally consist of two proteins, there are many examples of expanded systems [62-64]. Surveys on bacteria with completely sequenced genomes have indicated that a large number of non-canonical histidine-to-aspartate multi-step systems exist [65]. These systems can consist of an HK or RR with additional protein domains, resulting in "hybrid" proteins. Often a histidine phosphotransfer domain (HPt) is the additional domain present. The anaerobic sensor kinase ArcB found in a two-component system in *Escherichia coli*, has three domains, an HK domain, a receiver domain, and an HPt domain [66]. Additional stand-alone proteins are also found in specific pathways. For example, in the bacteria *Myxoccocus xanthus*, a "four-component system" is present [67]. Results from numerous studies have indicated that when multi-step systems are present in prokaryotes, they are found in organisms with distinct characteristics, such as cyanobacteria, pathogenic bacteria, or bacteria with

unusual life-cycle switching mechanisms [68]. This modularity is thought to allow for an increased versatility in signaling by allowing for a wider variety of output signals and more stringent regulation.

1.4 Histidine-to-aspartate two-component systems in eukaryotes

The original discovery of His-to-Asp pathways in eukaryotes occurred in 1993 when ETR1 in *Arabidopsis thaliana* and Sln1 in *Saccharomyces cerevisiae* were revealed [68, 69]. Prior to 1993 it was believed that eukaryotic organisms only contained the more "typical" phosphotransfer systems that involve threonine, serine, and tyrosine phosphorylation. When eukaryote genomes were further examined, it was shown that these pathways were not as uncommon as previously thought. However, unlike bacteria, eukaryotic His-to-Asp signaling most often consists of expanded multi-step pathways.

In these multi-step His-to-Asp signaling pathways, the sensor kinase has evolved to become a hybrid histidine kinase (HHK). This kinase, which contains both the sensor and effector domains found in canonical HK proteins, also contain their own receiver domain [68, 70]. These HHKs are highly diverse and often contain additional domains, such as GAF, PAS and HAMP domains [71]. ATP dependent autophosphorylation occurs at the conserved histidine residue, but instead of the phosphoryl group being transferred to a receiver domain of a downstream RR protein, it is transferred to a conserved aspartate residue in its own receiver domain **(Figure 1B)**. In order to maintain the histidine-to-aspartate signal transduction scheme, an additional stand-alone protein, a histidine phosphotransfer protein (HPt), is found as an intermediate between the HHK and the RR.

HPt proteins are generally small and often have low sequence homology to other HPt domains and stand-alone HPt proteins except in the region surrounding the conserved phosphorylatable histidine, which appears to be highly conserved [72]. They play a crucial role in regulating cellular functions of bacteria, eukaryotes and plants [5, 70, 73]. HPt domains or stand-alone proteins share a common structural motif, a four α-helix bundle as a core structure, with the conserved phospho-accepting histidine residue exposed to solvent [72, 74, 75]. From the crystal structure of Ypd1 (PDB ID: 1QSP), an HPt from *S. cerevisiae*, a conserved four helix bundle is observed similar that that seen in the DHp domain of HK proteins [28, 76].

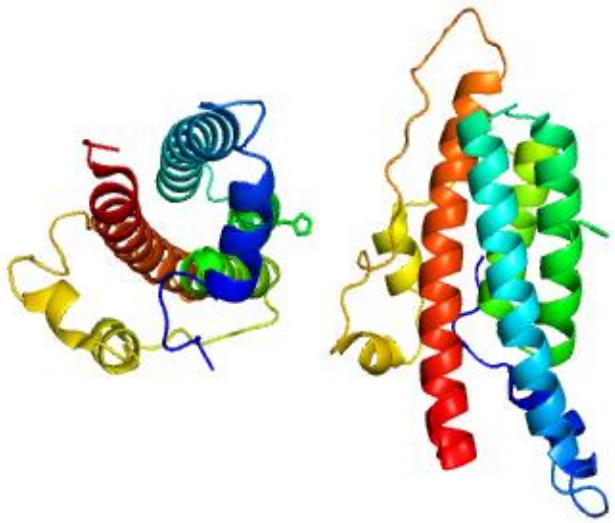


Figure 4. Crystal structure of histidine containing phosphotransfer protein ScYpd1 from *Saccharomyces cerevisiae*
Ribbon diagram of the HPt protein ScYpd1 (PDB ID: 1QSP). The protein is composed of the core four-helix bundle which is surrounded by 2 additional small helices. Phospho-accepting histidine residue (H64) is shown in stick representation.

In addition to the HPt protein, a second RR protein is often present in eukaryotic pathways [77]. As with prokaryotic systems, the RR often contains a DNA binding domain and is responsible for enhancing or suppressing gene expression. However,

because of the compartmentalization of cellular organelles in eukaryotic organisms, RR proteins are sequestered from each other, generally with a single RR protein located in the cytoplasm, and another located in the nucleus [42, 78]. In the fungal pathogen *Candida albicans* a third RR protein, Srr1, was discovered to be localized in the mitochondria [79].

In yeast and fungi, these His-to-Asp multi-step pathways have been shown to be responsible for both upstream regulation of the serine/threonine/tyrosine phosphotransfer cascades as well as direct regulation of gene expression. Until recently, elucidation of these eukaryotic pathways has mainly focused on ascomycetes such as *Saccharomyces cerevisiae, Candida albicans,* and *Aspergillus fumigatus,* as well as pathogenic organism such as the basidiomycete fungi *Cryptococcus neoformans*. However, with increased genetic data available studies of more species is rapidly increasing.

Recently, studies of proteomic data available have revealed that some species encode very large expansions of HK and RR gene families [74, 80]. Filamentous fungi have been reported to have as many as 18 HK proteins, and plant species have been shown to have as many as 8. In addition to the HK proteins, these eukaryotes also have larger numbers of RR proteins [9]. Although in general, fungi are typically shown to have only one HPt protein present, several plant species encode multiple HPts [9]. This may be due to the more diverse sensing activities of these higher eukaryotes as well as activities related to pathogenesis.

1.5 Research focus

My research has focused on better understanding the HPt proteins found in two eukaryotic organisms, Ypd1 homologs from the "baker's yeast" *Saccharomyces cerevisiae* and the human fungal pathogen *Cryptococcus neoformans*. While the hyperosmotic stress pathway in *S. cerevisiae* has been extensively studied [81, 82], there are still questions that we would like to address. One residue, G68 located at the *H+4* position relative to the phosphorylatable histidine on the surface of ScYpd1, has been shown to have a greatly diminished phosphotransfer ability to ScSsk1 relative to wild-type levels of phosphotransfer [83]. This residue is located near the active site of the protein near a series of small residues, and is hypothesized to be required for proper protein-protein interactions with its binding partner. Bioinformatics was used to elucidate the exceedingly high conservation of a glycine in this *H+4* position. A series of point mutants were constructed and analyzed using phosphoryl transfer assays, fluorescence-based binding assays, X-ray crystallography and molecular dynamics techniques. This work was completed as a lab collaboration and will help to elucidate why this particular residue is of seemingly high important for protein function.

Very little is currently known about the biochemistry involved in the His-to-Asp multi-step signal transduction pathways that are found in *C. neoformans*. All information available to date regarding these pathway has been obtained through genetic studies and complementation *in vivo* experiments [84, 85]. My objectives were to further characterize the CnYpd1 phosphotransfer protein. The site of phosphorylation was confirmed, CnYpd1 was analyzed for functional differences distinct from other HPt proteins, such as structural, oligomeric state, and phosphorylated protein stability.

According to sequence alignments, CnYpd1 contains an extended N-terminal. Homology models have not yielded any information about what possible function of the N-terminal region may confer to the protein. Mutation studies, phosphotransfer assays, size exclusion chromatography assays, and ICP-MS were used to try to address these questions as well as to investigate the possible function of the N-terminal region.

1.6 Significance

Further studies of the functions and mechanisms of His-to-Asp signal transduction pathways will allow for a greater understanding of how organisms use these pathways are used to respond to stresses and control virulence.

For all signal transduction pathways, proteins must interact with each other in order to elicit the proper response. For branched pathways, such as those found in *S. cerevisiae* and *C. neoformans*, proteins must be able to distinguish between multiple binding partners. In both *S. cerevisiae* and *C. neoformans*, the HPt protein Ypd1 is found at a crucial branch point of the pathway, and has a fundamental role in determining which downstream RR protein should be activated through phosphotransfer. The basis of this activation has to be in the form of a proper response to the type of external stimuli that was sensed by the HHK protein. Further understanding of how specificity is conferred by the HPt would greatly further our understanding of how these branched signal transduction pathways function.

References

1. Lim, W. A. 2002. The modular logic of signaling proteins: building allosteric switches from simple binding domains. *Current Opinion in Structural Biology* 12 (1): 61-68.

2. Davis, R. J. 1993. The mitogen-activated protein kinase signal transduction pathway. *Journal of Biological Chemistry* 268 (20): 14553-14556.

3. Seger, R. and Krebs, E. G. 1995. The MAPK signaling cascade. *The FASEB Journal* 9 (9): 726-735.

4. Chen, Z., Gibson, T. B., Robinson, F., Silvestro, L., Pearson, G., Xu, B., Wright, A., Vanderbilt, C., and Cobb, M. H. 2001. MAP kinases. *Chemical Reviews* 101 (8): 2449-2476.

5. Stock, A. M., Robinson, V. L., and Goudreau, P. N. 2000. Two-component signal transduction. *Annual Review of Biochemistry* 69 (1): 183-215.

6. Binnewies, T. T., Motro, Y., Hallin, P. F., Lund, O., Dunn, D., La, T., Hampson, D. J., Bellgard, M., Wassenaar, T. M., and Ussery, D. W. 2006. Ten years of bacterial genome sequencing: comparative-genomics-based discoveries. *Functional & Integrative Genomics* 6 (3): 165-185.

7. Kiil, K., Ferchaud, J. B., David, C., Binnewies, T. T., Wu, H., Sicheritz-Pontén, T., Willenbrock, H., and Ussery, D. W. 2005. Genome update: distribution of two-component transduction systems in 250 bacterial genomes. *Microbiology* 151 (11): 3447-3452.

8. Laub, M. T. and Goulian, M. 2007. Specificity in two-component signal transduction pathways. *Annual Review of Genetics* 41 121-145.

9. Schaller, E. G., Shiu, S.-H., and Armitage, J. P. 2011. Two-component systems and their co-option for eukaryotic signal transduction. *Current Biology* 21 (9): R320-30.

10. Loomis, W. F., Kuspa, A., and Shaulsky, G. 1998. Two-component signal transduction systems in eukaryotic microorganisms. *Current Opinion in Microbiology* 1 643-648.

11. Urao, T., Yamaguchi-Shinozaki, K., and Shinozaki, K. 2000. Two-component systems in plant signal transduction. *Trends in plant science* 5 (2): 67-74.

12. Mizuno, T. 1998. His-Asp phosphotransfer signal transduction. *Journal of Biochemistry* 123 (4): 555-563.

13. Chang, C. and Stewart, R. C. 1998. The two-component system: regulation of diverse signaling pathways in prokaryotes and eukaryotes. *Plant Physiology* 117 723-731.

14. Perraud, A.-L., Weiss, V., and Gross, R. 1999. Signalling pathways in two-component phosphorelay systems. *Trends Microbiology* 7 (3): 115-120.

15. Bhate, M. P., Molnar, K. S., Goulian, M., and Degrado, W. F. 2015. Signal transduction in histidine kinases: insights from new structures. *Structure* 23 (6): 981-94.

16. Mascher, T., Helmann, J. D., and Unden, G. 2006. Stimulus perception in bacterial signal-transducing histidine kinases. *Microbiology and Molecular Biology Reviews* 70 (4): 910-938.

17. Estelle, M. 2001. Cytokinin receptor: just another histidine kinase. *Current Biology* 11 R271-R273.

18. Lina, G., Jarraud, S., Ji, G., Greenland, T., Pedraza, A., Etienne, J., Novick, R., P., and Vandenesch, F. 1998. Transmembrane topology and histidine protein kinase activity of AgrC, the *agr* signal receptor in *Staphylococcus aureus*. *Molecular Microbiology* 28 (3): 655-662.

19. Koteva, K., Hong, H.-J., Wang, X. D., Nazi, I., Hughes, D., Naldrett, M. J., Buttner, M. J., and Wright, G. D. 2010. A vancomycin photoprobe identifies the histidine kinase VanSsc as a vancomycin receptor. *Nature Chemical Biology* 6 327-329.

20. Cheung, J. and Hendrickson, W. A. 2010. Sensor domains of two-component regulatory systems. *Current Opinion in Microbiology* 13 (2): 116-123.

21. Patching, S. G., Edara, S., Ma, P., Nakayama, J., Hussain, R., Siligardi, G., and Phillips-Jones, M. K. 2012. Interactions of the intact FsrC membrane histidine kinase with its pheromone ligand GBAP revealed through synchrotron radiation circular dichroism. *Biochimica et Biophysica Acta (BBA)-Biomembranes* 1818 (7): 1595-1602.

22. Gudipaty, S. A. and McEvoy, M. M. 2014. The histidine kinase CusS senses silver ions through direct binding by its sensor domain. *Biochimica et Biophysica Acta (BBA)-Proteins and Proteomics* 1844 (9): 1656-1661.

23. Maslennikov, I., Klammt, C., Hwang, E., Kefala, G., Okamura, M., Esquivies, L., Mörs, K., Glaubitz, C., Kwiatkowski, W., and Jeon, Y. H. 2010. Membrane domain structures of three classes of histidine kinase receptors by cell-free

expression and rapid NMR analysis. *Proceedings of the National Academy of Sciences* 107 (24): 10902-10907.

24. Parkinson, J. S. and Kofoid, E. C. 1992. Communication modules in bacterial signaling proteins. *Annual Review of Genetics* 26 71-112.

25. Ferris, H. U., Coles, M., Lupas, A. N., and Hartmann, M. D. 2014. Crystallographic snapshot of the *Escherichia coli* EnvZ histidine kinase in an active conformation. *Journal of Structural Biology* 186 (3): 376-9.

26. Diensthuber, R. P., Bommer, M., Gleichmann, T., and Möglich, A. 2013. Full-length structure of a sensor histidine kinase pinpoints coaxial coiled coils as signal transducers and modulators. *Structure* 21 (7): 1127-1136.

27. Yamada, S., Akiyama, S., Sugimoto, H., Kumita, H., Ito, K., Fujisawa, T., Nakamura, H., and Shiro, Y. 2006. The signaling pathway in histidine kinase and the response regulator complex revealed by X-ray crystallography and solution scattering. *Journal of Molecular Biology* 362 123-139.

28. Casino, P., Rubio, V., and Marina, A. 2009. Structural insight into partner specificity and phosphoryl transfer in two-component signal transduction. *Cell* 139 (2): 325-36.

29. Marina, A., Waldburger, C. D., and Hendrickson, W. A. 2005. Structure of the entire cytoplasmic portion of a sensor histidine-kinase protein. *EMBO Journal* 24 4247-4259.

30. Kojetin, D. J., Sullivan, D. M., Thompson, R. J., and Cavanagh, J. 2007. Classification of response regulators based on their surface properties. *Methods in Enzymology* 422 141-169.

31. Re, S. D., Tolstykh, T., Wolanin, P. M., and Stock, J. B. 2002. Genetic analysis of response regulator activation in bacterial chemotaxis suggests an intermolecular mechanism. *Protein Science* 11 2644-2654.

32. Stock, A. M. and Guhaniyogi, J. 2006. A new perspective on response regulator activation. *Journal of Bacteriology* 188 (21): 7328-7330.

33. Halkides, C. J., McEvoy, M. M., Casper, E., Matsumura, P., Volz, K., and Dahlquist, F. W. 2000. The 1.9 Å resolution crystal structure of phosphono-CheY, an analogue of the active form of the response regulator, CheY. *Biochemistry* 39 5280-5286.

34. Gao, R., Mack, T. R., and Stock, A. M. 2007. Bacterial response regulators: versatile regulatory strategies from common domains. *Trends in Biochemical Sciences* 32 (6): 225-234.

35. Chooback, L. and West, A. H. 2003. Co-crystallization of the yeast phosphorelay protein YPD1 with the SLN1 response regulator domain and preliminary X-ray diffraction analysis. *Acta Crystallographica Section D: Biological Crystallography* D59 927-929.

36. Im, Y. J., Rho, S.-H., Park, C.-M., Yang, S.-S., Kang, J.-G., Lee, J. Y., Song, P.-S., and Eom, S. H. 2002. Crystal structure of a cyanobacterial phytochrome response regulator. *Protein Science* 11 614-624.

37. Lee, S.-Y., Cho, H. S., Pelton, J. G., Yan, D., Henderson, R. K., King, D. S., Huang, L.-s., Kustu, S., Berry, E. A., and Wemmer, D. E. 2001. Crystal structure of an activated response regulator bound to its target. *Nature Structural Biology* 8 (1): 52-56.

38. Bachhawat, P. and Stock, A. M. 2007. Crystal structures of the receiver domain of the response regulator PhoP from *Escherichia coli* in the absence and presence of the phosphoryl analog beryllofluoride. *Journal of Bacteriology* 189 (16): 5987-5995.

39. Wisedchaisri, G., Wu, M., Sherman, D. R., and Hol, W. G. J. 2008. Crystal structures of the response regulator DosR from *Mycobacterium tuberculosis* suggest a helix rearrangement mechanism for phosphorylation activation. *Journal of Molecular Biology* 378 (1): 227-242.

40. Galperin, M. Y. 2006. Structural classification of bacterial response regulators: diversity of output domains and domain combinations. *Journal of Bacteriology* 188 (12): 4169-4182.

41. Gouet, P., Chinardet, N., Welch, M., Guillet, V., Cabantous, S., Birck, C., Mourey, L., and Samama, J.-P. 2001. Further insights into the mechanism of function of the response regulator CheY from crystallographic studies of the CheY-CheA$_{124-257}$ complex. *Acta Crystallographica Section D: Biological Crystallography* D57 44-51.

42. Stock, J. B. and Da Re, S. 2000. Signal transduction: Response regulators on and off. *Current Biology* 10 R420-R424.

43. Yan, M., Dai, T., Deak, J. C., Kyriakis, J. M., Zon, L. I., Woodgett, J. R., and Templeton, D. J. 1994. Activation of stress-activated protein kinase by MEKK1 phosphorylation of its activator SEK1. *Nature* 372 798-800.

44. Mascher, T., Margulis, N. G., Wang, T., Ye, R. W., and Helmann, J. D. 2003. Cell wall stress responses in *Bacillus subtilis*: the regulatory network of the bacitracin stimulon. *Molecular Microbiology* 50 (5): 1591-1604.

45. Shiozaki, K. and Russell, P. 1996. Conjugation, meiosis, and the osmotic stress response are regulated by Spc1 kinase through Atf1 transcription factor in fission yeast. *Genes and Development* 10 2276-2288.

46. Raivio, T. L., Popkin, D. L., and Silhavy, T. J. 1999. The Cpx envelope stress response is controlled by amplification and feedback inhibition. *Journal of Bacteriology* 181 (17): 5263-5272.

47. Aldridge, P. and Jenal, U. 1999. Cell cycle-dependent degradation of a flagellar motor component requires a novel-type response regulator. *Molecular Microbiology* 32 (2): 379-391.

48. Jacobs, C., Domian, I. J., Maddock, J. R., and Shapiro, L. 1999. Cell cycle-dependent polar localization of an essential bacterial histidine kinase that controls DNA replication and cell division. *Cell* 97 (Apr. 2): 111-120.

49. Ryan, K. R., Judd, E. M., and Shapiro, L. 2002. The CtrA response regulator essential for *Caulobacter cresentus* cell-cycle progression requires a bipartite degradation signal for temporally controlled proteolysis. *Journal of Molecular Biology* 324 443-455.

50. Shiozaki, K., Shiozaki, M., and Russell, P. 1997. Mcs4 mitotic catastrophe suppressor regulates the fission yeast cell cycle through the Wik1-Wis1-Spc1 kinase cascade. *Molecular Biology of the Cell* 8 409-419.

51. Skerker, J. M., Prasol, M. S., Perchuk, B. S., Biondi, E. G., and Laub, M. T. 2005. Two-component signal transduction pathways regulating growth and cell cycle progression in a bacterium: a system-level analysis. *PLoS Biology* 3 (10): e334.

52. Huam, M., Harvill, E. T., and Miller, J. F. 1998. The BvgAS virulence control system regulates type III secretion in *Bordetella bronchiseptica*. *Molecular Microbiology* 28 (5): 945-959.

53. Pragman, A. A., Yarwood, J. M., Tripp, T. J., and Schlievert, P. M. 2004. Characterization of virulence factor regulation by SrrAB, a two-component system in *Staphylococcus aureus*. *Journal of Bacteriology* 186 (8): 2430-2438.

54. Suarez, J. M., Edwards, A. N., and McBride, S. M. 2013. The *Clostridium difficile* cpr locus is regulated by a noncontiguous two-component system in

response to type A and B lantibiotics. *Journal of Bacteriology* 195 (11): 2621-31.

55. DiRita, V. J. 1992. Co-ordinate expression of virulence genes by ToxR in *Vibrio cholerae*. *Molecular Microbiology* 6 (4): 451-458.

56. Pathak, A., Goyal, R., Sinha, A., and Sarkar, D. 2010. Domain structure of virulence-associated response regulator PhoP of *Mycobacterium tuberculosis*: role of the linker region in regulator-promoter interaction(s). *Journal of Biological Chemistry* 285 (45): 34309-18.

57. Tang, Y. T., Gao, R., Havranek, J. J., Groisman, E. A., Stock, A. M., and Marshall, G. R. 2012. Inhibition of bacterial virulence: drug-like molecules targeting the *Salmonella enterica* PhoP response regulator. *Chemical Biology & Drug Design* 79 (6): 1007-17.

58. Beier, D. and Gross, R. 2006. Regulation of bacterial virulence by two-component systems. *Current Opinion in Microbiology* 9 143-152.

59. Morgan, R., Kohn, S., Hwang, S.-H., Hassett, D. J., and Sauer, K. 2006. BdlA, a chemotaxis regulator essential for biofilm dispersion in *Pseudomonas aeruginosa*. *Journal of Bacteriology* 188 (21): 7335-7343.

60. Sun, Y.-C., Koumoutsi, A., and Darby, C. 2009. The response regulator PhoP negatively regulates *Yersinia pseudotuberculosis* and *Yersinia pestis* biofilms. *FEMS Microbiology Letters* 290 85-90.

61. Yildiz, F. H. and Visick, K. L. 2009. *Vibrio* biofilms: so much the same yet so different. *Trends in Microbiology* 17 (3): 109-118.

62. Eswaramoorthy, P., Duan, D., Dinh, J., Dravis, A., Devi, S. N., and Fujita, M. 2010. The threshold level of the sensor histidine kinase KinA governs entry into sporulation in *Bacillus subtilis*. *Journal of Bacteriology* 192 (15): 3870-3882.

63. Beier, D., Schwarz, B., Fuchs, T. M., and Gross, R. 1995. *In vivo* characterization of the unorthodox BvgS two-component sensor protein of *Bordetella pertussis*. *Journal of Molecular Biology* 248 596-610.

64. Arricau, N., Hermant, D., Waxin, H., Ecobichon, C., Duffey, P. S., and Popoff, M. Y. 1998. The RcsB-RcsC regulatory system of *Salmonella typhi* differentially modulates the expression of invasion proteins, flagellin and Vi antigen in response to osmolarity. *Molecular Microbiology* 29 (3): 835-850.

65. Galperin, M. Y., Nikolskaya, A. N., and Koonin, E. V. 2001. Novel domains of the prokaryotic two-component signal transduction systems. *FEMS Microbiology Letters* 203 11-21.

66. Kato, M., Mizuno, T., Shimizu, T., and Hakoshima, T. 1997. Insights into multistep phosphorelay from the crystal structure of the C-terminal HPt domain of ArcB. *Cell* 88 717-723.

67. Jagadeesan, S., Mann, P., Schink, C. W., and Higgs, P. I. 2009. A novel "four-component" two-component signal transduction mechanism regulates developmental progression in *Myxococcus xanthus*. *Journal of Biological Chemistry* 284 (32): 21435-21445.

68. Ota, I. M. and Varshavsky, A. 1993. A yeast protein similar to bacterial two-component regulators. *Science* 262 566-569.

69. Chang, C., Kwok, S. F., Bleecker, A. B., and Meyerowitz, E. M. 1993. *Arabidopsis* ethylene-response gene *ETR1*: similarity of product to two-component regulators. *Science* 262 539-544.

70. Saito, H. 2001. Histidine phosphorylation and two-component signaling in eukaryotic cells. *Chemical Reviews* 101 2497-2509.

71. Bahn, Y. S. 2008. Master and commander in fungal pathogens: the two-component system and the HOG signaling pathway. *Eukaryot Cell* 7 (12): 2017-36.

72. Xu, Q. and West, A. H. 1999. Conservation of structure and function among histidine-containing phosphotransfer (HPt) domains as revealed by the crystal structure of YPD1. *Journal of Molecular Biology* 292 1039-1050.

73. D'Agostino, I. B. and Kieber, J. J. 1999. Phosphorelay signal transduction: the emerging family of plant response regulators. *Trends in Biochemical Sciences* 24 (11): 452-456.

74. Fassler, J. S. and West, A. H. 2013. Histidine phosphotransfer proteins in fungal two-component signal transduction pathways. *Eukaryotic cell* 12 (8): 1052-1060.

75. Xu, Q., Carlton, D., Miller, M. D., Elsliger, M.-A., Krishna, S. S., Abdubek, P., Astakhova, T., Burra, P., Chiu, H.-J., and Clayton, T. 2009. Crystal structure of histidine phosphotransfer protein ShpA, an essential regulator of stalk biogenesis in *Caulobacter crescentus*. *Journal of Molecular Biology* 390 (4): 686-698.

76. Ashenberg, O., Keating, A. E., and Laub, M. T. 2013. Helix bundle loops determine whether histidine kinases autophosphorylate in cis or in trans. *Journal of Molecular Biology* 425 (7): 1198-209.

77. Brown, J. L., Bussey, H., and Stewart, R. C. 1994. Yeast Skn7p functions in a eukaryotic two-component regulatory pathway. *EMBO Journal* 13 (21): 5186-5194.

78. Izumitsu, K., Yoshimi, A., and Tanaka, C. 2007. Two-component response regulators Ssk1p and Skn7p additively regulate high-osmolarity adaptation and fungicide sensitivity in *Cochliobolus heterostrophus*. *Eukaryotic Cell* 6 (2): 171-181.

79. Mavrianos, J., Berkow, E. L., Desai, C., Pandey, A., Batish, M., Rabadi, M. J., Barker, K. S., Pain, D., Rogers, P. D., Eugenin, E. A., and Chauhan, N. 2013. Mitochondrial two-component signaling systems in Candida albicans. *Eukaryot Cell* 12 (6): 913-22.

80. Catlett, N. L., Yoder, O. C., and Turgeon, B. G. 2003. Whole-genome analysis of two-component signal transduction genes in fungal pathogens. *Eukaryotic cell* 2 (6): 1151-1161.

81. Hohmann, S., Krantz, M., and Nordlander, B. 2007. Yeast osmoregulation. *Methods in Enzymology* 428 29-45.

82. Saito, H. and Posas, F. 2012. Response to hyperosmotic stress. *Genetics* 192 (2): 289-318.

83. Janiak-Spens, F. and West, A. H. 2000. Functional roles of conserved amino acid residues surrounding the phosphorylatable histidine of the yeast phosphorelay protein YPD1. *Molecular Microbiology* 37 (1): 136-144.

84. Bahn, Y. S., Kojima, K., Cox, G. M., and Heitman, J. 2006. A unique fungal two-component system regulates stress responses, drug sensitivity, sexual development, and virulence of *Cryptococcus neoformans*. *Molecular Biology of the Cell* 17 (7): 3122-35.

85. Lee, J. W., Ko, Y. J., Kim, S. Y., and Bahn, Y. S. 2011. Multiple roles of Ypd1 phosphotransfer protein in viability, stress response, and virulence factor regulation in *Cryptococcus neoformans*. *Eukaryotic Cell* 10 (7): 998-1002.

Role of the highly conserved G68 residue in the yeast phosphorelay protein Ypd1: implications for interactions between histidine phosphotransfer and response regulator proteins

1.1 Introduction

Histidine phosphotransfer (HPt) proteins allow bacteria, yeast and plants to expand beyond canonical two-component signaling pathways into multi-step phosphorelay pathways. They play crucial roles in regulating numerous cellular functions including those essential for growth and viability [1-4]. In bacteria, HPt domains are found as additional domains in two-component signaling proteins [5-7]. In fungi and plants, HPts are often stand-alone proteins occupying branch points within multi-step His-to-Asp phosphorelays [8-11].

Multi-step phosphorelay systems consist of the transmembrane hybrid histidine kinase (HHK), an HPt protein, and often multiple downstream response regulators (RR). The multi-step His-to-Asp phosphorelay Sln1 pathway of *Saccharomyces cerevisiae* (Sc) has been extensively studied [12-16]. The ScSln1 hyperosmotic stress pathway consists of the transmembrane HHK protein ScSln1, the HPt protein ScYpd1, and two RR proteins ScSsk1 and ScSkn7 **(Figure 5)** [11, 17, 18]. While ScYpd1 is activated by a single upstream donor, it can phosphorylate both ScSsk1 and/or ScSkn7 depending on the encountered stress. ScSsk1 is responsible for osmotic stress response through the High Osmolarity Glycerol (HOG1) Mitogen Activated Protein Kinase (MAPK) pathway, while activation of ScSkn7 is in response to cell wall stress [19]. ScSkn7 functions through direct transcriptional regulation of cell wall genes [20, 21].

ScSln1 is a membrane-bound HHK. Under normal osmotic conditions, ScSln1 autophosphorylates on a conserved histidine residue, H576, by transfer of the γ-phosphoryl group from ATP; this autophosphorylation leads to transfer of the phosphoryl group to a conserved aspartate residue, D1144, in its own receiver domain [11].

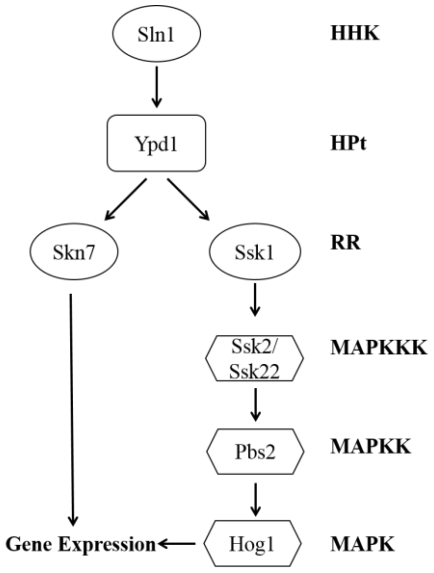


Figure 5. Sln1-Ypd1-Ssk1/Skn7 pathway in *S. cerevisiae*
ScSlnl is autophosphorylated on a histidine residue using ATP, this phosphoryl group is then transferred to an aspartic acid residue in the receiver domain of ScSlnl, and then to a histidine residue in ScYpdl. Subsequent phosphotransfer occurs to ScSsk1 or ScSkn7. Phosphorylated ScSskl serves to suppress the activation of the Hog1 MAP kinase pathway, while phosphorylated Skn7 regulates the expression genes related to cell wall stress.

Much is known regarding the structure/function relationship between the individual domains of ScSln1. ScSln1 has been shown to be evenly distributed throughout the cytoplasmic membrane, but rapidly clusters is response to hyperosmotic stress [22]. Systematic deletions mutants have shown that the periplasmic domain is essential for ScSln1 function [22]. A coiled-coil "linker" domain found between the transmembrane domains and the cytoplasmic

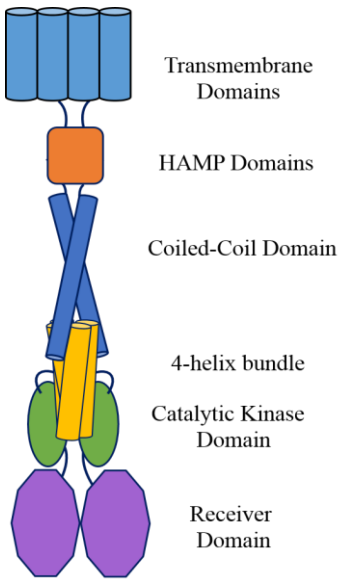


Figure 6. ScSln1 domain architecture
ScSln1 functions as a homodimer and is composed of multiple domains. The 4-helix bundle is composed of two domains from each monomer and is the location of the phosphorylatable histidine residue. The catalytic kinase domain is the binding site for ATP. The receiver domain is the location of the phosphorylatable aspartate residue.

kinase domain has also been shown to be essential for ScSln1 to function as an osmosensor [23] (**Figure 6**). After autophosphorylation, ScSln1 must pass the phosphoryl group from the reciever domain aspartate, D1144, to the a conserved histidine residue, H64, on the HPt protein ScYpd1.

The crystal structure of ScYpd1 revealed the same highly conserved fold found in other HPt structures [24, 25]. The ScYpd1 structure shows a common four-helix bundle core. The core is highly hydrophobic, and is protected from solvent by an extended linker region, the EF-linker [25]. The site of phosphorylation is completely solvent exposed and easily accessible for interaction with the reciever domains of its RR binding partners. Crystal structures of the receiver domain of ScSln1 in complex with ScYpd1 have helped to elucidate protein-protein interactions between HHK proteins and HPt proteins (**Figure 7**) [26, 27]. The structure revealed a buried hydrophobic patch surrounded by hydrophilic interactons, which may be distinct between different HPt:RR binding partners [26].

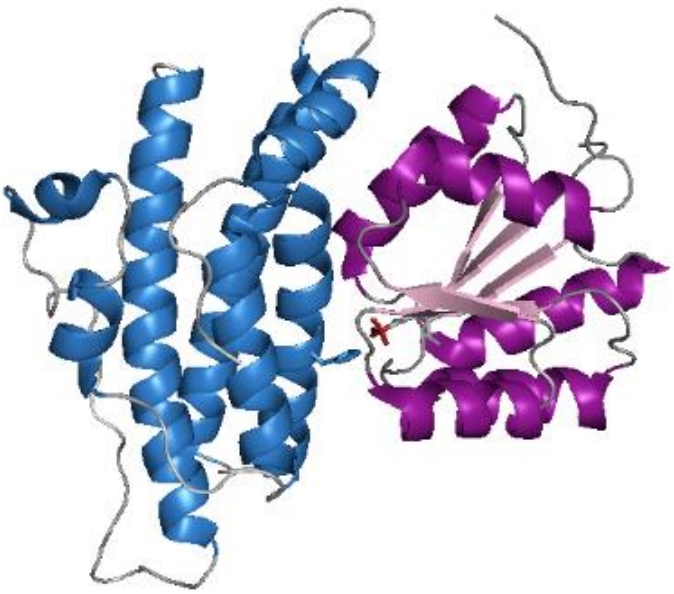


Figure 7. Crystal structure of complex between ScSln1-R1 and ScYpd1
The BeF_3^- activated complex of ScSln1-R1 (purple) and ScYpd1 (blue) demonstrates how the protein components interact with one another to form a complex for phosphotransfer to occur (PDB ID: 2R25).

Under normal osmotic conditions, the ScSln1-ScYpd1-ScSsk1 branch of the pathway is constitutively phosphorylated, and the downstream HOG1 pathway is repressed. Under hyperosmotic stress, ScSln1 ceases to autophosphorylate, allowing dephosphorylated ScYpd1 and ScSsk1 to accumulate. Unphosphorylated ScSsk1 is able to interact with the auto-inhibitory domain of ScSsk2/22, the most upstream component of the Hog1 MAPK cascade [17] and activate the pathway. Autophosphorylation of ScSsk2/ScSsk22 (MAPKKK) leads to phosphoryl group transfer to ScPbs2 (MAPKK) and finally transfer to ScHog1 (MAPK) [28]. Phosphorylated ScHog1 will then migrate into the nucleus and initiate expression of genes to respond to the loss of turgor pressure, which includes production of the compatible osmolyte glycerol [29-31] .

The ScSln1 pathway is required for cell viability through regulation of the ScHOG1 pathway [11, 17, 32]. Defects affecting any step of the ScSln1 pathway compromise the yeast's ability to respond to osmotic stress, leading to decreased cell viability.

Previous studies of the ScSln1 pathway using yeast two-hybrid assays and X-ray crystallography showed that ScYpd1 interacts with the receiver domains of its response regulator binding partners using a common hydrophobic binding surface [33, 34]. All known structures of HPt proteins, including *S. cerevisiae* ScYpd1, share a characteristic 4-helix bundle structure with this common hydrophobic binding surface [25, 35-40]. The phosphorylatable histidine residue is located just below this hydrophobic patch on the αC helix of the 4-helix bundle and is completely solvent-exposed [1, 41].

Despite their remarkably similar tertiary structure, HPt domains exhibit high sequence diversity. However, sequence conservation exist near the phosphorylatable histidine, including much of the αC helix. Conserved intramolecular interactions pull the side chains of nearby residues N61 and K67 of ScYpd1 away from the histidine leaving it accessible to the active site of cognate response regulators [38, 41, 42]. Phosphorylated half-life studies of ScYpd1 suggest that these residue may also be involved in the electrostatic stabilization of the phosphorylated histidine [27, 43].

A glycine located four residues from the phosphorylatable histidine (*H+4*), is highly conserved on the surface of HPt proteins, and has been shown to be involved in protein-protein interactions and/or phosphoryl transfer in both yeast and bacteria [33, 44-47]. Mutation of the *H+4* glycine in ScYpd1-G68Q was shown to have impaired binding of all RR receiver domains in an alanine scanning yeast two-hybrid assay [33]. The ability of the ScYpd1-G68Q to both accept and transfer phosphoryl groups was

severely impaired [44, 45]. Kinetic analysis shows that while there was a dramatic decrease in the rate of phosphoryl transfer between ScSln1-R1 and ScYpd1-G68Q, binding affinity remained similar to WT [44], indicating that the phenotypic changes observed during phosphotransfer may be related to catalysis and not a binding defect.

In order to further characterize the role that the *H+4* residue plays in protein-protein interactions between ScYpd1 and ScSsk1, a series of amino acids substitutions were made to the *H+4* glycine. This work was completed as a collaborative project with several individual members completing different aspects of the project. Here we report a comprehensive analysis of a set of point mutants at position 68 of Ypd1 to gain insights into the evolutionary constraints leading to the exceptionally high conservation of glycine at position *H+4* in HPts. We combine bioinformatics, phosphoryl transfer assays, X-ray crystallography, a fluorescence-based binding assay and molecular dynamics techniques to help explain the delicate balance of interatomic interactions required for phosphotransfer to occur between an HPt and its cognate RR. The conclusions that can be drawn clarify the importance of a small and/or hydrophilic residue in the *H+4* position.

1.2 Materials and Methods

1.2.1 Cloning

For expression of wild-type ScYpd1, the Sc*YPD1* gene was inserted into a modified pUC12 vector (pME43) as previously described [42]. The pUC-Sc*YPD1* plasmid was then used as a template to construct a set of ScYpd1-G68X mutants using site-directed mutagenesis PCR (primers listed in **Table 12** in **Appendix A**). Various

amino acid residues (S, A, V, L, E, Q) were introduced to the G68 position. For the PCR reaction, the denaturation temperature was set to 95°C for 1 minute, the annealing temperature was set to 55°C for 1 minute, and the extension temperature was set to 72°C for 7 minutes for 12 cycles.

The Sc*YPD1* gene was also inserted into a pET21a (+) vector for expression using the T7 promotor. To covalently attach a fluorescein molecule in close proximity of the active site of ScYpd1, T12 was mutated to a cysteine residue (ScYpd1-T12C) through two-step PCR site-directed mutagenesis. The resulting plasmid was then used as a template for creation of double mutants.

The expression vector encoding the ScSln1 kinase domain (GST-ScSln1-HK), was kindly provided by R. Deschenes (University of South Florida).

1.2.2 Protein purification

All ScYpd1 protein constructs used in this study were expressed in *Escherichia coli*, either DH5α for the constructs in pUC vectors, or BL21 (DE3) Star cells for constructs in the pET21a vector.

Proteins were purified by ammonium sulfate precipitation, anion exchange chromatography, and size exclusion chromatography as described previously with slight modifications [45]. The final size exclusion chromatography buffer used for the phosphotransfer reactions was modified to be 20 mM Tris-HCl pH 8.0 with 150 mM NaCl.

GST-ScSln1-HK was expressed and purified as a glutathione S-transferase (GST) fusion protein using glutathione Sepharose 4B resin. Protein was stored and used in assays in bead-bound form, as previously described [18].

The receiver domain from ScSln1 (ScSln1-R1) and the receiver domain of ScSsk1 (ScSsk1-R2) were inserted into a pFJS16 vector, as previously described [48]. These proteins were expressed in *E. coli* Rosetta (DE3) cells (Novagen) as a fusion protein containing C-terminal intein and chitin binding domains and was purified by chitin affinity chromatography and gel filtration, as described previously [18, 48].

1.2.3 Sequence alignment

Pfam was used to identify all sequences within the NCBI database containing an HPt domain, including both stand-alone HPt proteins and proteins with distinct HPt domains [49, 50]. This sequence list was edited with Jalview to remove redundancy (with a 98% cut-off) and duplicates were deleted to remove species bias. The number of non-redundant sequences remaining was found to be approximately 12000. Sequences were then sorted and counted based on residues in the *H+4* position. Jalview was used to construct a representative sequence alignment of HPts from various domains of life [51].

1.2.4 *In vitro* phosphorylation assay

The ScSln1-HK domain bound to glutathione-Sepharose 4B resin was phosphorylated via incubation with 0.66 μM [γ-^{32}P]-ATP (3000 Ci/mmol) for 30 min according to previously published protocols [14]. Unincorporated [γ-^{32}P]-ATP was washed from phospho~ScSln1-HK with 50 mM Tris-HCl, pH 8.0, 100 mM KCl, 15

mM $MgCl_2$, 2 mM DTT, and 20% glycerol by three consecutive centrifugations (1 min at 1000g). ScSln1-R1 was added to the reaction and incubated for 5 minutes with ScSln1-HK. ScSln1-HK was removed from the reaction through gentle centrifugation, leaving only ScSln1-R1 in solution. ScSln1-R1 was then used as a donor to phosphorylate all ScYpd1 proteins. ScYpd1 proteins were phosphorylated by incubation with an equimolar concentration of Sln1-R1 for 5 minutes. To test the ability of the ScYpd1-G68X mutants to transfer the phosphoryl group to downstream binding partners, ScYpd1~P was incubated with an equimolar concentration of ScSsk1-R2 and an aliquot was obtained at 5 minutes. Band intensities were quantified using ImageJ [52].

1.2.5 Fluorescence-based affinity assay (assay performed by Skyler Hebdon)

A mutation was made to ScYpd1 T12, adjacent to the hydrophobic binding patch, to introduce a unique, solvent exposed cysteine for thiol-specific labelling with a fluorescent probe. ScYpd1-T12C and ScYpd1-T12C-G68X mutants were purified according to the already published Ypd1 purification protocols [25] and buffer-exchanged into 50 mM potassium phosphate pH 9.0 and 1mM β-mercaptoethanol. Proteins were incubated in darkness for 2 hours at room temperature with a 7-fold molar excess of 5-iodoacetamidofluorescein (5-IAF) for covalent labeling of T12C. Unincorporated 5-IAF was removed by exchanging labelled ScYpd1 proteins into 20 mM Tris pH 8.0, 50 mM NaCl and 10 mM $MgCl_2$ using a GE HiTrap desalting column. The concentration of bound fluorescein was estimated by absorption at 492 nm, and protein concentration was estimated by BioRad protein assay revealing that 70-90% of

the ScYpd1 molecules were labelled. Fluorescently-labeled proteins were aliquoted and stored in the presence of 10% glycerol at -20 ˚C until ready for use.

ScSln1-R1 receiver domain as purified as described previously, but size exclusion was performed in fluorescence buffer (20 mM Tris pH 8.0, 50 mM NaCl and 10 mM $MgCl_2$). Chelex® resin (BioRad) was used to strip contaminating cations from the Tris-salt solution before magnesium chloride was added to the buffer.

Binding of Sln1-R1 to fluorescein labelled ScYpd1-T12C induces a change in the molar extinction of the fluorescein moiety. A Fluoromax 4 Spectrofluorometer from Horiba Scientific, temperature controlled to 23.0 °C, was used to observe changes in fluorescence caused by binding. 30 pmol of labelled ScYpd1-T12C was diluted to 1,900 μL in fluorescence buffer, and ScSln1-R1 was titrated into the reaction such that the concentration in the cuvette ranged from 10 nM to 6 μM. Upon addition of ScSln1-R1, the mixture was stirred with a magnetic stir bar for 30 seconds and allowed to rest for an additional 20 seconds before reading fluorescence intensity with absorbance at 492 nm and emission at 515 nm. Intensity after each addition (F) as a fraction of intensity from labelled ScYpd1 alone (F_0) was calculated for titration with ScSln1-R1 and buffer alone. The difference between these two normalized intensities (F/F_0, Sln1-R1 - F/F_0, buffer) indicates binding of ScSln1-R1 to labelled ScYpd1. Plotting change in fluorescence intensity caused by ScSln1-R1 versus concentration of ScSln1-R1 shows a binding curve with saturation at high concentrations. These curves were fitted using Mathematica to an expanded quadratic equation with parameters accounting for fluorescence from both the bound and unbound states of ScYpd1 and the dissociation

constant for the ScYpd1: ScSln1-R1 complex. The average dissociate constant and standard deviation of the mean are reported here.

1.2.6 Crystallization (structure determination completed by Dr. Smita Menon)

Hexagonal form ScYpd1-G68Q mutant crystals were grown using conditions obtained for wild ScYpd1 [42], a protein concentration of 10 mg/mL was used in a 0.1 M sodium acetate pH 5.0 buffer with 0.2 M ammonium acetate and 25-30% PEG 4000 (Fluka, 81242).

1.2.7 X-ray data collection and processing

Data were collected at the home source (OU Macromolecular Crystallography Lab) using CuKα radiation from a Rigaku Micromax 007HF X-ray generator set to 1.54 Å wavelength at 100 K by flash freezing crystals in a liquid N_2. High concentrations of PEG 4000 were used as a cryoprotectant. The data were recorded with a Dectris Pilatus P200K hybrid pixel detector using oscillations of 0.5° and processed using HKL2000 [53]. The space group was determined to be $P3_121$ after inspection of the electron density maps. The unit cell was determined to be $a = b = 76.7$ Å, $c = 66.7$ Å $\alpha = \beta = 90^{\circ}$, $\gamma = 120^{\circ}$. One molecule was found in the asymmetric unit with a resolution of 1.98 Å. Data processing and refinement statistics are presented in Table 1.

1.2.8 Structure solution and refinement

Molecular replacement using PHASER-MR from the Phenix (vs. 1.10pre_2131) [54-56] suite of programs was used to determine the initial phases using WT-ScYpd1 structure (1QSP) [42]. Refinement was carried out using Phenix-refine [57]. Clear

electron density difference was seen for the glutamine side chain at position 68 in a F_o-F_c electron density map. Coot [58] was used to place the glutamine into the electron density map and manually adjust the model after each cycle of refinement. The final the R_{work} was 17.1% with an R_{free} of 20.4%.

1.2.9 Molecular dynamics simulations (simulations performed by Clay Foster)

ScYpd1-G68X mutations were modeled using PyMOL version 1.83. For ScYpd1-G68Q and G68E (unpublished data), crystal structures were aligned to the existing Sln1-R1/Ypd1-BeF_3^- complex (PDB ID: 2R25). The mutant ScYpd1 and ScSln1-R1 molecules were then extracted for simulation. For the remaining substitutions, mutations were modeled directly onto the ScYpd1: ScSln1R1 activated structure (PDB ID: 2R25). In each model, the BeF_3^- ligand was replaced by PO_3^{2-}. Each system was stripped of crystallographic waters and ligands, with only the Mg^{2+} remaining at the active site. Structures were then placed in an orthorhombic solvent box using the TIP3P model. Finally, systems were neutralized and set to a concentration of 0.15 M NaCl. System preparation and visualization were done using Schrodinger Maestro [59]. Simulations were performed with Desmond using the OPLS 2005 force field [60, 61]. The default Desmond relaxation protocol was used, featuring a series of gradually diminishing restraints for ~270 ps, followed by a brief, 100 ps unrestrained NPT simulation. To preserve the pre-phosphotransfer active site and the relative locations of the phosphorylatable histidine and aspartate, a position restraint with a

force constant of 100 kcal/mol/Å was applied to the Nε2 atom of H64 and the phosphoryl during each simulation. Final structures were examined using PyMOL [62].

1.2.10 Molecular graphics

All molecular figures were generated using PyMOL version 1.83 [62].

1.3 Results

1.3.1 A glycine in the *H+4* position of HPt domains and stand-alone HPt proteins is highly conserved

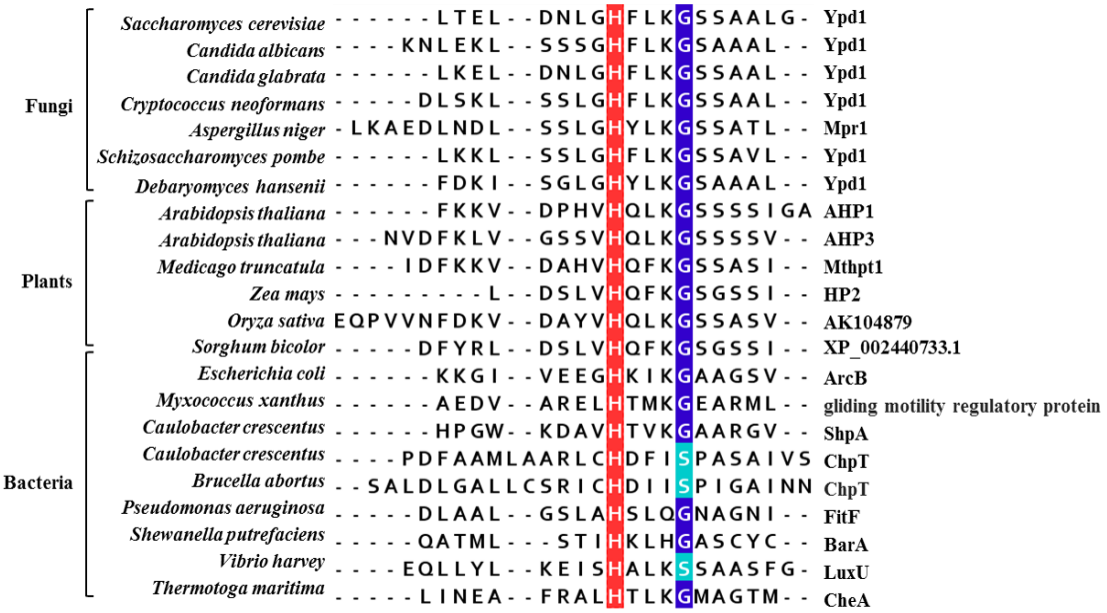


Figure 8. Representative sequence alignment of HPt proteins or domains from fungi, plants and bacteria

Representative sequence alignment of the αC region of stand-alone HPt proteins or HPt domains from fungi, plants and bacteria. The phosphorylatable histidine residue is highlighted in red and the *H+4* residue is highlighted in blue.

Table 2. Quantification of residues found in the *H+4* position of HPt proteins and HPt domains

Residue	Num. of Sequences	% of Total
G	10071	84.96
S	1392	11.74
P	115	0.970
A	92	0.77
T	72	0.60
N	42	0.35
H	22	0.18
E	11	0.09
V	10	0.08
R	10	0.08
I	6	0.05
C	2	0.01
D	2	0.01
L	2	0.01
Q	2	0.01
W	1	0.008
Y	1	0.008

Approximately 12000 non-redundant sequences in the NCBI database representing bacteria, fungi and plants were analyzed. The region spanning the predicted αC and αD helices of the core 4-helix bundle found in HPt proteins, as well as hybrid proteins containing HPt domains, was used to construct the alignment. Glycine was found to be present in ~85% of sequences that were aligned. The second most abundant amino acid at this position was found to be serine, which represented ~12% of sequences analyzed, followed by proline with ~1% (**Table 2**). A representative sequence alignment of the highly conserved region of HPt protein with the phosphorylatable histidine residue highlighted in red and the *H+4* glycine highlighted in blue is shown in (**Figure 8**).

1.3.2 Non-conservative mutations at ScYpd1 G68 disrupt phosphotransfer

Phosphorelay experiments were performed on each of the G68X mutants using ScSln1-R1 as a phospho-donor and ScSsk1-R2 as a phospho-recipient. ScYpd1-G68S and ScYpd1-G68A were both able to accept a phosphoryl group from ScSln1-R1 with approximately the same ability as wild-type ScYpd1 (**Table 3).** All other mutants showed various decreased levels of phosphorylation. Briefly, ScYpd1-G68Q showed a drastic decrease in its ability to accept a phosphoryl group (~40% of wild-type). ScYpd1-G68V, ScYpd1-G68L, and ScYpd1-G68E were almost completely unable to accept a phosphoryl group from ScSln1-R1 (**Figure 9**).

Table 3. Ability of ScYpd1-G68X mutants to function as a phosphorelay protein

Protein	Phospho-accepting ability (%)	Phospho-transfer ability (%)
WT	100 ± 0	100 ± 0
G68S	94.1± 3.6	80.9 ± 17.8
G68A	82.0 ± 15.6	80.4 ± 8.0
G68V	2.5 ±3.5	0.36 ± 0.6
G68L	0.4 ± 0.6	0.28 ± 0.5
G68E	0.3 ± 0.5	0.08 ± 0.15
G68Q	40.2 ± 8.3	0.9 ± 1.6

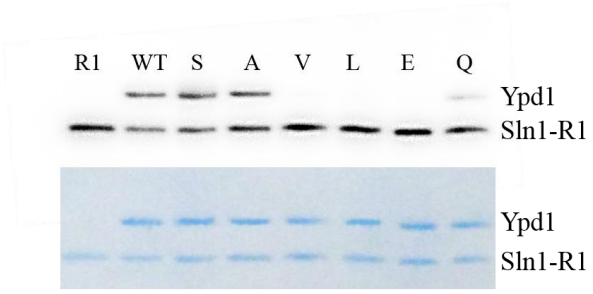


Figure 9. Phosphoryl transfer from phospho~ScSln1-R1 to ScYpd1
Phosphoryl transfer reactions contained equimolar concentrations of ScSln1-R1 and ScYpd1. Reaction was quenched at 5 mins. The autoradiographs were analyzed using ImageJ and the amount of radiolabel in ScYpd1-G68X mutants was quantified and compared with the amount of radio-label seen for the wild-type ScYpd1 band (set to 100%).

Full phosphorelay experiments were performed between ScSln1-R1, the set of ScYpd1-G68X mutants and ScSsk1-R2. ScYpd1-G68S and ScYpd1-G68A were able to

transfer a phosphoryl group to ScSsk1-R2 comparable to wild-type ScYpd1. Severe impairment of the ability of phospho~ScYpd1-G68Q to transfer the phosphoryl to ScSsk1-R2 was observed (**Figure 10**), consistent with previously published results [45]. Due to their inability to accept an initial phosphoryl group, no transfer could be observed between ScYpd1-G68V, ScYpd1-G68L and ScYpd1-G68E mutants and ScSsk1-R2.

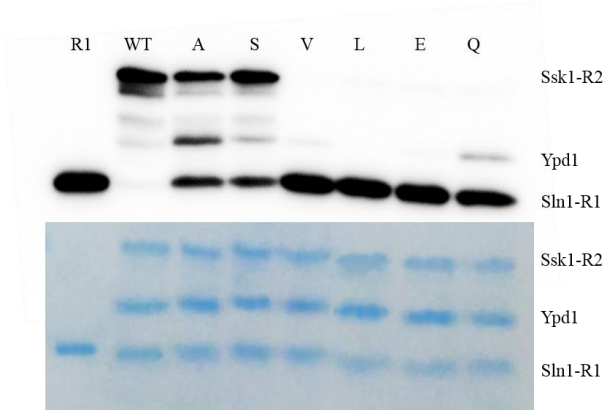


Figure 10. Phosphoryl transfer from phosopho~Ypd1 to Ssk1-R2
Phosphoryl transfer from phosopho-ScYpd1 to Ssk1-R2. Phosphoryl transfer reactions contained equimolar concentrations of ScSln1-R1, ScYpd1, and ScSsk1-R2 proteins. The autoradiographs were analyzed using ImageJ and the amount of radiolabel in ScSsk1-R2 bands in the presence of G68X mutants was quantified and compared with the amount of ScSsk1-R2 radiolabel in the presence of wild-type ScYpd1 band (set to 100%).

1.3.3 Substitutions at the G68 position cause only modest changes in affinity of ScYpd1 for ScSln1-R1 (Experiments performed by Skyler Hebdon)

Because a defect was observed in the ability for ScYpd1 to accept phosphoryl groups, a fluorescence based, *in vitro* binding assay was developed to test the possibility that large side chains at position 68 inhibit binding between ScYpd1 and ScSln1-R1. Addition of ScSln1-R1 to labelled ScYpd1 mutants increased fluorescence intensity

above baseline buffer dilutions, resulting in binding curves that appear to reach saturation at high concentrations (**Figure 11**).

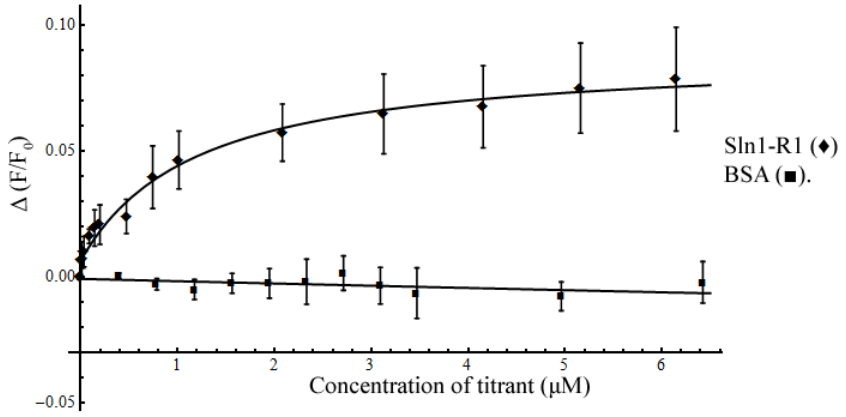


Figure 11. Representative titration of ScYpd1-T12C with ScSln1-R1
ScYpd1-T12C~F (♦) and ScYpd1-T12C-G68Q~F (■) titrated with ScSln1-R1. Curves were inverted and fitted to an expanded quadratic binding equation in order to calculate dissociation constants.

Dissociation constants (K_d) calculated from these binding curves for this panel of mutants ranged from 0.5 to 4 μM as shown in **Table 4**. The K_d for the ScSln1-R1 and ScYpd1-T12C interaction, 0.94 ± 0.38 μM, is in agreement with the K_d between ScSln1-R1 and wild-type ScYpd1 calculated from published kinetics data [44]. Though the K_d values observed for the mutants were within error of the wild-type protein, there was an observable trend that hydrophobic side chains decreased binding affinity and hydrophilic side chains increased affinity (**Table 4**).

Table 4. Binding constants for ScYpd1 with ScSln1-R1

WT	0.94 ± 0.38 μM
G68V	2.9 ± 0.08 μM
G68L	1.3 ± 0.09 μM
G68E	0.5 ± 0.13 μM
G68Q	0.6 ± 0.27 μM

Binding constants and standard deviations were derived from three replicates

1.3.4 Crystal structure of ScYpd1-G68Q (Structure solution determined by Dr. Smita Menon.)

The ScYpd1-G68Q mutant was crystallized in space group $P3_121$. The structure was solved using molecular replacement to a resolution of 1.98 Å. The model contains residues 2-167 with an average B-factor of 23.73 $Å^2$. Clear electron density is observed for the side chain of the glutamine substitution at position 68. Few differences exist between this structure and the previously reported ScYpd1 crystal structures (PDB ID: 1QSP) **(Figure 13**) [25, 27, 63].

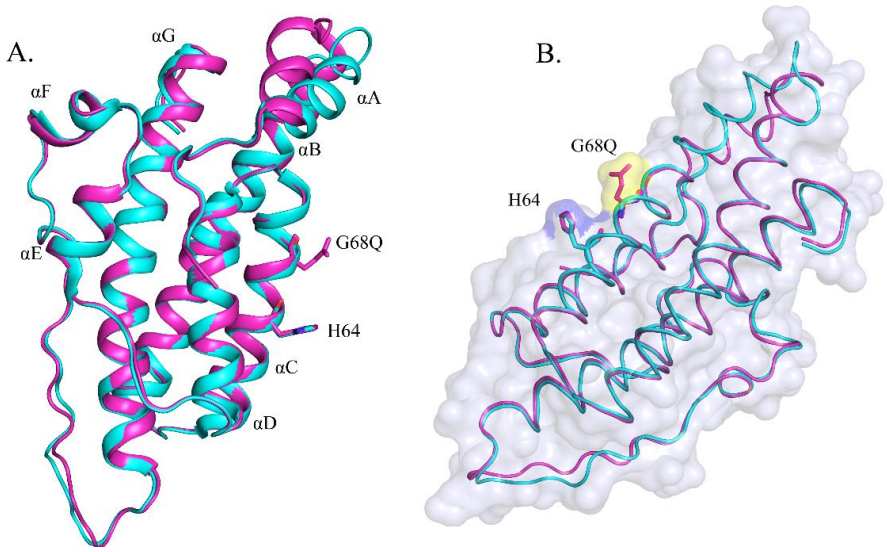


Figure 13. Overlay and surface representations of wild-type ScYpd1 (cyan) (PDB ID: 1QSP) and the ScYpd1-G68Q mutant (magenta)

A. The helices are numbered sequentially A to G from the N terminus to the C terminus with the four-helix bundle core composed of helices B, C, D and G. Phosphorylatable histidine and *H+4* glycine or glutamine are shown in stick representation. Movement of the αA helix is observed with a RMSD of 3.0 for this region.

B. The volume of the H64 surface is shown in blue and the added bulk of the glutamine side chain is shown in yellow.

The area around the site of phosphorylation is relatively unperturbed with an RMSD of 0.2 Å for all residues in αC and αD 1.4 Å. The highest deviation is seen in I18, which is displaced ~6.9 Å from its position in the wild-type structure (**Figure 12**). In unit cell, the αA helix is located between αB (in contact with residues 37-58) and αG (in contact with residues 130-140). The αA helix and the following turn (residues 10 – 27) show the largest shifts in



Figure 12. Shift in I18 residue of ScYpd1-G68Q

I18, which is displaced ~6.9 Å from its position in the wild-type structure.

Cα positions. The Cα RMSD between G68Q (10-27) and wild-type (10-27) is 3.0 Å. The movement of αA can be decomposed into two components. The αA helix rotates approximately 30° upwards from its wild-type position centered on the N-terminal end of the helix (L9). Secondly, the αA helix makes a ¼ rotation around its longitudinal axis (**Figure 13**). Upon the αA twisting movement, the originally exposed I13 and I17 are buried, E16 is shifted and L14 and I18 are now exposed. As a result, the alternative conformation of αA maintains hydrophobic interactions. Minor shifts in the orientations of exposed side chains account for the remainder of the deviation between ScYpd1 structures.

1.3.5 Mutations at the G68 position lead to changes in active site residues involved in catalysis (Molecular dynamics simulation performed by Clay Foster. Analysis of data completed in collaboration)

To better understand the effects of mutating the *H+4* residue in ScYpd1, mutations were modeled onto the existing ScSln1-R1/ScYpd1-BeF_3^- structure (PDB ID: 2R25). Short molecular dynamics runs were performed to allow the mutant active sites to relax. This let us to observe the local structural changes caused by each substitution. The following G68 mutants were simulated, in addition to a wild-type control: S, V, E, L and Q. Wild-type and G68S showed little structural perturbation upon relaxation, preserving the phosphoryl geometry and proper His-Asp alignment for phosphotransfer. G68V caused slight distortion of the phosphoryl geometry, but produced a significant shift in the β4α4 loop of ScSln1-R1, specifically at residue A1174. G68E demonstrated moderate distortion, but an even more dramatic shift in β4α4 loop region. In addition, the mutant glutamate formed direct interactions with ScSln1-R1 at both A1174 and the

highly conserved “switch” residue, T1173, which switches in orientation to form a new hydrogen bond upon RR activation. The positioning of the acidic side chain also appears to form a salt-bridge with K67 of ScYpd1. G68L led to severe distortion of the phosphoryl geometry, though the β4α4 loop of Sln1-R1 was unaffected. This distortion is most likely due to repulsive effects on the nearby ScSln1-R1 K1195, which is known to form a highly conserved salt-bridge with the phosphoryl group. Finally, G68Q caused moderate active site distortion, but had a negligible effect on the β4α4 loop of ScSln1-R1. The added glutamine side chain was also able to satisfy several additional hydrogen bonds outside of the active site.

1.4 Discussion

HPt proteins play critical roles in signal transduction. Their primary role is to transfer a phosphoryl group from the receiver domain of a HHK to the receiver domain of an RR protein. Deletion mutants of HPt proteins, resulting in the loss of signal transduction leads in decreased cell viability in both bacteria and yeast through suboptimal pathway regulation [11, 64-66]. The multi-domain protein ArcB (which consists of HK-RR-HPt domains) from *E. coli* transmits a signal to the terminal response regulator ArcA, mutants of residues in $ArcB^{C}$, notably the *H+4* residue G721, show a decrease in phosphotransfer ability [47]. When the *H+4* residue of the P1 domain from CheA (an HPt domain), G52, is mutated it has a highly detrimental effect on chemotaxis [46]. The ScYpd1-G68Q mutant from *S. cerevisiae* had a significantly diminished ability to both accept a phosphoryl group from the upstream ScSln1 and transfer it to the downstream ScSsk1 [45]. We aimed to investigate the role of this *H+4* residue in His-to-Asp multi-step phosphorelay systems.

In every currently known sequence containing an HPt domain, 98.4% of residues that occupy the *H+4* position relative to the phospho-accepting histidine are small. Glycine assumes this position in ~85% of cases, while ~12% contain a serine residue and ~2% are either proline or alanine. This observation suggests that evolutionary preservation of a small residue was necessary for HPt domain function or interaction with binding partners. We hypothesized that substituting an amino acid with a bulky side chain at this position could potentially interfere with complex formation based off of a previous study which showed a diminished ability of accept a phosphoryl group and transfer the phosphoryl to a downstream binding partner [45].

In this study, we used phosphotransfer assays, a fluorescence binding assay and X-ray crystallography to provide evidence that the *S. cerevisiae* HPt protein, ScYpd1, requires a small residue such as glycine in the *H+4* position. Without this small residue, phosphotransfer to its cognate response regulator, Ssk1, is inhibited.

By creating a series of amino acid substitutions in the *H+4* location, we determined that substitutions by smaller residues (S, A) at the *H+4* position still allowed for phosphotransfer at near wild-type levels in ScYpd1. Mutations introducing larger side chain volumes (V, L, E) drastically inhibited phosphotransfer as both an acceptor and donor. The only exception was the G68Q substitution, where a large hydrophilic side chain still allowed for moderate phosphotransfer activity.

To test if the functional defects observed for the *S. cerevisiae* ScYpd1-G68Q mutant were a result of loss of structural integrity, we used X-ray crystallography to solve the structure of the ScYpd1-G68Q mutant. We did not observe any broad overall structural changes, with the exception of movement of the AA helix and the significant

bulk at the interface's surface. The intrinsic flexibility of αA suggests that the observed movement is likely due to crystal packing and not a static structural alteration; this helix is known to be the most flexible region in the HPt protein structure [41].

In vitro fluorescence-based binding experiments between ScSln1-R1 and ScYpd1-G68X mutants showed no substantial changes in binding affinity as a consequence of the substitutions. These data demonstrate that the diminished phosphotransfer activity that we see in most of the larger mutants is not a consequence of changes in HPt:RR complex formation. Taken together, our results suggest the interface perturbations introduced by the non-functional mutants at position 68 are most likely negatively affecting the catalysis of the phosphotransfer reaction.

Our lab previously showed that there is a hydrophobic docking site on ScYpd1 for all three of its cognate binding partners. It consists of the αA, N-terminus of αB and C-terminus of αC helices of ScYpd1 [33]. From the crystal structures of ScSln1-R1 in complex with ScYpd1, we noted that the interfaces are highly complementary. The small volume of the active site cavity would not easily accommodate the addition of a bulky side chain without substantial rearrangement. If this additional bulk does not inhibit binding, as our fluorescence-based binding data confirms, then these rearrangements must be interfering with key residues involved in the phosphotransfer reaction. When the structures of ScYpd1-G68Q and ScYpd1 from the BeF_3^- activated complex are aligned, the mutant glutamine side chain clashes with the highly conserved K1195 of ScSln1-R1 (**Figure 14**).

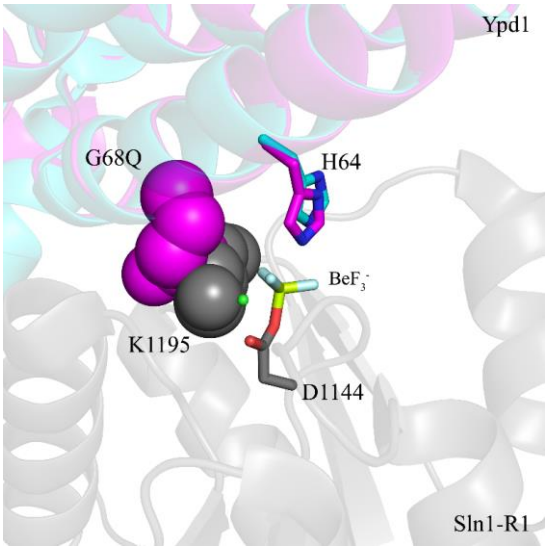


Figure 14. Overlay of the ScYpd1-G68Q mutant (magenta)(PDB ID: 5JH4) with the ScYpd1•Sln1-R1•Mg^{2+}•BeF_3^- complex (cyan) (PDB ID: 2R25)
The Q68 residue (magenta) of ScYpd1 occupies the same space as the K1195 residue (grey) of ScSln1-R1 (gray). Q68 and K1195 are shown in space filling representation. Bound Mg^{2+} is colored green and BeF_3^- is shown in stick representation.

K1195 has been implicated in the stabilization of the transition state formed during the His-Asp phosphotransfer event [67]. Any changes to its ability to neutralize the negatively charged transition state may have a significant effect on phosphotransfer between ScSln1-R1 and ScYpd1.

In addition to K1195, the molecular dynamics simulations we performed showed several other factors that may be affected by the substitutions. The geometry of the donor and acceptor atoms is critical for His-to-Asp phosphotransfer. Crystal structures of BeF_3^- bound complexes, such as ScSln1-R1/ScYpd1 (PDB ID: 2R25) [26, 27] suggest a conserved in-line orientation is necessary for nucleophilic attack and transfer between the residues. Correct geometry is maintained for HPts and their RRs by a narrow channel through which the histidine can access the aspartate. In the Sln1-R1/Ypd1 complex, this is formed by adjacent residues on both proteins, including highly conserved positions such as Q1146, T1173, A1174 and K1195 on Sln1-R1, and K67, G68 and Q86 on ScYpd1. Any disruption to the arrangement of these residues would distort the in-line geometry. This is observed in the simulations of the larger substitutions (V, L, E, Q), with G68L causing the most severe phosphoryl distortion. The obvious explanation for this is the introduction of a large hydrophobic group into a mostly polar/charged active site. A related effect is shifting of β4α4 loop on ScSln1-R1. Upon phosphorylation, ScSln1-R1 undergoes a significant conformational change involving the β4α4 region. This allows for the transfer channel to form, and also for T1173 (side chain) and A1174 (main chain) to hydrogen bond with the oxygen atoms on either side of the tetrahedral phosphoryl group. In the case of Asp-to-His phosphotransfer, such as between the upstream ScSln1-R1 and ScYpd1, these interactions likely serve a similar purpose as K1195 in stabilizing the negatively charged pentavalent transition state. G68V and G68E both caused large shifts in this region, increasing the distance between A1174 and the phosphoryl oxygen. The G68Q substitution caused only moderate distortion, while leaving the β4α4 region largely

unaffected. This can explain why ScYpd1-G68Q was still able to function in phosphotransfer, albeit in a diminished capacity due to its moderate distortion. The additional hydrogen bonds satisfied by the glutamine side chain may also simply make it more favorable and/or stable than leucine or valine in the same environment.

Interestingly, while both HPt and HK domains interact with receiver domains using phosphorylatable histidine residues, the strict *H+4* conservation of HPt domains does not translate to HK domains. In most HKs, a threonine or asparagine occupies the *H+4* position in the conserved H-box motif of the DHp domain [68-70]. Comparison of HK:RR structures HK853:RR468 (PDB ID: EDGE) and ThkA:TrrA from *Thermotoga maritima* (PDB ID: 3A0R) with HPt:RR structures ScSln1-R1: ScYpd1 (PDB ID: 10XB) and CheA-P1:CheY (PDB ID: 2LP4) demonstrates that the protein-protein interactions occur in different regions on the RR partner. RR proteins interact with HK proteins using primarily the β3α3/β4α4 regions, but interact with HPt proteins using the β1α1/ β2α2/β3α3 regions. An altered orientation allows for the larger residues found near the phosphorylatable histidine on most HKs. Large residues on the surface of the HPt in the *H+4* location, as we have shown through radio-labeled phosphotransfer assays and molecular dynamic simulations, displace residues crucial for proper HPt: RR interactions due to their shifted binding orientations. Additional structural complexes of HK:RR cognate pairs as well as HPt:RR pairs would provide further insight.

References

1. Fassler, J. S. and West, A. H. 2013. Histidine phosphotransfer proteins in fungal two-component signal transduction pathways. *Eukaryotic cell* 12 (8): 1052-1060.

2. Stock, A. M., Robinson, V. L., and Goudreau, P. N. 2000. Two-component signal transduction. *Annual Review of Biochemistry* 69 (1): 183-215.

3. Saito, H. 2001. Histidine phosphorylation and two-component signaling in eukaryotic cells. *Chemical Reviews* 101 2497-2509.

4. D'Agostino, I. B. and Kieber, J. J. 1999. Phosphorelay signal transduction: the emerging family of plant response regulators. *Trends in Biochemical Sciences* 24 (11): 452-456.

5. Tsuzuki, M., Ishige, K., and Mizuno, T. 1995. Phosphotransfer circuitry of the putative multi-signal transducer, ArcB, of *Escherichia coli*: *in vitro* studies with mutants. *Molecular Microbiology* 18 953-962.

6. Bilwes, A. M., Alex, L. A., Crane, B. R., and Simon, M. I. 1999. Structure of CheA, a signal-transducing histidine kinase. *Cell* 96 131-141.

7. Freeman, J. A. and Bassler, B. L. 1999. Sequence and function of LuxU: a two-component phosphorelay protein that regulates quorum sensing in *Vibrio harveyi*. *Journal of Bacteriology* 181 (3): 899-906.

8. Calera, J. A., Herman, D., and Calderone, R. 2000. Identification of *YPD1*, a gene of *Candida albicans* which encodes a two-component phosphohistidine intermediate protein. *Yeast* 16 1053-1059.

9. Lee, J. W., Ko, Y. J., Kim, S. Y., and Bahn, Y. S. 2011. Multiple roles of Ypd1 phosphotransfer protein in viability, stress response, and virulence factor regulation in *Cryptococcus neoformans*. *Eukaryotic Cell* 10 (7): 998-1002.

10. Miyata, S., Urao, T., Yamaguchi-Shinozaki, K., and Shinozaki, K. 1998. Characterization of genes for two-component phosphorelay mediators with a single HPt domain in *Arabidopsis thaliana*. *FEBS Letters* 437 11-14.

11. Posas, F., Wurgler-Murphy, S. M., Maeda, T., Witten, E. A., Thai, T. C., and Saito, H. 1996. Yeast HOG1 MAP kinase cascade is regulated by a multistep phosphorelay mechanism in the SLN1-YPD1-SSK1 "two-component" osmosensor. *Cell* 86 865-875.

12. Saito, H. and Posas, F. 2012. Response to hyperosmotic stress. *Genetics* 192 (2): 289-318.

13. Levin, D. E. 2005. Cell wall integrity signaling in *Saccharomyces cerevisiae*. *Microbiology and Molecular Biology Reviews* 69 (2): 262-291.

14. Fassler, J. S. and West, A. H. 2010. Genetic and Biochemical Analysis of the SLN1 Pathway in *Saccharomyces cerevisiae*. *Methods in Enzymology* 471 291-317.

15. Hohmann, S. 2002. Osmotic stress signaling and osmoadaptation in yeasts. *Microbiology and Molecular Biology Reviews* 66 (2): 300-372.

16. Hohmann, S. 2009. Control of high osmolarity signalling in the yeast Saccharomyces cerevisiae. *FEBS Letters* 583 (24): 4025-4029.

17. Posas, F. and Saito, H. 1998. Activation of the yeast SSK2 MAP kinase kinase kinase by the SSK1 two-component response regulator. *EMBO Journal* 17 (5): 1385-1394.

18. Li, S., Ault, A., Malone, C. L., Raitt, D., Dean, S., Johnston, L. H., Deschenes, R. J., and Fassler, J. S. 1998. The yeast histidine protein kinase, Sln1p, mediates phosphotransfer to two response regulators, Ssk1p and Skn7p. *EMBO Journal* 17 (23): 6952-6962.

19. Wurgler-Murphy, S. M. and Saito, H. 1997. Two-component signal transducers and MAPK cascades. *Trends in Biochemical Sciences* 22 172-176.

20. Fassler, J. S. and West, A. H. 2011. Fungal Skn7 stress responses and their relationship to virulence. *Eukaryotic Cell* 10 (2): 156-167.

21. Li, S., Dean, S., Li, Z., Horecka, J., Deschenes, R. J., and Fassler, J. S. 2002. The eukaryotic two-component histidine kinase Sln1p regulates OCH1 via the transcription factor, Skn7p. *Mol Biol Cell* 13 412-424.

22. Reiser, V., Raitt, D. C., and Saito, H. 2003. Yeast osmosensor Sln1 and plant cytokinin receptor Cre1 respond to changes in turgor pressure. *Journal of Cell Biology* 161 (6): 1035-1040.

23. Tao, W., Malone, C. L., Ault, A. D., Deschenes, R. J., and Fassler, J. S. 2002. A cytoplasmic coiled-coil domain is required for histidine kinase activity of the yeast osmosensor, SLN1. *Molecular Microbiology* 43 (2): 459-473.

24. Kato, M., Shimizu, T., Mizuno, T., and Hakoshima, T. 1999. Structure of the histidine-containing phosphotransfer (HPt) domain of the anaerobic sensor

protein ArcB complexed with the chemotaxis response regulator CheY. *Acta Crystallographica Section D: Biological Crystallography* D55 1257-1263.

25. Xu, Q. and West, A. H. 1999. Conservation of structure and function among histidine-containing phosphotransfer (HPt) domains as revealed by the crystal structure of YPD1. *Journal of Molecular Biology* 292 1039-1050.

26. Xu, Q., Porter, S. W., and West, A. H. 2003. The yeast YPD1/SLN1 complex: Insights into molecular recognition in two-component systems. *Structure* 11 (12): 1569-1581.

27. Zhao, X., Copeland, D. M., Soares, A. S., and West, A. H. 2008. Crystal structure of a complex between the phosphorelay protein YPD1 and the response regulator domain of SLN1 bound to a phosphoryl analog. *Journal of Molecular Biology* 375 (4): 1141-1151.

28. Maayan, I. and Engelberg, D. 2009. The yeast MAPK Hog1 is not essential for immediate survival under osmostress. *FEBS Letters* 583 2015-2020.

29. Tamás, M. J., Luyten, K., Sutherland, F. C. W., Hernandez, A., Albertyn, J., Valadi, H., Li, H., Prior, B. A., Kilian, S. G., Ramos, J., Gustafsson, L., Thevelein, J. M., and Hohmann, S. 1999. Fps1p controls the accumulation and release of the compatible solute glycerol in yeast osmoregulation. *Molecular Microbiology* 31 (4): 1087-1104.

30. Capaldi, A. P., Kaplan, T., Liu, Y., Habib, N., Regev, A., Friedman, N., and O'Shea, E. K. 2008. Structure and function of a transcriptional network activated by the MAPK Hog1. *Nature Genetics* 40 (11): 1300-1306.

31. Jacoby, T., Flanagan, H., Faykin, A., Seto, A. G., Mattison, C., and Ota, I. 1997. Two protein-tyrosine phosphatases inactivate the osmotic stress response pathway in yeast by targeting the mitogen-activated protein kinase, Hog1. *Journal of Biological Chemistry* 272 17749-17755.

32. Albertyn, J., Hohmann, S., Thevelein, J. M., and Prior, B. A. 1994. GPD1, which encodes glycerol-3-phosphate dehydrogenase, is essential for growth under osmotic stress in *Saccharomyces cerevisiae*, and its expression is regulated by the high-osmolarity glycerol response pathway. *Molecular and Cellular Biology* 14 (6): 4135-4144.

33. Porter, S. W. and West, A. H. 2005. A common docking site for response regulators on the yeast phosphorelay protein YPD1. *Biochimica et Biophysica Acta* 1748 138-145.

34. Porter, S. W., Xu, Q., and West, A. H. 2003. Ssk1p response regulator binding surface on histidine-containing phosphotransfer protein Ypd1p. *Eukaryotic Cell* 2 (1): 27-33.

35. Sugawara, H., Kawano, Y., Hatakeyama, T., Yamaya, T., Kamiya, N., and Sakakibara, H. 2006. Crystal structure of the histidine-containing phosphotransfer protein ZmHP2 from maize. *Protein Science* 14 202-208.

36. Kato, M., Mizuno, T., Shimizu, T., and Hakoshima, T. 1999. Refined structure of the histidine-containing phosphotransfer (HPt) domain of the anaerobic sensor kinase ArcB from *Escherichia coli* at 1.57 Å resolution. *Acta Crystallographica Section D: Biological Crystallography* D55 1842-1849.

37. Ulrich, D. L., Kojetin, D., Bassler, B. L., Cavanagh, J., and Loria, J. P. 2005. Solution structure and dynamics of LuxU from *Vibrio harveyi*, a phosphotransferase protein involved in bacterial quorum sensing. *Journal of Molecular Biology* 347 297-307.

38. Ruszkowski, M., Brzezinski, K., Jedrzejczak, R., Dauter, M., Dauter, Z., Sikorski, M., and Jaskolski, M. 2013. Medicago truncatula histidine-containing phosphotransfer protein: structural and biochemical insights into the cytokinin transduction pathway in plants. *FEBS Journal* 280 (15): 3709-20.

39. Rogov, V. V., Bernhard, F., Lohr, F., and Dotsch, V. 2004. Solution structure of the Escherichia coli YojN histidine-phosphotransferase domain and its interaction with cognate phosphoryl receiver domains. *Journal of Molecular Biology* 343 1035-1048.

40. Bauer, J., Reiss, K., Veerabagu, M., Heunemann, M., Harter, K., and Stehle, T. 2013. Structure–function analysis of *Arabidopsis thaliana* histidine kinase AHK5 bound to its cognate phosphotransfer protein AHP1. *Molecular plant* 6 (3): 959-970.

41. Xu, Q., Carlton, D., Miller, M. D., Elsliger, M.-A., Krishna, S. S., Abdubek, P., Astakhova, T., Burra, P., Chiu, H.-J., and Clayton, T. 2009. Crystal structure of histidine phosphotransfer protein ShpA, an essential regulator of stalk biogenesis in *Caulobacter crescentus*. *Journal of Molecular Biology* 390 (4): 686-698.

42. Xu, Q., Nguyen, V., and West, A. H. 1999. Purification, crystallization, and preliminary X-ray diffraction analysis of the yeast phosphorelay protein YPD1. *Acta Crystallographica Section D: Biological Crystallography* D55 291-293.

43. Janiak-Spens, F., Sparling, D. P., and West, A. H. 2000. Novel role for an HPt domain in stabilizing the phosphorylated state of a response regulator domain. *Journal of Bacteriology* 182 (23): 6673-6678.

44. Janiak-Spens, F., Cook, P. F., and West, A. H. 2005. Kinetic analysis of YPD1-dependent phosphotransfer reactions in the yeast osmoregulatory phosphorelay system. *Biochemistry* 44 (1): 377-386.

45. Janiak-Spens, F. and West, A. H. 2000. Functional roles of conserved amino acid residues surrounding the phosphorylatable histidine of the yeast phosphorelay protein YPD1. *Molecular Microbiology* 37 (1): 136-144.

46. Nishiyama, S.-I., Garzón, A., and Parkinson, J. 2014. Mutational analysis of the P1 phosphorylation domain in Escherichia coli CheA, the signaling kinase for chemotaxis. *Journal of Bacteriology* 196 (2): 257-264.

47. Matsushika, A. and Mizuno, T. 1998. The structure and function of the histidine-containing phosphotransfer (HPt) signaling domain of the *Escherichia coli* ArcB sensor. *Journal of Biochemistry* 124 440-445.

48. Janiak-Spens, F., Sparling, J. M., Gurfinkel, M., and West, A. H. 1999. Differential stabilities of phosphorylated response regulator domains reflect functional roles of the yeast osmoregulatory SLN1 and SSK1 proteins. *Journal of Bacteriology* 181 (2): 411-417.

49. Finn, R. D., Coggill, P., Eberhardt, R. Y., Eddy, S. R., Mistry, J., Mitchell, A. L., Potter, S. C., Punta, M., Qureshi, M., Sangrador-Vegas, A., Salazar, G. A., Tate, J., and Bateman, A. 2016. The Pfam protein families database: towards a more sustainable future. *Nucleic Acids Research* 44 (D1): D279-85.

50. Geer, L. Y., Marchler-Bauer, A., Geer, R. C., Han, L., He, J., He, S., Liu, C., Shi, W., and Bryant, S. H. 2009. The NCBI biosystems database. *Nucleic Acids Research* 38 D492-6.

51. Waterhouse, A. M., Procter, J. B., Martin, D. M., Clamp, M., and Barton, G. J. 2009. Jalview Version 2—a multiple sequence alignment editor and analysis workbench. *Bioinformatics* 25 (9): 1189-1191.

52. Schneider, C. A., Rasband, W. S., and Eliceiri, K. W. 2012. NIH Image to ImageJ: 25 years of image analysis. *Nature Methods* 9 (7): 671-675.

53. Otwinowski, Z. and Minor, W. 1997. Processing of X-ray diffraction data collected in oscillation mode. *Methods in Enzymology* 276 307-326.

54. Adams, P. D., Afonine, P. V., Bunkóczi, G., Chen, V. B., Davis, I. W., Echols, N., Headd, J. J., Hung, L.-W., Kapral, G. J., and Grosse-Kunstleve, R. W. 2010. PHENIX: a comprehensive Python-based system for macromolecular structure solution. *Acta Crystallographica Section D: Biological Crystallography* 66 (2): 213-221.

55. McCoy, A. J., Grosse-Kunstleve, R. W., Adams, P. D., Winn, M. D., Storoni, L. C., and Read, R. J. 2007. Phaser crystallographic software. *Journal of Applied Crystallography* 40 (4): 658-674.

56. Terwilliger, T. C., Grosse-Kunstleve, R. W., Afonine, P. V., Moriarty, N. W., Zwart, P. H., Hung, L.-W., Read, R. J., and Adams, P. D. 2008. Iterative model building, structure refinement and density modification with the PHENIX AutoBuild wizard. *Acta Crystallographica Section D: Biological Crystallography* 64 (1): 61-69.

57. Afonine, P. V., Grosse-Kunstleve, R. W., Echols, N., Headd, J. J., Moriarty, N. W., Mustyakimov, M., Terwilliger, T. C., Urzhumtsev, A., Zwart, P. H., and Adams, P. D. 2012. Towards automated crystallographic structure refinement with phenix. refine. *Acta Crystallographica Section D: Biological Crystallography* 68 (4): 352-367.

58. Emsley, P. and Cowtan, K. 2004. Coot: model-building tools for molecular graphics. *Acta Crystallographica Section D: Biological Crystallography* D60 2126-2132.

59. Maestro, v., Schrödinger, LLC, New York, NY, 2016.

60. Banks, J. L., Beard, H. S., Cao, Y., Cho, A. E., Damm, W., Farid, R., Felts, A. K., Halgren, T. A., Mainz, D. T., and Maple, J. R. 2005. Integrated modeling program, applied chemical theory (IMPACT). *Journal of Computational Chemistry* 26 (16): 1752-1780.

61. Bowers, K. J., Chow, E., Xu, H., Dror, R., Eastwood, M. P., Gregersen, B. A., Klepeis, J. L., Kolossvary, I., Moraes, M. A., and Sacerdoti, F. D. Scalable algorithms for molecular dynamics simulations on commodity clusters. in SC 2006 Conference, Proceedings of the ACM/IEEE. 2006. IEEE.

62. DeLano, W. L., The PyMOL molecular graphics system. 2002, San Carlos, CA: DeLano Scientific.

63. Xu, Q., Porter, S. W., and West, A. H. 2003. The yeast YPD1/SLN1 complex: Insights into molecular recognition in two-component systems. *Structure* 11 1569-1581.

64. Biondi, E. G. 2006. A phosphorelay system controls stalk biogenesis during cell cycle progression in *Caulobacter cresentus*. *Molecular Microbiology* 59 (2): 386-401.

65. Bahn, Y. S., Kojima, K., Cox, G. M., and Heitman, J. 2006. A unique fungal two-component system regulates stress responses, drug sensitivity, sexual development, and virulence of *Cryptococcus neoformans*. *Molecular Biology of the Cell* 17 (7): 3122-35.

66. Hsu, J. L., Chen, H. C., Peng, H. L., and Chang, H. Y. 2008. Characterization of the histidine-containing phosphotransfer protein B-mediated multistep phosphorelay system in *Pseudomonas aeruginosa* PAO1. *Journal of Biological Chemistry* 283 (15): 9933-9944.

67. Schuster, M., Silversmith, R. E., and Bourret, R. B. 2001. Conformational coupling in the chemotaxis response regulator CheY. *Proceedings of the National Academy of Sciences* 98 (11): 6003-6008.

68. Wolanin, P. M., Thomason, P. A., and Stock, J. B. 2002. Histidine protein kinases: key signal transducers outside the animal kingdom. *Genome Biology* 3 (10): reviews3013.1-3013.8.

69. Grebe, T. W. and Stock, J. B. 1999. The histidine protein kinase superfamily. *Advances in Microbial Physiology* 41 139-227.

70. Kim, D. and Forst, S. 2001. Genomic analysis of the histidine kinase family in bacteria and archaea. *Microbiology* 147 (5): 1197-1212.

Extended N-terminal region of the essential phosphorelay signaling protein Ypd1 from *Cryptococcus neoformans* contributes to structural stability, phospho-stability, and binding of calcium ions

2.1 Introduction

Histidine-to-aspartate (His-to-Asp) multi-step phosphorelay systems are used extensively by bacteria and lower eukaryotes to sense and respond to changes in their external environment and to regulate critical cellular functions such as progression through the cell cycle, mating, and the production of virulence factors [1-5]. While these signaling pathways are abundant in bacteria and lower eukaryotes, they are absent in humans and other higher eukaryotes making these promising targets for development of new antifungal therapeutics [6-9]. In bacteria, "two-component systems" generally consist of a single sensor histidine kinase (HK), and a response regulator protein (RR) [10-12]. In plants and fungi, this canonical two-component system has been expanded into as a multi-step phosphorelay system [13]. The HK is often replaced with a hybrid histidine kinase (HHK), which in addition to an HK domain includes a receiver domain typically found in RR proteins, a histidine phosphotransfer (HPt) protein, and multiple downstream RR proteins [14-16].

The histidine phosphotransfer protein Ypd1, or a close homolog, is found at the branch point of multi-step His-to-Asp signal transduction pathways in several fungal organisms including *Saccharomyces cerevisiae*, *Candida albicans*, *Schizosaccharomyces pombe*, and *Cryptococcus neoformans* [17-19]. Ypd1 is often the sole HPt encoded by fungal organisms [20].

The hyperosmotic stress response pathway in *S. cerevisiae* has been extensively characterized [21, 22]. This pathway consists of a membrane bound HHK protein, ScSln1, the HPt protein, ScYpd1, and two RR proteins, ScSsk1 and ScSkn7. The ScSln1-ScYpd1-ScSsk1 branch of this pathway is responsible for regulation of the High Osmolarity Glycerol Pathway (HOG1) MAP kinase pathway that responds to external osmotic stress by production of the compatible osmolyte glycerol.

The human fungal pathogen *Cryptococcus neoformans* (Cn) utilizes a homologous pathway to that found in *S. cerevisiae* **(Figure 15)**, however, much less is understand about this pathway.

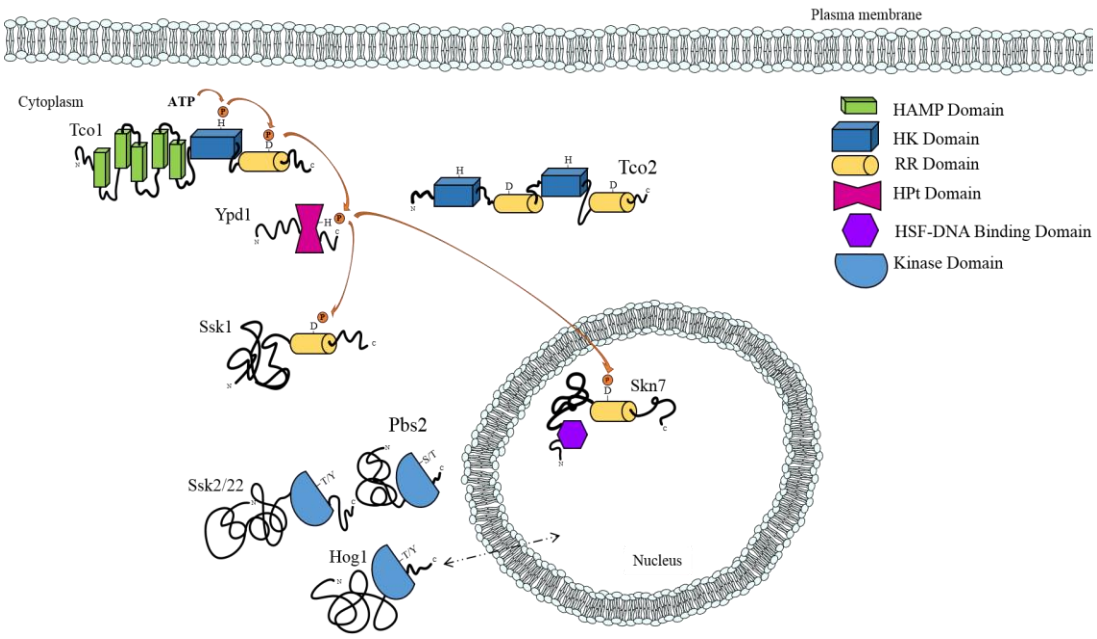


Figure 15. Multi-step histidine-to-aspartate pathway in *C. neoformans*
The multi-step histidine-to-aspartate pathway found in *C. neoformans* consists of at least two HHK proteins, CnTco1 and CnTco2, as well as an HPt protein, CnYpd1, and two RR proteins, CnSsk1 and CnSkn7.

In *S. cerevisiae* only one HHK protein is encoded by the genome, while in *C. neoformans*, seven HHK proteins (CnTco1-7) are encoded. Only one of the proteins,

CnTco5, is predicted to contain transmembrane domains similar to ScSln1, while the remaining CnTco proteins are all predicted to be cytosolic [14]. CnTco1 and CnTco2, have been found to interact with CnYpd1 under osmotic stress conditions [19, 23].

Disruption of Cn*TCO1* results in increased resistance to fludioxonil (an antifungal drug), and increased the production of melanin (a virulence factor) both of which are comparable phenotypes found when the Cn*HOG1* gene is disrupted [19]. Independent of Hog1 MAPK pathway activation, Cn*TCO1* also plays a role in sexual reproduction, and disruption of the gene results in defective cell-cell fusion during mating [19]. CnTco1 and CnTco2 have been found to play redundant roles in resistance to fludioxonil but have also been shown to have roles independent of each other. Disruption of the Cn*TCO1* gene but not the Cn*TCO2* gene results in attenuation of virulence, while disruption of the Cn*TCO2* gene results in sensitivity to hydrogen peroxide [19]. Another interesting characteristic of the CnTco1 and CnTco2 proteins are their unique domain architecture. CnTco1 is proposed to contain five HAMP domain repeats, while CnTco2 is proposed to contain repeating HK and RR domains **(Figure 16)** [19]. The functions of the other CnTco proteins remain unknown.

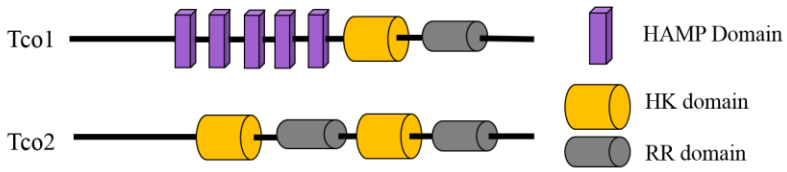


Figure 16. Proposed domain architecture of Tco1 and Tco2 HHK proteins found in *C. neoformans*
Several CnTco proteins are proposed to have unique domain architecture. CnTco1 is proposed to contain five HAMP domain repeats, while CnTco2 is proposed to contain repeating HK and RR domains.

CnYpd1 is the sole HPt protein present in *C. neoformans* [24], and initial attempts at gene disruption were unsuccessful [19]. Severe growth defects were observed when Cn*YPD1* was not transcribed upon subsequent replacement of the Cn*YPD1* promotor with an inducible promoter, indicating that Cn*YPD1* is essential for viability [23]. CnYpd1 has been shown to be an intermediate in the regulation of the Hog1 MAPK pathway, as well as having roles that are independent of the Hog1 pathway [23].

C. neoformans also contains two response regulators homologous to the *S. cerevisiae* RR proteins found in the Sln1 Pathway, CnSsk1 and CnSkn7 [19]. CnSsk1 has been implicated as being the major upstream regulator of the Hog1 MAPK pathway, with disruption of the Cn*SSK1* gene resulting in increased sensitivity to osmotic shock, UV irradiation, high temperature, and hydrogen peroxide, increased resistance to fludioxonil, enhanced mating, and increased virulence factor production of melanin and capsule [19]. The role of CnSkn7 is thought to be mainly independent of the Hog1 pathway, with deletion of the Cn*SKN7* gene resulting in more severely attenuated virulence than Cn*HOG1* disruption mutants [19].

C. neoformans is ubiquitous to the environment and can be isolated from air and soil containing pigeon excrement. Through serological studies it has been shown that up to 70% of children over the age of two living in urban areas such as the Bronx have been exposed to C. *neoformans* [25]. These infections very rarely progress to disease in individuals who are immunocompetent but there have been reported incidents [26].

Fungal infections caused by *C. neoformans* are increasing at an alarming rate as the number of immunocompromised individuals (AIDS patients, organ transplant

recipients, and cancer patients) also increases. There are greater than 1 million cryptococcosis infections worldwide annually [27]. *C. neoformans* is the most common cause of fungal infections in HIV patients, reported to be annually responsible for over 620,000 deaths within 3 months of infection in this population [28].

When *C. neoformans* causes symptomatic disease it often results in pneumonia-like illnesses. The fungi can disseminate through the blood to the central nervous system to cause meningoencephalitis [29]. This most often occurs in individuals who are immunocompromised, including those with HIV/AIDS in underdeveloped countries such as Southeast Asia and Africa [30]. HIV infected patients who acquire *Cryptococcus* infections are at a very high risk of death, with as many as 60% of all diagnoses resulting in patient death [28]. There are four serotypes of *C. neoformans*: serotype A (var. *grubii*), serotype B and serotype C (var. *gattii*), and serotype D (var. *neoformans*). Serotype A is the most virulent, accounting for 95% of clinical isolates worldwide and 95% of isolates from AIDS patients [30].

Because *C. neoformans* has vast implications in human health, this work could result in the further help with the development of antifungal medications. The emergence of drug resistant strains of microorganisms has recently become more common, so there is a need for new medications to treat these infections. The most common drugs used in treating *C. neoformans* infections, Amphotericin B and Flucytosine, are highly toxic and often treatment with the drugs has to cease despite treatment being incomplete and fungal infection remaining [31]. The toxicity and the number of side effects that are associated with the current most common antifungal medications are extensive and with the requirement of long term use these medications

in the treatment in HIV/AIDs patients for cryptococcosis fungal infections, this has become increasingly problematic [32]. Because the His-to-Asp signal transduction pathways found in pathogenic fungi like *C. neoformans* are not found in humans or other higher eukaryotes, and protein components such as CnYpd1 have been shown to be associated with virulence and are essential for viability, His-to-Asp pathway proteins are excellent targets for the development of new antifungal medications.

Here I report my work on the biochemical characterization of the predicted histidine phosphotransfer protein Ypd1 from the fungal human pathogen *C. neoformans*. Results from this study indicate that the extended N-terminal amino acid sequence confers structural stability, contributes to the phosphorylated life-time of the protein, and provides binding sites for calcium ions. Results from our studies will contribute to a better understanding of how HPt proteins mediate multi-step phosphorelay signaling pathways in pathogenic fungi.

2.2 Material and Methods

2.2.1 Materials

All chemicals for protein expression and purification were of ultrapure grade from Ameresco® or Sigma®. The pTrcHis-TOPO® TA Expression Kit was purchased from Invitrogen for gene cloning. Ni-NTA affinity resin was purchased from McLab (NiNTA). HiTrapQ columns were purchased from GE Healthcare and were used on an AKTÄ prime chromatography system from GE Healthcare. [γ-^{32}P] ATP (3000 Ci/mmol) was purchased from Perkin Elmer. TEV protease was produced in our

laboratory from an expression plasmid that was kindly given to us by J. Doudna at University of California, Berkeley [33].

2.2.2 Cloning

All constructs used in this study were confirmed by DNA sequencing at the Oklahoma Medical Research Foundation DNA Sequencing Facility. The Cn*YPD1* gene was PCR amplified from cDNA (kindly provided by Dr. Jan Fassler, University of Iowa), into a pTrcHis-TOPO vector **(Figure 17)** using the pTrcHis TOPO® TA Expression Kit (Life Technologies) to construct the plasmid pTrcHis-Cn*YPD1*. The primers 768/769 in **Table 12** in **Appendix A** were used for the PCR reaction. The PCR program used was 95°C for 30 seconds, 65°C for 1 minute, 72°C for 1 minute, repeated for 20 cycles, and 72°C for 5 minutes. After transformation into *E. coli* DH5α cells and overnight culture, plasmid DNA was isolated using the QIAprep Spin Miniprep Kit (Qiagen).

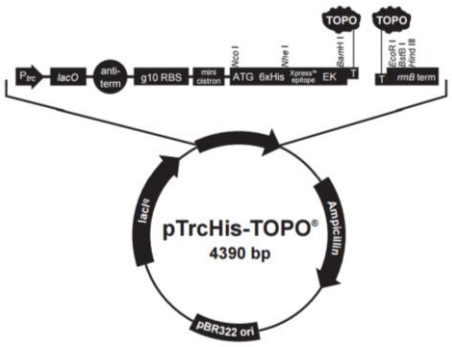


Figure 17. Plasmid map of pTrcHis-TOPO vector

Site-directed mutagenesis PCR was used to remove the enterokinase (EK) site present in the pTrcHis-TOPO vector and replace it with a TEV protease cleavage site for higher cleavage specificity. Primers 809/810 listed in **Table 12** in **Appendix** were used for PCR reaction. The resulting plasmid was called TrcHis-*CnYPD1-TEV*. For the PCR reaction for replacement of the EK site the programmed method was 95°C for 30

seconds, five cycles of 95°C for 30 seconds, 52°C for 1 minute, 72°C for 7 minutes, followed by thirteen cycles of 95°C for 30 seconds, 55°C for 1 minute, and 72°C for 7 minutes. DpnI (10 U) was used to digest methylated parental DNA while retaining the newly synthesized DNA.

The pTrcHis-Cn*YPD1* plasmid served as a template for making a series of N-terminal truncation constructs (Δ5, Δ19, Δ43, Δ50, Δ60, Δ77, Δ83, and Δ100) using primers listed in **Table 12** in **Appendix A**. For the PCR reaction, the denaturation temperature was set to 95°C for 1 minute, the annealing temperature was set to 55°C for 1 minute, and the extension temperature was set to 72°C for 7 minutes for 20 cycles.

The hypothetical phospho-accepting histidine residue of CnYpd1, H138, was mutated to a glutamine residue by site-directed mutagenesis PCR in both the pTrcHis-Cn*YPD1* and pTrcHis-Cn*YPD1-TEV* plasmids to create the pTrcHis-Cn*YPD1-H138Q* and pTrcHis-Cn*YPD1-H138Q-TEV* plasmids. For the PCR reaction, the denaturation temperature was set to 95°C for 1 minute, the annealing temperature was set to 55°C for 1 minute, and the extension temperature was set to 72°C for 7 minutes for 12 cycles with primers 721/722 listed in **Table 12** in **Appendix A.** DpnI (10 U) was used to digest methylated parental DNA while retaining the newly synthesized DNA.

Three mutants were constructed using pTrcHis-Cn*YPD1* as a template in order to determine which specific residues are involved in metal ion binding, E48A-E54A, E58A and D60A-E67A. CnYpd1-E58A was cloned using site-directed mutagenesis PCR with the same PCR program used to create the pTrcHis-Cn*YPD1-H138Q* mutant. E48A-E54A and D60A-E67A were cloned using ligation independent cloning [34]. Primers used are listed in **Table 12** of **Appendix A.**

The receiver domain (nucleotides 3022-3780) of Cn*SSK1* from *C. neoformans* strain H99 (CnSsk1-R2) was PCR amplified from cDNA into a pET-21a vector by Dr. Katie Branscum using oligo pairs 711/712 found in **Table 12** of **Appendix A**.

The receiver domain of Cn*SKN7* (nucleotides 2062-3159) from *C. neoformans* strain H99 (CnSkn7-R3) were amplified from cDNA using oligo pairs 711/712 found in **Table 12** of **Appendix A** and into the TrcHis-Topo vector by Brittany Kitchens.

2.2.3 Protein expression and purification

All plasmids were transformed into *Escherichia coli* DH5α cells for protein expression. Protein purification and growth conditions was consistent for all constructs. Ten mL overnight cultures were used to inoculate 1 L of Luria Broth (LB). Protein expression was induced with 0.4 M isopropyl β-D-1-thiogalactopyranoside (IPTG) (Gold Biotechnology) when at OD_{600} reached 0.5. Cells were grown at 37°C and harvested at approximately 10 hours. The cells were pelleted by centrifugation at 5000 *g* and then suspended in lysis buffer (20 mM Bis-tris pH 6.5, 500 mM NaCl, and 20 mM imidazole). Cells were lysed using sonication and the supernatant was clarified by centrifugation at 17000 *g*. The clarified supernatant was applied to a 5 mL Ni-NTA agarose column and protein was eluted from the column using elution buffer (20 mM Bis-tris pH 6.5, 50 mM NaCl, and 300 mM imidazole). Elution fractions containing the Ypd1 protein were applied to a 5 mL HiTrap Q anion exchange column (GE Life Sciences) using an AKTÄ Prime chromatography system.

CnYpd1 eluted from the Q column at approximately 300 mM NaCl. CnYpd1 containing fractions were combined and concentrated to approximate 500 µL using a Amicon Ultra-15 centrifugation unit with a 10 kDa molecular weight cutoff (Millipore) and loaded onto a Superdex 200-Increase column (GE Life Sciences) equilibrated in 50 mM Tris-HCl pH 8.0 and 150 mM NaCl using an AKTÄ Pure M1 system in the Protein Production Core at the University of Oklahoma. Fractions containing pure CnYpd1 proteins were pooled and protein concentration was determined by absorbance at 280 nm using a calculated extinction coefficient for each CnYpd1 construct **(Table 5)**. Protein appears to be approximately 95% pure and yield was approximately 40 mg/L of cell culture.

Table 5. Calculated molecular weight, extinction coefficient and pI information for CnYpd1 constructs

Protein	Calculated molecular weight (g/mol)	Calculated extinction coefficient (M^{-1} cm^{-1})	Calculated pI
$CnYpd1_{tag}$	27586	18575	4.46
$CnYpd1_{notag}$	23449	17085	4.33
CnYpd1 ΔN5	27115	16960	4.35
CnYpd1 ΔN15	26175	18575	4.46
CnYpd1 ΔN19	25773	18575	4.46
CnYpd1 ΔN43	22970	18575	4.40
CnYpd1 ΔN50	22254	18450	4.40
CnYpd1 ΔN60	21226	18575	4.47
CnYpd1 ΔN70	20065	18575	4.73
CnYpd1 ΔN 77	15184	18450	4.88
CnYpd1ΔN84	18443	18575	4.94
CnYpd1ΔN100	16393	18450	5.96

CnSsk1-R2 (~29 kDa) and CnSkn7-R3 (~40 kDa) were expressed in BL21 (DE3) Rosetta cells and DH5α cells respectively. Cells were grown at 16°C for approximately 18 hours. Cells were lysed by French Press in lysis buffer (20 mM Na/K Phosphate pH 7.4, 500 mM NaCl, 10 mM Imidazole). Supernatant was passed over a 5 mL Ni-NTA column, column was washed with wash buffer (Na/K Phosphate pH 7.4, 500 mM NaCl, 30 mM Imidazole). Proteins were eluted from column with 400 mM imidazole. Protein containing fractions were pooled and buffer exchanged into a buffer

containing 20 mM Na/K Phosphate pH 7.4, 50 mM NaCl for anion exchange chromatography. Protein containing fractions were concentrated using an Amicon centrifugation unit with a 10 kDa molecular weight cut off. Pure proteins were aliquoted and stored at -20°C in the presence of 10% glycerol.

The *S. cerevisiae* phosphorelay proteins, histidine kinase and receiver domains from ScSln1 (ScSln1-HKR1), and receiver domain from ScSsk1 (ScSsk1-R2), were purified following methods described previously in our laboratory [35, 36].

2.2.4 Determination of oligomeric state of CnYpd1

Size exclusion chromatograph, size exclusion chromatography with multi-angle light scattering analysis and native gel analysis were performed on CnYpd1 protein samples in order to determine the oligomeric state of the protein in solution. CnYpd1 was purifies as previously described and subjected to SEC on a calibrated S200 column in the Protein Production Core at the University of Oklahoma. *S. cerevisiae* ScYpd1 was purified according to previously published protocols [37]. SEC was repeated on a protein sample containing both ScYpd1 and CnYpd1 in a 20 mM Tris pH 8.0, 50 mM NaCl buffer. Similarly, SEC was performed on a series of protein constructs (ScYpd1, CnYpd1, CnYpd1 ΔN50, CnYpd1 ΔN60, and CnYpd1 ΔN70) on a calibrated Superdex 200 Increase column in a 50 mM Tris pH 7.0, 150 mM NaCl buffer.

To determine if cysteine residues were involved in the elution volume of the protein, SEC was performed on CnYpd1 samples in the presence and absence of 1mM βME.

Native gel analysis was performed on CnYpd1 protein samples. Protein was purified in a buffer containing 20 mM Tris pH 8.0 and 150 mM NaCl. Additives were added to protein samples and protein was separated on a 15% native gel.

Size exclusion chromatography with multi-angle light scattering analysis (SEC-MALS) was performed on CnYpd1 protein samples from anion exchange fractions. Protein was buffer exchanged into a 50 mM Tris pH 8.0, 150 mM NaCl buffer and SEC-MALS was performed.

2.2.5 Pull down assay with receiver domain of CnSkn7 (CnSkn7-R3)

Pure CnSkn7-R3 protein was bound to a 5 mL Ni-NTA column and unbound protein was washed from the column with wash buffer (50 mM Tris pH 8.0 and 150 mM NaCl). Pure CnYpd1 protein was then passed over the column. The column was again washed with wash buffer. Proteins were then eluted from the column with wash buffer containing 300 mM imidazole. Aliquots were taken of each step and were separated on a 15% SDS-PAGE gel.

2.2.6 Solubility studies of CnYpd1 N-terminal deletion constructs

E. coli cells expressing various constructs of CnYpd1 were grown in 500 mL cultures at 37°C for 6 hours. Samples were taken prior and subsequent to induction with IPTG, and of the clarified supernatant and pellet fractions subsequent to sonication. The percentage of CnYpd1 distributed in the supernatant versus pellet fractions were estimated using ImageJ software [38].

2.2.7 *In vitro* phosphorylation assay

To test the ability of CnYpd1 to function as an HPt protein, the HK and RR domains of the *S. cerevisiae* HHK Sln1 were used as a phosphoryl donor. GST-tagged ScSln1-HKR1 was purified and left bound to glutathione–sepharose 4B resin (Amersham Pharmacia Biotech AB) as described previously ([39]). Autophosphorylation of the bead-bound GST-Sln1-HKR1 protein using γ-^{32}P-ATP (Perkin Elmer) was performed according to previously published protocols from our laboratory [40]. Phospho~GST-ScSln1-HKR1 (GST-ScSln1-HKR1~P) was then added to tubes containing an equal molar amount of an HPt protein alone, or HPt protein with a RR receiver domain (ScSsk1-R2), aliquots were obtained and the reaction was quenched with stop buffer (250 mM Tris, pH 6.8, 40% glycerol, 8% sodium dodecyl sulfate (SDS), 50 mM EDTA. All CnYpd1 constructs were phosphorylated in this manner. For visualization of the reaction, samples were applied to a 15% SDS polyacrylamide gel and electrophoresed at 200 V for 45 min. The SDS gels were wrapped in plastic wrap and exposed to a phosphorimager screen. The radioactivity of each band was quantified using a Typhoon phosphorimager (Molecular Dynamics).

For phosphorylated life-time studies, CnYpd1 or a CnYpd1 N-terminal deletion mutant, was incubated with Bead-bound GST-ScSln1-HKR1~P for 10 minutes. After the 10 minute incubation, GST-tagged ScSln1-HKR1 was removed from the reaction by gentle centrifugation (**Figure 18).** The supernatant containing only phospho~HPt protein was placed into a separate Eppendorf tube, aliquots were removed at specific

time points and the reaction was quenched with stop buffer.

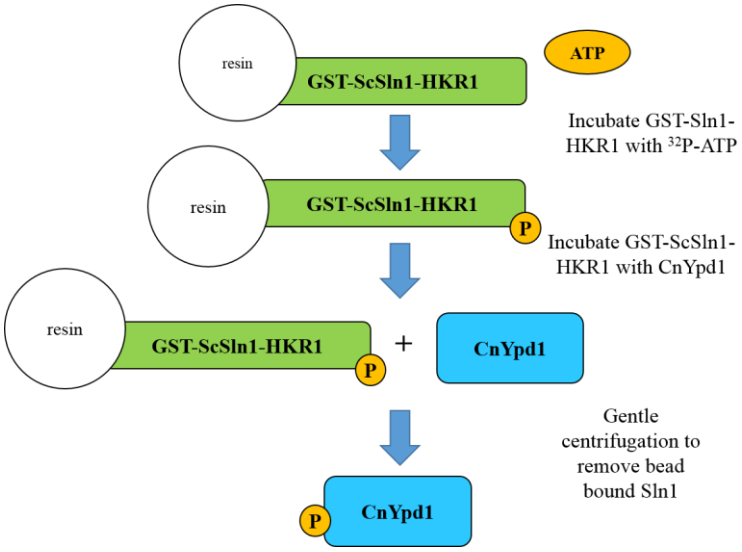


Figure 18. Schematic for phosphorylation of CnYpd1
Heterologous donor ScSln1-HKR1 was used to phosphorylate CnYpd1 and removed from reaction by gentle centrifugation.

2.2.8 Size exclusion chromatography analysis for metal binding studies

Pure CnYpd1 protein was buffer exchanged into a buffer containing either 20 mM Sodium Citrate pH 5, 50 mM NaCl, and 1 mM EDTA or 20 mM Tris pH 8, 50 mM NaCl, and 1 mM EDTA using an Amicon Ultra-15 Centrifugation Unit with a 10 kDa molecular weight cutoff. All buffers were passed over a 10 mL Chelex® column to remove trace metal ions. Proteins were subjected to size exclusion chromatography on a Superdex 200 Increase column using an AKTÄ Pure M1 system equilibrated with the corresponding buffer in the Protein Production Core Facility at the University of Oklahoma. Fractions containing CnYpd1 protein were pooled and buffer exchanged into the corresponding buffer without EDTA. Protein was then split into four equal parts. Metal ions were re-introduced to the solution by the addition of 10mM $MgCl_2$, 10

mM $MnCl_2$, 10 mM $CaCl_2$, or 10 mM $CoCl_2$ to the split protein fraction. Proteins were incubated in the presence of the metal ion for 3 hours. Protein samples were then loaded onto the Superdex 200 Increase column equilibrated in the corresponding buffer. Fractions containing the CnYpd1 protein were collected and analyzed by SDS-PAGE analysis.

2.2.9 Inductively coupled plasma atomic emission spectroscopy (ICP-MS) analysis

Inductively coupled plasma mass spectrometry (ICP-MS) analysis was performed on CnYpd1 to determine whether metal ions were bound to the native protein and, if so, the molar concentration. All purification buffers were passed through a column of Chelex® resin to remove trace metal ions. Chelex® treated water was used to rinse all glassware and centricon concentration units. Protein was concentrated to approximately 50 mg/mL and sent overnight on dry ice to Dr. Martina Ralle at the Elemental Analysis Core at Oregon Health and Science University where ICP-MS was performed. Protein samples were analyzed for magnesium, cobalt, calcium, copper, nickel and zinc ions. A second analysis was performed on a separate purification of CnYpd1, CnYpd1 ΔN50, and CnYpd1 ΔN70 with protein concentrations of approximately 1 mg/mL, metal ion concentration was only determined for calcium. To examine possible metal binding sites, CnYpd1 E58A, E48A-E54A and D60A-E67A mutants were also subjected to ICP-MS.

2.3 Results

2.3.1 CnYpd1 functions as a histidine phosphotransfer protein

CnYpd1 was purified to approximately 95% purity (**Figure 19**) and when necessary the affinity tag used during protein purification was cleaved using TEV protease.

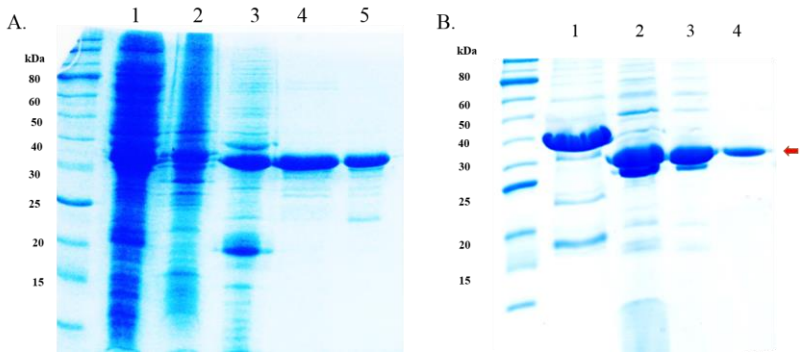


Figure 19. Purification summary for CnYpd1
15% coomassie stained SDS-PAGE gels showing the protein purification summary of CnYpd1 and TEV cleavage. CnYpd1 protein indicated by red arrow.

- **A.** Lane 1: Supernatant after cell lysis, Lane 2: Pellet after cell lysis, Lane 3: Elution from Ni-NTA column, Lane 4: Pooled fractions from HiTrap Q anion exchange chromatography, Lane 5: Pooled fractions from size exclusion chromatography.
- **B.** Lane 1: Pooled fractions from SEC prior to cleavage with TEV protease, Lane 2: Subsequent to overnight cleavage, Lane 3 and 4: Flow through from Ni-NTA column wash containing CnYpd1.

HPt proteins or domains range in size from approximately 150 to 300 amino acids, they often have low sequence homology except in the region surrounding the conserved phospho-accepting histidine, which is more highly conserved [41]. Currently, only one HPt protein has been identified in *C. neoformans*, CnYpd1 [19]. While CnYpd1 is expected to be homologous in structure and function to ScYpd1, amino acid sequence identity between the two proteins is only about 29%. An extension at the N-terminal region of CnYpd1 accounts for the difference in sizes between CnYpd1 and

ScYpd1 (209 and 167 amino acids, respectively) as shown in **Figure 20**. This extended N-terminal region shares no close sequence homology with any other protein domains, including other HPt proteins with extended N-terminal regions such as Mpr1 from *Schizzosaccharomyces pombe* and *Wallemia ichthyophaga*, or AHP2 from *Arabidopsis thaliana* (**Figure 20**).

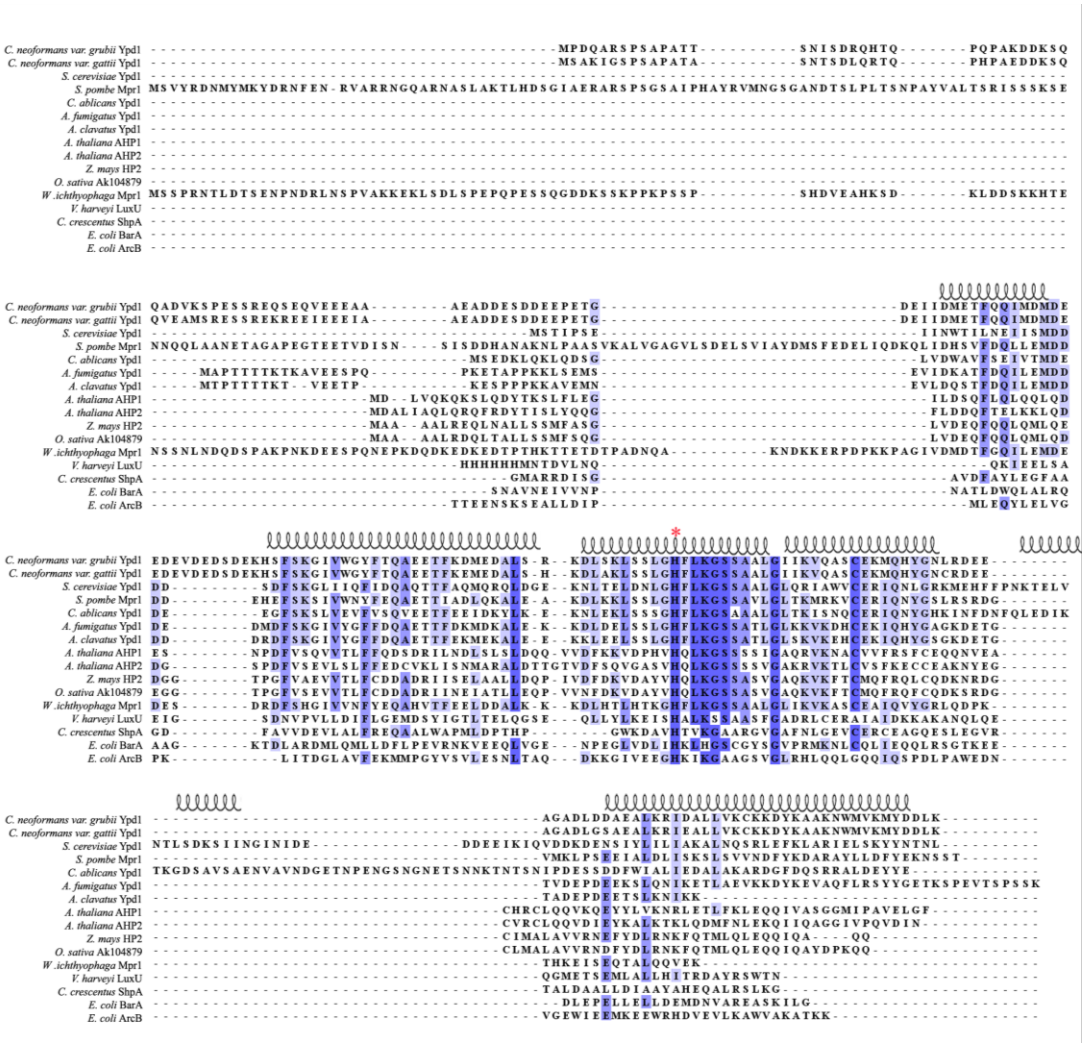


Figure 20. Representative sequence alignment of HPt proteins
Amino acid sequences of HPt proteins were aligned using ClustalX 2.1 and visualized using Jalview 2.8.2. Highly conserved residues are shaded dark blue, while less conserved residues are shaded in lighter blue. The phospho-accepting histidine residue is denoted by a red asterisk (*). Secondary structure of the known crystal structure of Ypd1 from *S. cerevisiae* (PDB ID: 1QSP) is diagrammed above the alignment.

Cloning of full-length genes and protein expression proved to be difficult, in our hands, for the two upstream HHK proteins in *C. neoformans,* CnTco1 and CnTco2, and the two downstream RR proteins, CnSsk1 and CnSkn7 that are known to interact with CnYpd1 [19]. These HHK and RR proteins are very large multi-domain proteins of greater than 1000 residues. When further attempts to isolate individual domains of each of these proteins were made, the protein products were found to be highly insoluble or have very low yields during expression in *E. coli*. Because of these difficulties, a heterologous system using purified HHK ScSln1 and RR ScSsk1 proteins from *S. cerevisiae* were used instead to characterize biochemical properties of CnYpd1 *in vitro*.

CnYpd1 is able to function *in vitro* as a HPt protein by accepting phosphoryl groups from the heterologous upstream donor ScSln1 from *S. cerevisiae* (ScSln1-HKR1), as well as transferring phosphoryl groups to a downstream RR protein ScSsk1 (ScSsk1-R2) (**Figure 21**). Radiolabeled phosphoryl groups from phospho~GST-ScSln1-HKR1 were shown to be almost completely transferred to CnYpd1 within 1 minute of incubation. Based on a sequence alignment of HPt proteins, residue H138 was predicted to be the site of phosphorylation. When H138 was mutated to a glutamine (H138Q), the ability of CnYpd1 to accept phosphoryl groups was completely abolished, confirming that H138 is the site of phosphorylation.

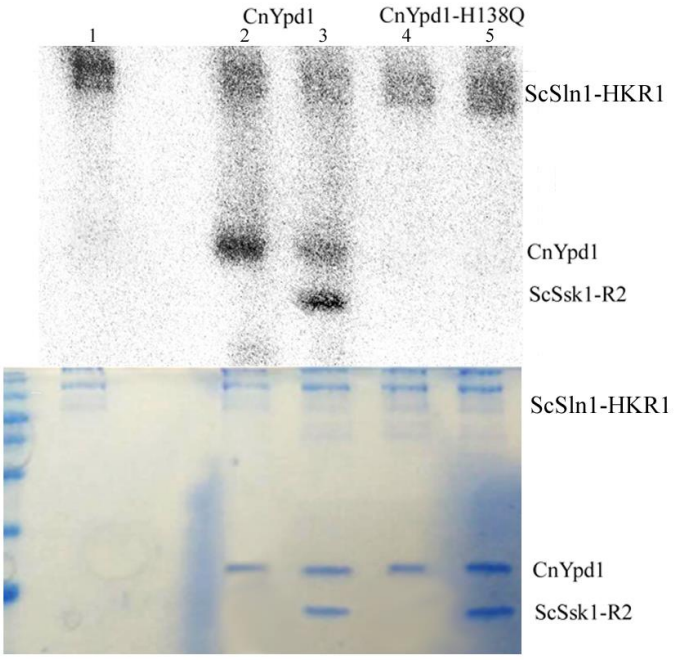


Figure 21. Phosphorylation of CnYpd1 from a heterologous phosphodonor
The HK and RR domains from a heterologous donor, Sln1 from *S. cerevisiae* (Sln1-HKR1), were used to phosphorylate CnYpd1. ScSln1-HKR1 was autophosphorylated using 0.1 μM γ-^{32}P-labeled ATP (lane 1). ScSln1-HKR1 was incubated with CnYpd1 alone (Lane 2) or with ScSsk1-R2 (lane 3), CnYpd1-H138Q alone (lane 4) or with ScSsk1-R2 (lane 5).

2.3.2 CnYpd1 interactions with downstream RR proteins

C. neoformans encodes two RR proteins which interact with CnYpd1, CnSsk1 and CnSkn7. These proteins are very large multi-domain proteins, both are composed of over 1000 amino acids. Initial attempts at cloning full length genes from cDNA were unsuccessful, possibly because of low DNA concentration or sheering of mRNA during isolation, the focus was predominantly on isolating receiver domains which interact with CnYpd1. Extensive attempts by Dr. Katie Branscum to expression and purify CnSsk1 failed to result in protein that was available for assay. Information on constructs and protein expression/purification can be found in her dissertation [42].

Attempts by myself to alter expression and buffer conditions also did not improve protein yield/activity. Full length protein may be necessary for complete solubility and function.

Initial cloning and expression of the receiver domains of CnSkn7 (CnSkn7-R3) were performed by Brittany Kitchens, Jamie Sykes performed initial expression and protein purification experiments. Yield was very low due to both low expression and poor solubility. I attempted to improve expression and solubility by altering expression strains and conditions as well as buffer conditions for purification. Expression at low temperatures in *E. coli* DH5α cells (generally only used for cloning) appeared to slightly improve expression as did use of high concentrations of NaCl during lysis. A large percentage of the protein was still found to be insoluble and yield was very low (**Figure 22**).

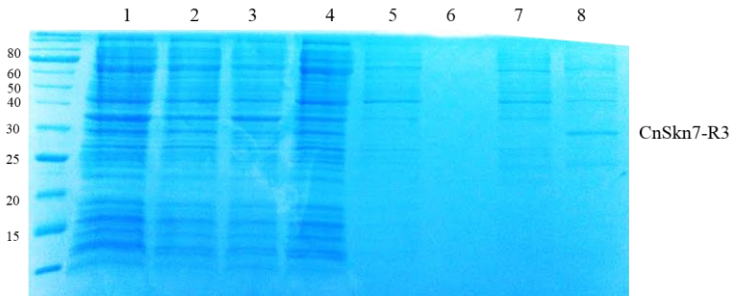


Figure 22. Expression and purification of CnSkn7-R3
15% coomassie stained SDS-PAGE gel showing the protein purification of CnSkn7-R3. Lane 1: Whole cell prior to lysis, Lane 2: Supernatant after cell lysis, Lane 3: Pellet after cell lysis, Lane 4: Wash with 10 mM imidazole, Lane 5: Wash with 50 mM imidazole Lane 6: Wash with 100 mM imidazole, Lane 7: Elution with 250 mM imidazole, Lane 8: Elution with 400 mM imidazole.

A pull down experiment was performed to test if CnYpd1 and CnSkn7-R3 are able to interact *in vitro*. Both CnSkn7-R3 and CnYpd1 are purified using affinity chromatography with 6X-HIS tags. The affinity tag for CnYpd1was removed using

TEV protease. Results indicate that CnYpd1 and CnSkn7-R3 can form a stable interaction (**Figure 23A**). Some CnYpd1 was present in the wash, indicating that not all CnYpd1 bound to CnSkn7-R3. Preliminary results also show that CnYpd1 is also able to pass a phosphoryl group to CnSkn7-R3. The transfer from CnYpd1 to CnSkn7 was observed to be very weak, however, and appeared to take a relatively long amount of for the transfer to occur (**Figure 23B**). It is possible that an alternate construct of CnSkn7 may yield better results.

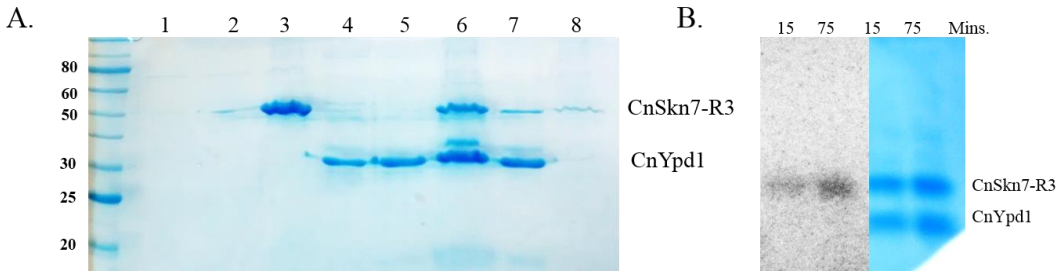


Figure 23. Pull down assay and phosphotransfer between CnYpd1 and CnSkn7-R3

A. CnSkn7-R3 was bound to a 5 mL Ni-NTA column. Unbound protein was washed from the column. CnYpd1 was passed over the column and unbound CnYpd1 was removed by washing with wash buffer (150 mM Tris pH 8.0, 150 mM NaCl). The proteins were then eluted from the column with wash buffer containing 300 mM imidazole. Samples were taken at each step and separated on a 15% SDS-PAGE gel. Lane 1: CnSkn7-R3 flow through, Lane 2. CnSkn7-R3 wash, Lane 3: Resin containing CnSkn7-R3, Lane 4: CnYpd1 flow through, Lane 5: CnYpd1 wash, Lane 6: Resin containing both CnYpd1 and CnSkn7-R3, Lane 7: Elution, Lane 8: Resin after elution.

B. Phosphotransfer from Phospho~CnYpd1 to Skn7. Aliquots were taken at 15 and 75 minutes and separated on a 12% SDS-PAGE gel.

2.3.3 N-terminal region of CnYpd1 important for structural integrity

A series of N-terminal deletion mutants were created and analyzed with respect to protein folding/stability, phosphotransfer activity, phospho-stability and ability to bind metal ions. N-terminal deletion mutants were created using secondary structure predictions from PSIPRED [43] (**Figure 24**).

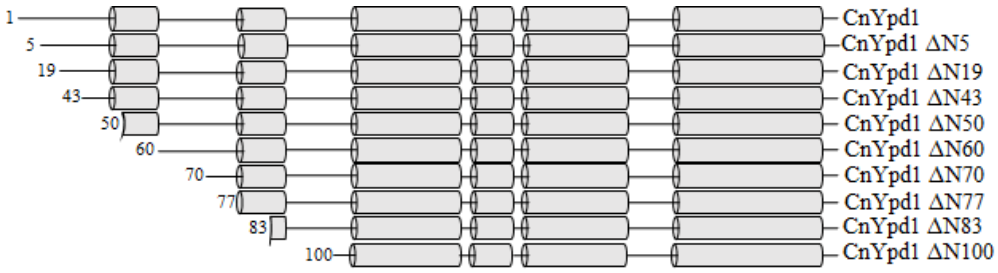


Figure 24. CnYpd1 N-terminal deletion mutants
Secondary structure predictions were performed using PSIPRED. Deletion mutants were created based on position of helices and region predicted to be an HPt domain.

Whole-cell, supernatant, and pellet samples after lysis were analyzed for each N-terminal deletion mutant (**Figure 25**).

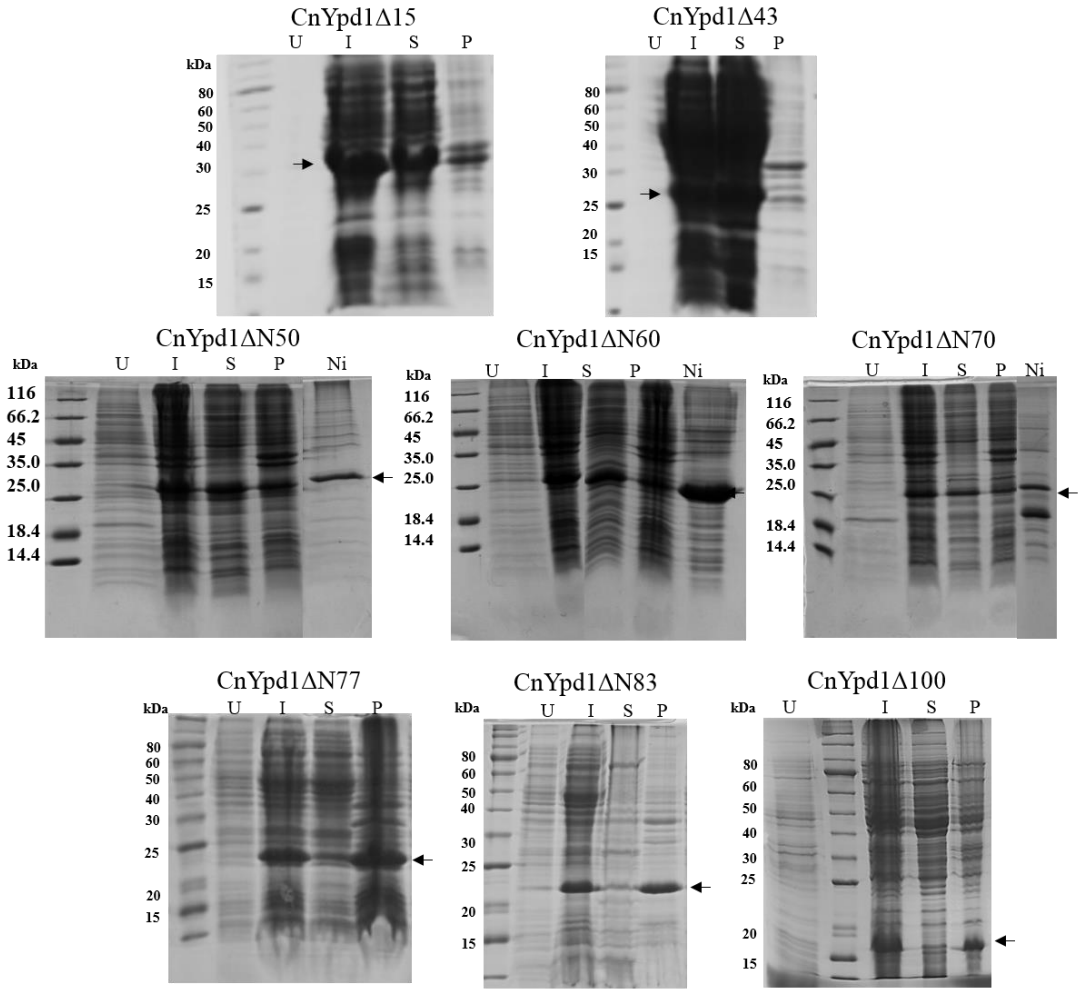


Figure 25. Solubility studies of CnYpd1 deletion constructs

Comparison of amount of protein for each CnYpd1 deletion construct found soluble in supernatant and/or insoluble in pellet after cell lysis.

Full length CnYpd1, CnYpd1 ΔN5, ΔN19, and ΔN43 were found to be completely soluble with approximately 100% of the protein found in the supernatant.

CnYpd1 ΔN50, ΔN60, and ΔN70 were all found to be approximately 50% soluble. CnYpd1 ΔN77, ΔN83, and ΔN100 were found to be completely insoluble **(Table 6)**.

All soluble N-terminal deletion mutants were able to accept phosphoryl groups to the same extent as wild-type CnYpd1 (**Figure 26**).

Table 6. Approximate percentage of CnYpd1 ΔN protein found in supernatant and pellet after lysis

Protein construct	% Soluble Protein	% Insoluble Protein
CnYpd1	100	0
CnYpd1 Δ5	100	0
CnYpd1 Δ19	100	0
CnYpd1 Δ43	100	0
CnYpd1 Δ50	50	50
CnYpd1 Δ60	60	40
CnYpd1 Δ70	50	50
CnYpd1 Δ77	10	90
CnYpd1 Δ84	0	100
CnYpd1 Δ100	0	100

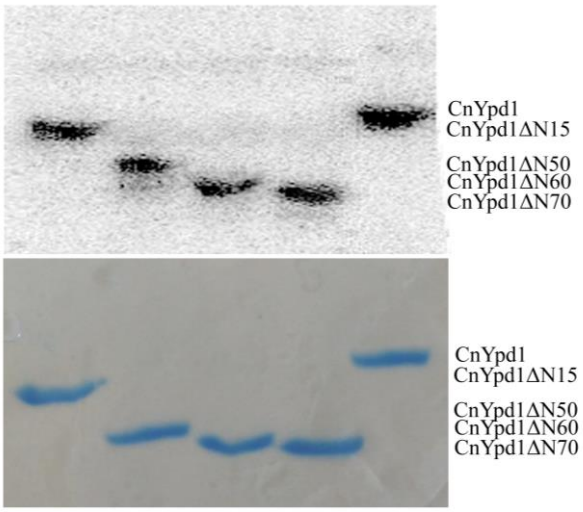


Figure 26. Phosphorylation of CnYpd1 ΔN constructs
CnYpd1, CnYpd1 ΔN15, ΔN50, ΔN60, and ΔN70 were incubated with phospho~GST-ScSln1-HKR1. GST-ScSln1-HKR1 was removed from the reaction after a 5 minute incubation. Aliquots were removed of only CnYpd1 construct and mixed with stop buffer to quench the reaction.

These results indicate that while the first 40 residues are dispensable for protein folding/solubility, subsequent removal of residues causes the protein to become increasingly insoluble. Secondary structure predictions using PSIPRED [43] indicates

that residues 75-85 may form an α-helix that would correspond to the αA helix found in other HPt proteins (**Figure 24**). Our solubility studies indicate that this helix may be important for protein stabilization and solubility. Structural information available for *S. cerevisiae* Ypd1 (PDB ID: 1QSP) and *A. thaliana* AHP2 (PDB ID: 4PAC) show that this helix has amphipathic character and forms a "cap" covering a larger hydrophobic patch composed of the core helices of the four α-helix bundle, suggesting that it is important for structural stabilization and proper alignment of these helices as well as protection from solvent.

2.3.4 CnYpd1 functions a monomer in solution

To determine the oligomeric state of CnYpd1, size exclusion chromatography was performed on a calibrated Superdex 200 (S200) column in the Protein Production Core at the University of Oklahoma. The predicted molecular weight of CnYpd1 is expected to be approximately 28 kDa, however, the protein eluted from a calibrated S200 size exclusion column at the same elution volume as a globular protein with a molecular weight of approximate 70 kDa (**Figure 27**). There is no indication of a lower molecular weight peak eluting from the column, indicating that the protein is in a single form.

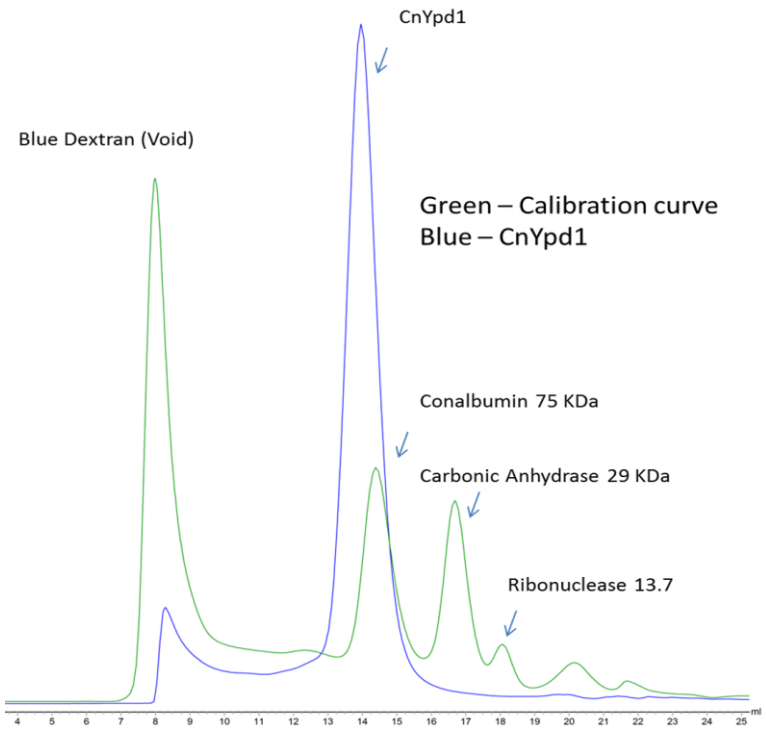


Figure 27. CnYpd1 apparent molecular weight on a calibrate S00 column
CnYpd1 elutes on a calibrated S200 column as a protein with an apparent molecular weight of approximately 75 kDa.

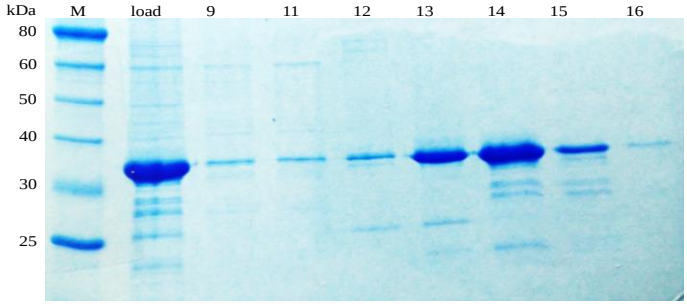


Figure 28. SDS-PAGE gel of CnYpd1 protein
Aliquots obtained from fractions collected from SEC performed on CnYpd1 protein to determine oligomeric state.

This apparent molecular weight may be a result of CnYpd1 being a dimer or non-globular in shape as the result of the addition N-terminal amino acid sequence. The crystal structure of the Ypd1 protein from *S. cerevisiae* (ScYpd1) shows a monomeric

protein that is oblong in shape rather than globular (PDB ID: 1QSP). SEC was performed on a protein sample containing both ScYpd1 and CnYpd1 in a 20 mM Tris pH 8.0, 150 mM NaCl buffer (**Figure 29**).

ScYpd1 has a calculated molecular weight of ~20 kDa and elutes from the S200 Increase column with an apparent molecular of ~30kDa, showing a protein of 1.5 times the predicted molecular weight. CnYpd1 with a calculated molecular weight of ~28 kDa eluted from the column with an apparent molecular weight of ~63 kDa, 2.2 times the predicted molecular weight (**Table 7**).

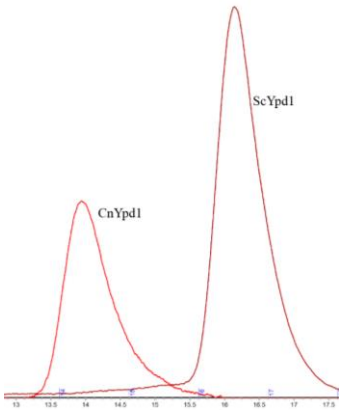


Figure 29. Elution profile of ScYpd1 with CnYpd1 on a S200 column
SEC was performed on a combined sample of ScYpd1 and CnYpd1 in a 20 mM Tris pH 8.0, 50 mM NaCl buffer.

Table 7. Predicted and apparent molecular weights of ScYpd1 and CnYpd1

Protein	Elution Volume	Predicted Molecular Weight (kDa)	Apparent Molecular Weight (kDa)	Ratio (Apparent: Predicted)
ScYpd1	16.2	19.7	30.0	1.5
CnYpd1	14.1	27.6	62.9	2.3

ScYpd1 does not behave in an "ideal" manner on the SEC column, most likely due to its oblong shape. This results in an apparent Stokes radius that is larger than is predicted for the monomeric protein. Results of a ratio of apparent molecular weight to predicted molecular weight using SEC alone would not indicate monomeric or dimeric state of ScYpd1. Consequently, a ratio of an apparently vs. predicted molecular weight

of 2.3 for CnYpd1 appears to indicate that CnYpd1 is a dimer in solution, but is not completely rule out an irregularly shaped oblong protein.

If CnYpd1 behaves as a dimer, the most likely dimerization interface location should be in the N-terminal region. It is crucial for the phospho-accepting histidine residue to remain solvent exposed, so it is unlikely that the C-terminal HPt domain would be a dimerization interface. Full length CnYpd1, N-terminal deletion mutants of CnYpd1 and ScYpd1 were all subjected to SEC on a S200 increase column equilibrated in a 50 mM Tris pH 7.0, 150 mM NaCl buffer (**Table 8**).

Table 8. Predicted and apparent molecular weights of ScYpd1, full length CnYpd1 and CnYpd1 ΔN constructs

Protein	Elution volume	Predicted Molecular Weight (kDa)	Apparent Molecular Weight (kDa)	Apparent:Predicted Molecular Weight Ratio
ScYpd1	16.2	19.8	30	1.5
CnYpd1 FL	14.1	27.6	74	2.7
CnYpd1 ΔN50	15.5	22.2	42	1.9
CnYpd1 ΔN60	16.1	21.2	31	1.5
CnYpd1 ΔN70	16.2	20.0	30	1.5

Complete remove of the N-terminal region (CnYpd1 ΔN70) results in a protein that appears to elute from the SEC S200 column in a similar manner to ScYpd1, a known monomer. Conversely, full length CnYpd1 has an apparent to predicted molecular weight ratio of 2.7. These results may indicate that CnYpd1 functions as a dimer in solution taking into account the oblong shape and addition N-terminal region which may form a small domain which acts as a dimerization domain.

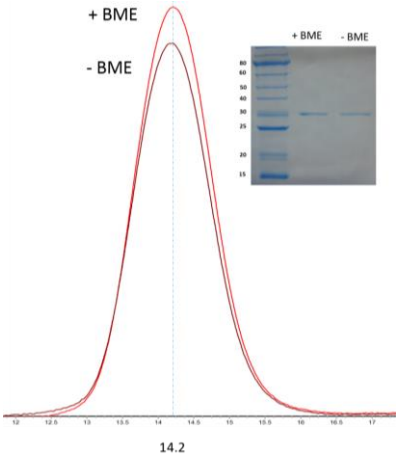


Figure 30. SEC elution profile of CnYpd1 in presence and absence of reducing agent
SEC was performed on CnYpd1 protein samples in the absence or addition of 1 mM BME. Protein was incubated with BME for 1 hour before SEC was performed.

CnYpd1 contains 2 cysteine residues, C96 and C130. In order to eliminate the possible that these residues were involved in potential dimerization SEC was performed on protein samples in the presence and absence of reducing agent (1 mM β-mercaptoethanol (BME)). Results show no change in elution profile with the addition of reducing agent, indicating that cysteine residues are not involved with potential dimerization (**Figure 30**).

If CnYpd1 ΔN70 and ScYpd1 behave in a similar manner during SEC the N-terminal region must be responsible for causing either dimerization or a drastic shape change from ScYpd1. If CnYpd1 is a dimer in solution, there should be a way to break apart dimer into monomers. It is also possible that, depending on how much of the potential dimerization region is removed, heterodimers may form between different

CnYpd1 protein constructs. Native gel assays were performed using CnYpd1, CnYpd1 ΔN50 and CnYpd1 ΔN 70.

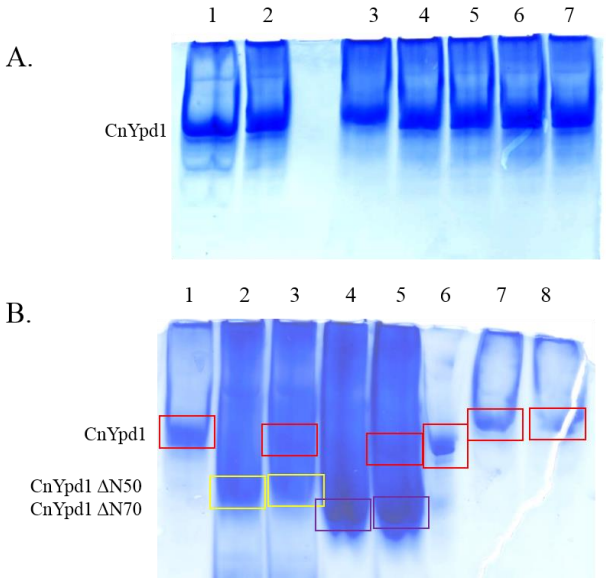


Figure 31. Native gel analysis of CnYpd1 constructs
Pure CnYpd1, CnYpd1 ΔN50 and CnYpd1 ΔN 70 were subjected to native gel analysis. Protein was in buffer containing 50 mM Tris pH 8.0 and 150 mM NaCl, Each addition component was added to protein sample and incubated for 15 minutes before being separated on a 15% Native gel.

- **A.** Lane 1: CnYpd1, Lane 2: 5% Trixton-X, Lane 3: 250 mM NaCl, Lane 4: 500 mM NaCl, Lane 5: 750 mM NaCl, Lane 6: 1 M NaCl, Lane 7:2 M NaCl
- **B.** Red boxes indicate CnYpd1, yellow boxes indicate CnYpd1 ΔN50, and purple boxes indicate CnYpd1 ΔN70. Lane1: CnYpd1, Lane 2: CnYpd1 ΔN50, Lane 3: CnYpd1 + CnYpd1 ΔN50, Lane 4: CnYpd1 ΔN70, Lane 5: CnYpd1 + CnYpd1 ΔN70, Lane 6: 2 mM EDTA, Lane 7: 2 M Sodium Thiocynate, Lane 8: CnYpd1 2 M Potasium Thiocynate

Results from the native gel analysis indicate no evidence of a "monomer" present in in the presence of an increasing concentration of NaCl , high concentrations of different chaotropic salts such as sodium or potassium thiocyanate, high percentages of detergent, or high concentrations of EDTA (**Figure 31**). There was also no evidence of hetero-dimer formation between full length CnYpd1 and either CnYpd1 ΔN50 or CnYpd1 ΔN70. From SEC experiments there is no evidence of second peak at lower MW during chromatography.

Size exclusion chromatography with multi-angle light scattering analysis was performed on CnYpd1 protein fractions collected from anion exchange. The theoretical molecular weight for CnYpd1 was calculated to be ~27.6 kDa. The experimentally determined molecular weight obtained from SEC-MALS calculates was determined to be 27.1 ± 1.99 kDa. These results indicate that CnYpd1 functions in solution as a monomer. Experiment was performed in triplicate.

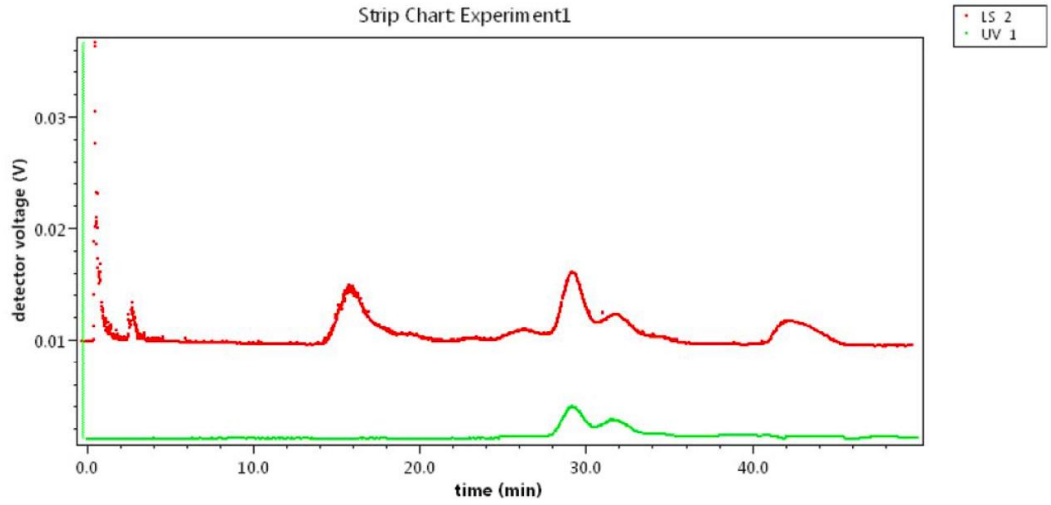


Figure 32. SEC-MALS of CnYpd1
SEC-MALS was performed on CnYpd1 in a 20 mM Tris pH 8.0, 150 mM NaCl buffer. Red indicates light scattering signal and green indicates UV signal.

Taken together there is more evidence to support CnYpd1 functioning as a monomer in solution than a dimer, contrary to SEC results predicted molecular weight results. This observation is most likely due to the irregular shape of the protein Additional experiments such as analytical ultracentrifugation would need to be performed in order to determine with certainty the oligomeric state of CnYpd1.

2.3.5 CnYpd1 exhibits an extended phosphorylated lifetime in comparison to other HPt proteins

To investigate the stability of the phosphoryl group on CnYpd1, phospho-stability experiments were performed, again using ScSln1-HKR1 as a phosphoryl donor. CnYpd1 was phosphorylated in the presence of ScSln1-HKR1 for 5 minutes, ScSln1-HKR1 was removed from solution and aliquots were taken over time of CnYpd1 (**Figure 33**). Significant protein degradation was observed after 42 hours. In comparison to ScYpd1, which has a phosphorylated half-life of approximately 4 hours [39], CnYpd1 exhibited a significantly extended phosphorylated life-time.

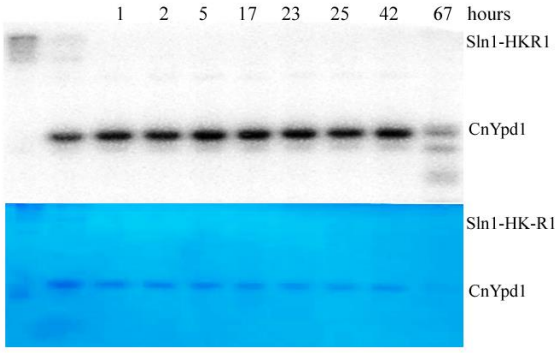


Figure 33. Extended phosphorylated life-time of CnYpd1
The histidine kinase and receiver domains from the heterologous donor ScSln1 (ScSln1-HKR1) were used as a phospho-donor for CnYpd1. Phosphorylated ScSln1-HKR1 was removed from the reaction and aliquots of CnYpd1 were taken at specified time points. Three replicates were performed.

Experiments were performed on both protein with the affinity tag present, and with the affinity tag removed to ensure that the extended phospho-stability observed was not a result of the presence of the affinity tag. A comparable phospho-stability was observed, indicating that the affinity tag was not responsible for the extended phospho-stability (**Figure 34**).

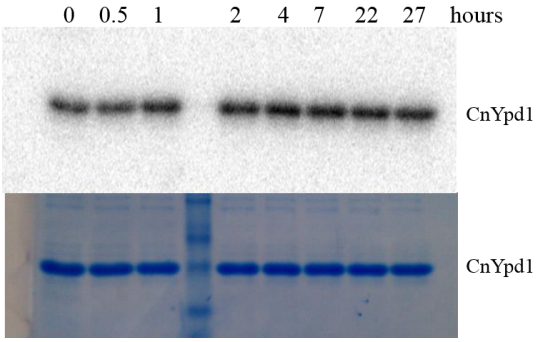


Figure 34. Phosphoryl stability of CnYpd1 after affinity tag removal
Affinity tag was removed from pure CnYpd1 protein with TEV protease. Bead bound GST-ScSln1-HKR1 was used as a phospho-donor to phosphorylate CnYpd1. GST-ScSln1-HKR1 was removed from the reaction once transfer from GST-ScSln1-HKR1 to CnYpd1 was complete and aliquots of CnYpd1 were taken at specific time points and quenched with stop buffer. 0 hour time point was removed at approximately 1 min.

2.3.6 N-terminal region stabilizes phosphoryl group on CnYpd1

According to sequence alignments of CnYpd1 with ScYpd1 and other Ypd1 homologs (**Figure 20**), CnYpd1 contains an extended N-terminal. Because ScYpd1 lacks the extended N-terminal region present in CnYpd1, it was hypothesized that it is this region which is responsible for the stabilization of the phosphoryl group on CnYpd1. CnYpd1 ΔN70 was chosen to repeat phospho-stability experiments. CnYpd1 ΔN70 is most similar to ScYpd1 in that it is predominantly composed of only an HPt domain and subsequent deletion mutants (ΔN77, ΔN83, and ΔN100) were found to be insoluble (**Table 6**). Phospho~GST-ScSln1-HKR1 was used as a donor to phosphorylate CnYpd1 ΔN70 and removed from the reaction by gentle centrifugation, leaving only CnYpd1 ΔN70 present in the reaction. Aliquots were removed at specific time points. The phosphorylated half-life of CnYpd1 ΔN70 was determined to be 3.4 ± 0.63 hours (N=4) (**Figure 35**). This half-life is significantly different than that of full

length protein, for which a half-life was not able to be determined. These data suggests a role for N-terminal region of CnYpd1 in stabilizing the phosphoryl group.

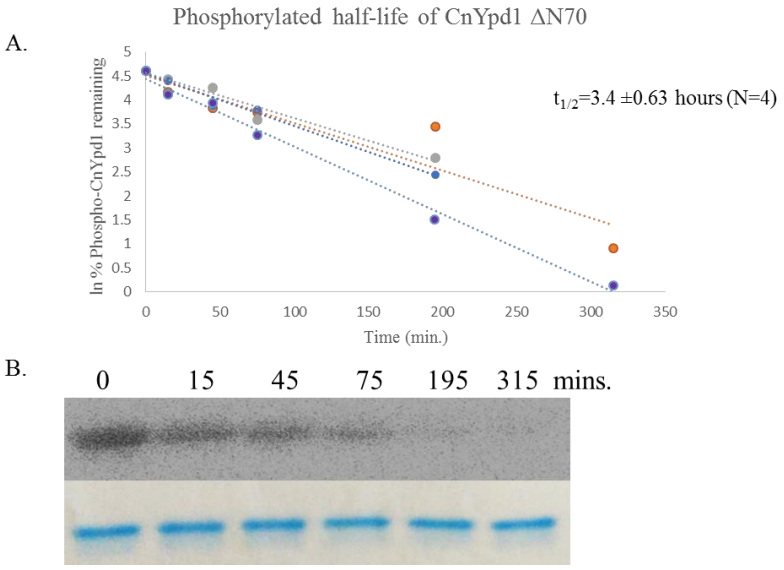


Figure 35. CnYpd1 ΔN70 dephosphorylation
CnYpd1 ΔN70 was incubated with phospho~GST-ScSln1-HKR1. GST-ScSln1-HKR1 was removed from the reaction. Aliquots were removed and mixed with stop buffer to quench the reaction. **(A)** All data points for phosphorylated half-life experiments for CnYpd1 ΔN70. **(B)** Representative phosphorimage that shows dephosphorylation of CnYpd1 ΔN70 over time. A phosphorylated half-life of 3.4 ± 0.63 hours (N=4) was calculated.

2.3.7 CnYpd1 binds calcium ions in a 2:1 molar ratio

An observation was made while performing size exclusion during protein purification that the addition of EDTA resulted in a slight but reproducible shift in the elution volume of CnYpd1 on a calibrated S200 column. A shift from an elution volume of 14.7 in the absence of EDTA to 14.93 in the presence of EDTA was observed (**Figure 36**).

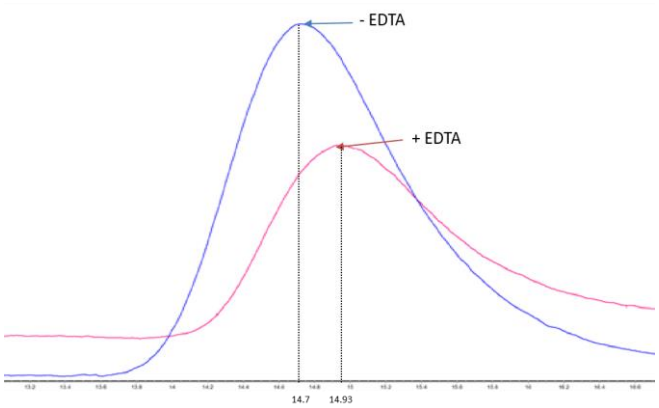


Figure 36. CnYpd1 shows a shift in elution volume in the presence and absence of EDTA
Chromatograms obtained from Superdex 200 column using AKTÄ Pure M1 system when CnYpd1 was applied to the S200 column in the presence and absence of EDTA.

In order to test whether the elution volume shift was simply a result of column variability or due to the presence or absence of EDTA, an experiment involving the re-introduction of metal ions to the protein sample was performed. In order to test whether this shift in elution volume was simply a result of column variability or due to the presence or absence of metal ions, an experiment involving the re-introduction of metal ions to the protein sample was performed. CnYpd1 protein was treated with 1 mM EDTA for 3 hours. EDTA was removed by buffer exchange into buffer lacking EDTA. Metal ions were reintroduced to the protein by incubation with each metal ion for 3

hours. SEC was then performed on each sample (**Figure 37**).

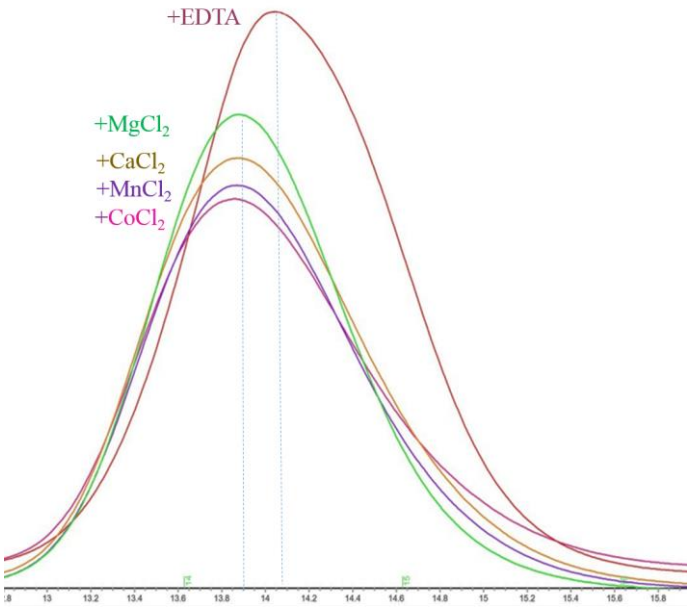


Figure 37. Re-introduction of metal ions to CnYpd1 causes a change in the elution volume during SEC
Chromatograms obtained from Superdex 200 column using AKTÄ Pure M1 system. Protein sample was tested at pH 5 (a) and pH 8 (b) in the presence of EDTA. Fractions were pooled and split into 4 equal parts. Metal ions were re-introduced into protein and incubated for ~3 hours. Fractions were re-tested on the column in the presence of each metal ion separately.

Re-introduction of metal ions after treatment of the protein samples with 1 mM EDTA resulted in a small shift in the elution volume of the protein from 14.1 to 13.8 at pH 8. Several divalent metal ions were chosen (calcium, cobalt, manganese, and magnesium) based on literature searches. Magnesium is often required for proper phosphotransfer to occur in His-to-Asp systems, and other metal ions such as calcium have been previously shown to inhibit phosphotransfer [44]. There was no observable change in the elution volume of CnYpd1 based on which metal ion was present (**Figure**

37), indicating that any divalent metal ion present may be a possible substitution for the naturally occurring metal ion.

ICP-MS experiments were performed on CnYpd1, CnYpd1 ΔN50 and CnYpd1 ΔN70 to determine the type of metal present and molar ratio. Metal ion concentrations were determined for calcium, cobalt, copper, magnesium, nickel and zinc for wild-type CnYpd1. All metal ions with the exception of calcium in the full length protein were found in insignificant concentrations (**Table 9**). Subsequent ICP-MS experiments only determined the concentration of calcium present.

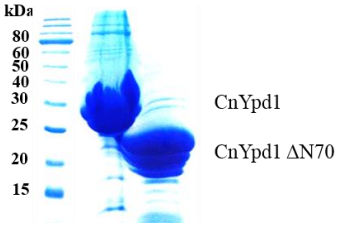


Figure 38. CnYpd1 and CnYpd1 ΔN70 protein samples for ICP-MS
Coomassie stained protein samples sent to OHSU for ICP-MS studies.

Table 9. Micromolar concentrations of metal ions determined by ICP-MS

Protein	Protein [uM]	Ca [uM]	Mg [uM]	Co [uM]	Ni [uM]	Cu [uM]	Zn [uM]
CnYpd1 FL	1812.51	3968.00	1.38	0.04	0.84	0.53	3.56
CnYpd1 FL	1812.51	3230.00	1.77	0.03	0.87	0.63	4.31
CnYpd1 ΔN70	2242.71	12.64	1.04	0.03	5.39	1.49	31.92
Buffer	---	7.01	0.70	0.00	0.01	0.04	0.23
Protein	**Protein [uM]**	**Ca [uM]**	---	---	---	---	---
CnYpd1 FL	36.25	83.83	---	---	---	---	---
CnYpd1 ΔN70	49.84	21.35	---	---	---	---	---
CnYpd1 Δ50	44.94	3.76	---	---	---	---	---
Buffer	---	7.26	---	---	---	---	---
Protein	**Protein [uM]**	**Ca [uM]**	---	---	---	---	---
E58A	18.13	18.13	---	---	---	---	---
D60A-E67A	29.0	14.50	---	---	---	---	---
E48A-E54A	1.81	3.63	---	---	---	---	---
Buffer	---	3.99	---	---	---	---	---

Molar ratios of each metal ion per protein molecule were calculated **(Table 10)**. The ratio of calcium ions per CnYpd1 full-length protein was determined to be 2:1, whereas calcium was far below stoichiometric amounts for the CnYpd1 ΔN70 and ΔN50 mutants (essentially a 0:1 ratio). This suggests that the first 70 residues of CnYpd1 of the extended N-terminal region are responsible for metal ion binding.

Table 10. Calculated molar ratio of metal ions per protein based on ICP-MS

Protein	Ca^{2+}
CnYpd1 ΔN70	**0.0**
CnYpd1 FL	**2.19**
CnYpd1 FL	**1.78**
Protein	
CnYpd1 FL	**2.11**
CnYpd1 ΔN70	**0.28**
CnYpd1 ΔN50	**0.08**
Protein	
CnYpd1 E58A	**0.92**
CnYpd1 D60A-E67A	**0.23**
CnYpd1 E48A-E54A	**2.05**

A comprehensive sequence alignment was performed on all stand-alone HPt proteins found in the NCBI data base. Of the 2000 sequences found for stand-alone HPt proteins, approximately 80 were found to contain an extended N-terminal extension. These proteins were realigned using only the non-HPt containing region using ClustalX2. Two regions of higher sequence homology were observed (**Figure 39**) [45] corresponding to highly acidic segments of the N-terminal region of CnYpd1, residues from approximately E48 to E67 . BLAST results obtained using this region of CnYpd1 indicated that it was also homologous to proteins known to bind both calcium and zinc metal ions.

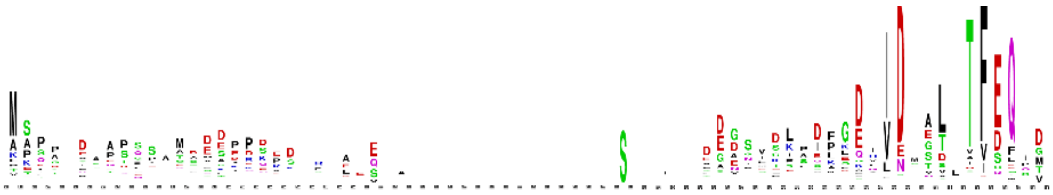


Figure 39. Highly homologous region of N-terminal sequence alignment.
Frequency of residues found in highly homologous region of HPt proteins with N-terminal extensions. Height of residue indicates higher frequency.

Three mutant CnYpd1 constructs were created, E58A, E48A-E54A, and D60A-E67A, and subjected to ICP-MS analysis. Previous results indicated that wild-type CnYpd1 is able to bind calcium ions in a 2:1 molar ratio. CnYpd1 E58A showed the presence of only one calcium ion per protein molecule, while the E48A-E54A mutant showed two calcium ions bound per protein molecule and the D60A-E67A mutant showed no calcium present (**Table 10**). These results suggest that residue E58 and the region between D60 to E67 of the N-terminal domain are responsible for calcium ion binding.

2.3.8 Calcium is not required for phosphorylation of CnYpd1

To determine if the bound calcium ions are required for phosphorylation of CnYpd1, metal ions were removed from the protein by addition of EDTA for 30 minutes. EDTA was removed from the protein sample using a HiTrap Desalting column on an AKTA prime chromatography system. Untreated CnYpd1 was used as a control. Samples were subjected to a phosphotransfer assay. The phosphotransfer reaction was performed in the presence of both calcium (**Figure 40A**) and magnesium (**Figure 40B**) . Untreated CnYpd1 was used as a control. Samples was subjected to a phosphotrasnfer assay The phosphotransfer reaction was done in the presence of both calcium (**Figure**

40A) and magnesium (**Figure 40B**).

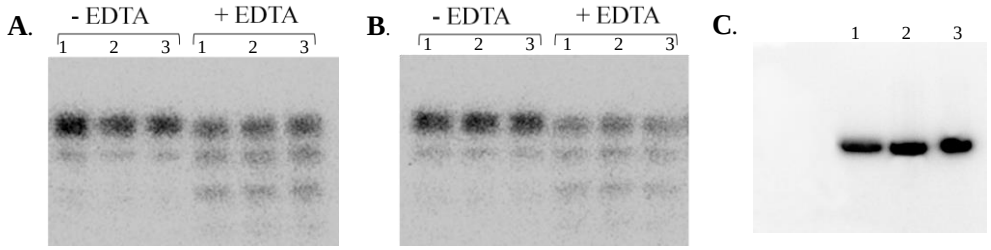


Figure 40. Phosphorylation of CnYpd1, CnYpd1 E58A and CnYpd1 D60A-E67A

Phospho~ScSln1-HKR1 was used as a donor to CnYpd1 constructs and removed from the reaction after 2 minutes. **(A)** Autophosphorylation of bead-bound ScSln1-HKR1 was performed in the presence of 10 mM $MgCl_2$. Bead-bound ScSln1-HKR1 was split into two fractions and each was washed by gentle pelleting of resin and addition of reaction buffer with either 10 mM $MgCl_2$ or $CaCl_2$. CnYpd1 was added to each ScSln1-HKR1 in the presence of $CaCl_2$ **(A)** or $MgCl_2$ **(B)** containing tube, ScSln1-HKR1 was removed from the reaction after 1 minute and aliquots were taken of only CnYpd1 at 1, 5, and 15 minutes (lane designations indicate time points). **(C)** CnYpd1 E58A and CnYpd1 D60A-E67A were phosphorylated using ScSln1-HKR1. ScSln1-HKR1 was removed from the reaction after 1 minute and aliquots were taken Lane 1: WT CnYpd1, Lane 2: CnYpd1 E58A, lane 3: CnYpd1 D60A- E67A.

Only slight differences were observed for phosphorylation of CnYpd1 in the presence of calcium versus magnesium, indicating that calcium is not required for phosphotransfer. Furthermore, it was noted that degradation of the protein occurred for the EDTA-containing protein samples suggesting that calcium may be required for structural integrity. CnYpd1 E58A and CnYpd1 D60A-E67A were also subjected to phosphotransfer assay. Neither the E58A mutant nor the D60A-E67A double mutant showed any difference in the ability to accept a phosphoryl group from ScSln1-HKR1 (**Figure 40C**). These results indicate that the calcium bound to CnYpd1 is not required for phosphorylation of CnYpd1, and likely serves other functions such as stabilizing the structure of the N-terminal region.

2.3.9 Crystallization attempts for CnYpd1

Extensive crystallography attempts were made using several CnYpd1 constructs. Attempts included variations in initial protein conditions, such as protein concentration, buffer components (salts, pH) and protein constructs. Most results from broad screens yielded spherulite-like crystals that could not be further optimized (see **Appendix B: Crystallography attempts for CnYpd1**). DLS was performed on CnYpd1 protein sample prepared in PBS. Results from DLS indicated that the most suitable buffer for mono-dispersity was 50 mM Tris pH 8.0 and 200 mM NaCl (**Figure 41**).

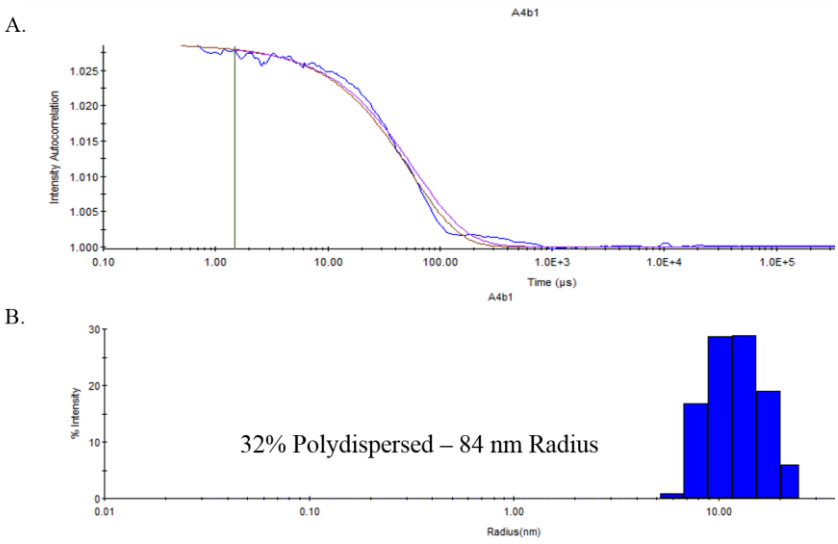


Figure 41. Analysis of oligomeric distribution of CnYpd1 by DLS
0.7 mg/mL CnYpd1 was prepared in PBS buffer. Protein was diluted in 50 mM Tris pH 8.0, 200 mM NaCl buffer.

Further DLS studies were completed in protein prepared in this 50 mM Tris pH 8.0 and 200 mM NaCl buffer using additive screens (**Figure 42** and **Figure 43)**.

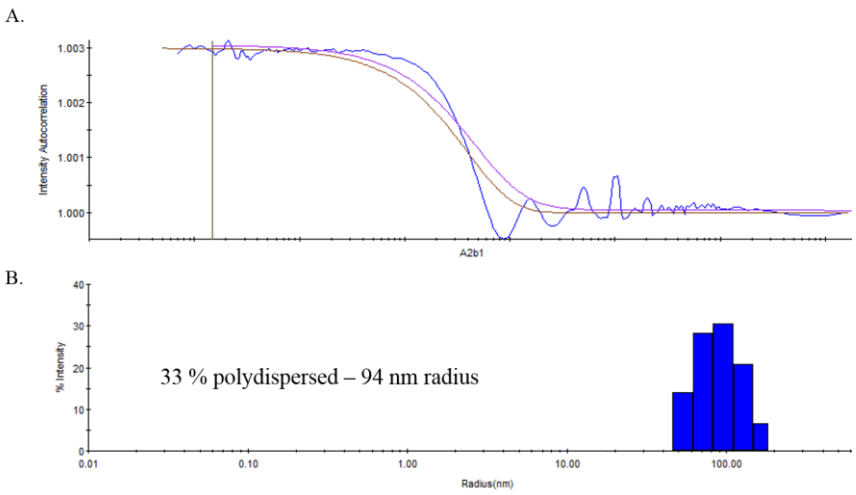


Figure 42. Analysis of oligomeric distribution of CnYpd1 by DLS
1.5 mg/mL CnYpd1 was prepared in 50 mM Tris pH 8.0 and 200 mM NaCl. A final concentration of 0.06% Tween 20 was added to the protein.

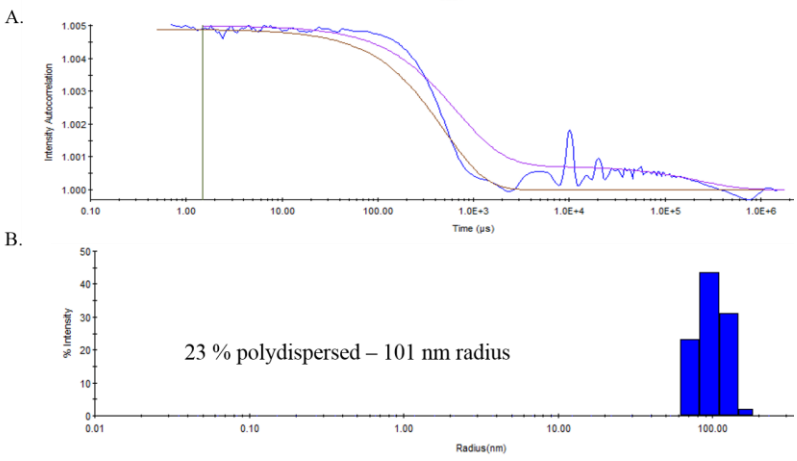


Figure 43. Analysis of oligomeric distribution of CnYpd1 by DLS
1.5 mg/mL CnYpd1 was prepared in 50 mM Tris pH 8.0 and 200 mM NaCl. A final concentration of 20 mM n-Octyl-β-D-glucoside (OG) was added to the protein.

Crystallography attempts were repeated based on the best results found from DLS experiments. These attempts also yielded spherulite-like crystals. Other attempts using additive screens produced long fiber like crystals that did not diffract well for data collection.

2.3.10 Discussion

Very few HPt proteins with N-terminal domains are found in nature. A phylogenetic tree of organisms which encode stand-alone HPt proteins with extended N-terminal domains was created using phyloT and visualized using iTOL [46] (**Figure 44**). Analysis of the phylogenetic tree revealed that the vast majority of organisms which contain these proteins have either been shown to be pathogenic to humans or plants, or to live in highly diverse environments, such as locations of extreme cold. The majority of the species with HPt proteins with an extended N-terminal region belong to *Ascomycota* phylum, but several are also found in the *Basidiomycota* phylum.

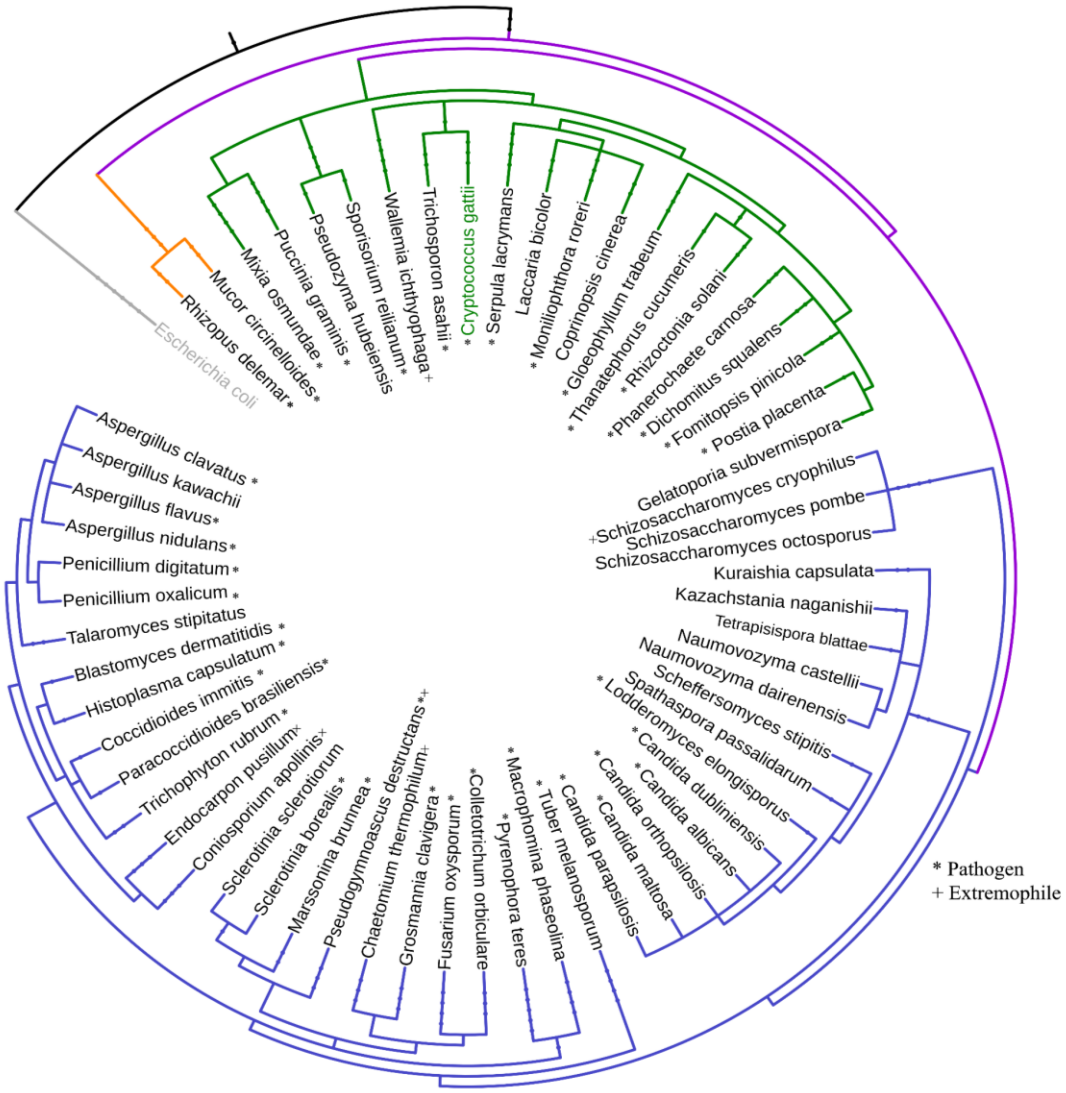


Figure 44. Phylogenetic tree of HPt proteins with extended N-terminal region
Phylogenetic tree created based on sequence alignment of stand-alone HPt proteins with extended N-terminal regions. An 'extended' N-terminal domain was defined as any encoded sequence extended greater than at least 20 residues from the start site of S. cerevisiae Ypd1. *Escherichia coli* was used as an out group and is designated in grey. Purple represents the Fungi kingdom, orange the phylum *Zygomycota*, green Basidiomycota, and blue *Ascomycota*. Pathogenic organisms are denoted by a * and extremophiles by a +.

Although the model yeast *S. cerevisiae* encodes a single HHK, a single HPt, and 2 RR proteins compartmentalized to the cytoplasm and nucleus, filamentous and pathogenic *Ascomycetes* and *Basidiomycetes* fungi have been observed to have

expanded families of HHK and RR proteins. The number of HHKs encoded by an organism is highly variable: the plant pathogen *Bipolaris maydis* encodes 21 HHK proteins; human pathogens *C. albicans* encodes 3 HHK proteins, *Trichosporon asahii* has 8 HHK proteins and *C. neoformans* has 7 HHKs [16]. Although the number of HHK proteins encoded has been greatly expanded, the majority of fungal organisms still only encode 2-5 RR, proteins and a single HPt protein [13]. This makes the HPt protein solely responsible for shuttling the phosphoryl group from numerous HHK proteins to the cognate RR protein depending on the stimuli sensed by the HHK. Addition of an N-terminal extension to the HPt protein may allow for more specific interaction between the HHK and the HPt or the HPt and the RR. For example, the extended N-terminal region of the Ypd1 homolog Mpr1 from *S. pombe* has been shown to influence phosphotransfer effiency between its cognate HHK binding partner Mak2 by contributing to the protein-protein interactions [47]. Thus, diverse functions, such as metal ion binding or stabilization of the phosphoryl group, may allow for specific functions of the N-terminal region and alter the way that the HPt interacts with its binding partners.

In summary, we show that the C-terminal region of the Ypd1 homolog from *C. neoformans* indeed functions as an HPt domain. It is able to accept and transfer phosphoryl groups to heterologous donors/acceptors, with residue H138 being the site of phosphorylation. Our data indicates that the N-terminal region of CnYpd1 confers the following structural and functional properties to CnYpd1 that differentiates this protein from other HPt domains that lack the N-terminal region. The N-terminal region (i) is essential for protein solubility, (ii) stabilizes the phosphorylated conformation, and

(iii) binds 2 calcium ions per protein monomer. A question remains with regard to the primary function of metal ion binding. We find that Ca^{2+}-binding is not required for phosphorylation of CnYpd1 and is more likely to contribute to the structural integrity of the N-terminal domain alone and/or full-length protein or perhaps is involved in a yet undetermined sensory function of N-terminal domain.

Funding

This work was supported by grants from the National Science Foundation MCB 1158319 and the Oklahoma Center for the Advancement of Science and Technology (HR12-059). This paper reports data obtained in the University of Oklahoma Protein Production Core, which is supported by an Institutional Development Award (IDeA) from the National Institute of General Medical Sciences of the National Institutes of Health under grant number P20GM103640.

Acknowledgements

We would like to thank Dr. Martina Ralle at the Elemental Core Analysis Facility at Oregon Health and Science University for performing ICP-MS analysis. We are grateful to Dr. J. Doudna (University of California, Berkeley) for the gift of a TEV-expression plasmid and Dr. J. Fassler (University of Iowa) for providing *C. neoformans* cDNA. The authors state that there are no conflicts of interest to declare.

References

1. O'Meara, T. R. and Alspaugh, J. A. 2012. The *Cryptococcus neoformans* capsule: a sword and a shield. *Clinical Microbiology Reviews* 25 (3): 387-408.

2. Urao, T., Yamaguchi-Shinozaki, K., and Shinozaki, K. 2000. Two-component systems in plant signal transduction. *Trends in plant science* 5 (2): 67-74.

3. Dziejman, M. and Mekalanos, J. J., Two-component signal transduction and its role in the expression of bacterial virulence factors, in Two-component signal transduction, Hoch, J.A. and Silhavy, T.J., Editors. 1995, American Society for Microbiology: Washington, D.C. p. 305-317.

4. Skerker, J. M., Prasol, M. S., Perchuk, B. S., Biondi, E. G., and Laub, M. T. 2005. Two-component signal transduction pathways regulating growth and cell cycle progression in a bacterium: a system-level analysis. *PLoS Biology* 3 (10): e334.

5. Bahn, Y. S. and Jung, K. W. 2013. Stress signaling pathways for the pathogenicity of *Cryptococcus*. *Eukaryotic Cell* 12 (12): 1564-77.

6. Gotoh, Y., Eguchi, Y., Watanabe, T., Okamoto, S., Doi, A., and Utsumi, R. 2010. Two-component signal transduction as potential drug targets in pathogenic bacteria. *Current Opinion in Microbiology* 13 (2): 232-239.

7. Worthington, R. J., Blackledge, M. S., and Melander, C. 2013. Small-molecule inhibition of bacterial two-component systems to combat antibiotic resistance and virulence. *Future Medicinal Chemistry* 5 (11): 1265-1284.

8. Bem, A. E., Velikova, N., Pellicer, M. T., Baarlen, P. v., Marina, A., and Wells, J. M. 2014. Bacterial histidine kinases as novel antibacterial drug targets. *ACS Chemical Biology* 10 (1): 213-224.

9. Shor, E. and Chauhan, N. 2015. A case for two-component signaling systems as antifungal drug targets. *PLoS Pathogens* 11 (2): e1004632.

10. West, A. H. and Stock, A. M. 2001. Histidine kinases and response regulator proteins in two-component signaling systems. *Trends in Biochemical Sciences* 26 (6): 369-376.

11. Goulian, M. 2010. Two-component signaling circuit structure and properties. *Current Opinion in Microbiology* 13 184-189.

12. Jung, K., Fried, L., Behr, S., and Heermann, R. 2012. Histidine kinases and response regulators in networks. *Current Opinion in Microbiology* 15 (2): 118-124.

13. Schaller, E. G., Shiu, S.-H., and Armitage, J. P. 2011. Two-component systems and their co-option for eukaryotic signal transduction. *Current Biology* 21 (9): R320-30.

14. Bahn, Y. S. 2008. Master and commander in fungal pathogens: the two-component system and the HOG signaling pathway. *Eukaryot Cell* 7 (12): 2017-36.

15. Fassler, J. S. and West, A. H. 2011. Fungal Skn7 stress responses and their relationship to virulence. *Eukaryotic Cell* 10 (2): 156-167.

16. Defosse, T. A., Sharma, A., Mondal, A. K., Dugé de Bernonville, T., Latgé, J. P., Calderone, R., Giglioli-Guivarc'h, N., Courdavault, V., Clastre, M., and Papon, N. 2015. Hybrid histidine kinases in pathogenic fungi. *Molecular Microbiology* 95 (6): 914-924.

17. Calera, J. A., Herman, D., and Calderone, R. 2000. Identification of *YPD1*, a gene of *Candida albicans* which encodes a two-component phosphohistidine intermediate protein. *Yeast* 16 1053-1059.

18. Posas, F., Wurgler-Murphy, S. M., Maeda, T., Witten, E. A., Thai, T. C., and Saito, H. 1996. Yeast HOG1 MAP kinase cascade is regulated by a multistep phosphorelay mechanism in the SLN1-YPD1-SSK1 "two-component" osmosensor. *Cell* 86 865-875.

19. Bahn, Y. S., Kojima, K., Cox, G. M., and Heitman, J. 2006. A unique fungal two-component system regulates stress responses, drug sensitivity, sexual development, and virulence of *Cryptococcus neoformans*. *Molecular Biology of the Cell* 17 (7): 3122-35.

20. Fassler, J. S. and West, A. H. 2013. Histidine phosphotransfer proteins in fungal two-component signal transduction pathways. *Eukaryotic cell* 12 (8): 1052-1060.

21. Hohmann, S., Krantz, M., and Nordlander, B. 2007. Yeast osmoregulation. *Methods in Enzymology* 428 29-45.

22. Saito, H. and Posas, F. 2012. Response to hyperosmotic stress. *Genetics* 192 (2): 289-318.

23. Lee, J. W., Ko, Y. J., Kim, S. Y., and Bahn, Y. S. 2011. Multiple roles of Ypd1 phosphotransfer protein in viability, stress response, and virulence factor regulation in *Cryptococcus neoformans*. *Eukaryotic Cell* 10 (7): 998-1002.

24. Loftus, B. J., Fung, E., Roncaglia, P., Rowley, D., Amedeo, P., Bruno, D., Vamathevan, J., Miranda, M., Anderson, I. J., Fraser, J. A., Allen, J. E., Bosdet, I. E., Brent, M. R., Chiu, R., Doering, T. L., Donlin, M. J., D'Souza, C. A., Fox, D. S., Grinberg, V., Fu, J., Fukushima, M., Haas, B. J., Huang, J. C., Janbon, G., Jones, S. J., Koo, H. L., Krzywinski, M. I., Kwon-Chung, J. K., Lengeler, K. B., Maiti, R., Marra, M. A., Marra, R. E., Mathewson, C. A., Mitchell, T. G., Pertea, M., Riggs, F. R., Salzberg, S. L., Schein, J. E., Shvartsbeyn, A., Shin, H., Shumway, M., Specht, C. A., Suh, B. B., Tenney, A., Utterback, T. R., Wickes, B. L., Wortman, J. R., Wye, N. H., Kronstad, J. W., Lodge, J. K., Heitman, J., Davis, R. W., Fraser, C. M., and Hyman, R. W. 2005. The genome of the basidiomycetous yeast and human pathogen *Cryptococcus neoformans*. *Science* 307 (5713): 1321-4.

25. Goldman, D. L., Khine, H., Abadi, J., Lindenberg, D. J., Pirofski, L.-a., Niang, R., and Casadevall, A. 2001. Serologic evidence for *Cryptococcus neoformans* infection in early childhood. *Pediatrics* 107 (5): e66-e66.

26. Thompson, H. I. 2005. Not your "typical patient": cryptococcal meningitis in an immunocompetent patient. *The Journal of neuroscience nursing: journal of the American Association of Neuroscience Nurses* 37 (3): 144.

27. Brown, G. D., Denning, D. W., Gow, N. A., Levitz, S. M., Netea, M. G., and White, T. C. 2012. Hidden killers: human fungal infections. *Science Translational Medicine* 4 (165): 165rv13-165rv13.

28. Park, B. J., Wannemuehler, K. A., Marston, B. J., Govender, N., Pappas, P. G., and Chiller, T. M. 2009. Estimation of the current global burden of cryptococcal meningitis among persons living with HIV/AIDS. *AIDS* 23 (4): 525-530.

29. Coelho, C., Bocca, A. L., and Casadevall, A. 2014. The intracellular life of *Cryptococcus neoformans*. *Annual Review of Pathology: Mechanisms of Disease* 9 219-238.

30. Bicanic, T. and Harrison, T. S. 2004. Cryptococcal meningitis. *British Medical Bulletin* 72 99-118.

31. Loyse, A., Thangaraj, H., Easterbrook, P., Ford, N., Roy, M., Chiller, T., Govender, N., Harrison, T. S., and Bicanic, T. 2013. Cryptococcal meningitis: improving access to essential antifungal medicines in resource-poor countries. *The Lancet Infectious Diseases* 13 (7): 629-637.

32. Perfect, J. R., Dismukes, W. E., Dromer, F., Goldman, D. L., Graybill, J. R., Hamill, R. J., Harrison, T. S., Larsen, R. A., Lortholary, O., and Nguyen, M.-H. 2010. Clinical practice guidelines for the management of cryptococcal disease: 2010 update by the Infectious Diseases Society of America. *Clinical Infectious Diseases* 50 (3): 291-322.

33. Lucast, L. J., Batey, R. T., and Doudna, J. A. 2001. Large-scale purification of a stable form of recombinant tobacco etch virus protease. *Biotechniques* 30 (3): 544-6, 548, 550 passim.

34. Scholz, J., Besir, H., Strasser, C., and Suppmann, S. 2013. A new method to customize protein expression vectors for fast, efficient and background free parallel cloning. *BMC Biotechnology* 13 (1): 1.

35. Janiak-Spens, F., Sparling, J. M., Gurfinkel, M., and West, A. H. 1999. Differential stabilities of phosphorylated response regulator domains reflect functional roles of the yeast osmoregulatory SLN1 and SSK1 proteins. *Journal of Bacteriology* 181 (2): 411-417.

36. Janiak-Spens, F., Cook, P. F., and West, A. H. 2005. Kinetic analysis of YPD1-dependent phosphotransfer reactions in the yeast osmoregulatory phosphorelay system. *Biochemistry* 44 (1): 377-386.

37. Xu, Q., Nguyen, V., and West, A. H. 1999. Purification, crystallization, and preliminary X-ray diffraction analysis of the yeast phosphorelay protein YPD1. *Acta Crystallographica Section D: Biological Crystallography* D55 291-293.

38. Schneider, C. A., Rasband, W. S., and Eliceiri, K. W. 2012. NIH Image to ImageJ: 25 years of image analysis. *Nature Methods* 9 (7): 671-675.

39. Janiak-Spens, F. and West, A. H. 2000. Functional roles of conserved amino acid residues surrounding the phosphorylatable histidine of the yeast phosphorelay protein YPD1. *Molecular Microbiology* 37 (1): 136-144.

40. Kaserer, A. O., Andi, B., Cook, P. F., and West, A. H. 2010. Kinetic measurements for studying phosphorelay signaling. *Methods in Enzymology* 471 291-317.

41. Xu, Q. and West, A. H. 1999. Conservation of structure and function among histidine-containing phosphotransfer (HPt) domains as revealed by the crystal structure of YPD1. *Journal of Molecular Biology* 292 1039-1050.

42. Branscum, K. 2015. Structural and Mutagenesis Studies of the Yeast Phosphorelay Signaling Proteins Ypd1 and Ssk1.

43. Buchan, D. W., Minneci, F., Nugent, T. C., Bryson, K., and Jones, D. T. 2013. Scalable web services for the PSIPRED Protein Analysis Workbench. *Nucleic Acids Research* 41 (W1): W349-W357.

44. Lukat, G. S., Stock, A. M., and Stock, J. B. 1990. Divalent metal ion binding to the CheY protein and its significance to phosphotransfer in bacterial chemotaxis. *Biochemistry* 29 5436-5442.

45. Crooks, G. E., Hon, G., Chandonia, J.-M., and Brenner, S. E. 2004. WebLogo: a sequence logo generator. *Genome Research* 14 (6): 1188-1190.

46. Letunic, I. and Bork, P. 2016. Interactive tree of life (iTOL) v3: an online tool for the display and annotation of phylogenetic and other trees. *Nucleic Acids Research* gkw290.

47. Tan, H., Janiak-Spens, F., and West, A. H. 2007. Functional characterization of the phosphorelay protein Mpr1p from *Schizosaccharomyces pombe*. *FEMS Yeast Res* 7 912-921.

Appendix A: Table of West Lab plasmids, cell strains, and primers

Table 11. OU Construct Summary

Organism	Protein	Oligos	Restriction Sites	Plasmid	Storage Strain	Expression Strain
Cn	Ypd1	n/a	Nde1/BamH1	OU421 pET16-Ypd1	OU623 (DH5α)	OU639
Cn	Ypd1-H138Q	721/722	Nde1/BamH1	OU421 pET16-Ypd1-H138Q	OU642 (DH5α)	OU644 (RIL)
Cn	Ypd1	768/769	Nde1/Pst1	OU434 trcCnYpd1	OU684 (DH5α)	OU684 (DH5α)
Cn	Ypd1-H138Q	721/722	721/722	OU435 trcCnYpd1-H138Q	OU685 (DH5α)	OU685 (DH5α)
Cn	Ypd1	768/769	Nde1/Pst1	OU434 trcCnYpd1	OU684 (DH5α)	OU667 (Gold)
Cn	Ypd1	809/810	Nde1/Pst1	OU497 trcCnYpd1-TEV	OU719 (DH5α)	OU719 (DH5α)
Cn	Ypd1-H138Q	809/810	Nde1/Pst1	OU498 trcCnYpd1-H138Q-TEV	OU836 (DH5α)	OU836 (DH5α)
Cn	Ypd1-ΔN5	928/769	Nde1/Pst1	OU476 trcCnYpd1 ΔN5	OU775 (DH5α)	OU775 (DH5α)
Cn	Ypd1-ΔN19	997/769	Nde1/Pst1	OU477 trcCnYpd1 ΔN19	OU779 (DH5α)	OU779 (DH5α)
Cn	Ypd1-ΔN77	899/769	Nde1/Pst1	OU478 trcCnYpd1 ΔN77	OU776 (DH5α)	OU776 (DH5α)
Cn	Ypd1-ΔN83	900/769	Nde1/Pst1	OU479 trcCnYpd1 ΔN83	OU778 (DH5α)	OU778 (DH5α)
Cn	Ypd1-ΔN100	901/769	Nde1/Pst1	OU480 trcCnYpd1 ΔN100	OU777 (DH5α)	OU777 (DH5α)
Cn	Ypd1-ΔN15	930/769	Nde1/Pst1	OU490 trcCnYpd1 ΔN15	OU795 (DH5α)	OU795 (DH5α)
Cn	Ypd1-ΔN43	898/769	Nde1/Pst1	OU491 trcCnYpd1 ΔN43	OU796 (DH5α)	OU796 (DH5α)
Cn	Ypd1-ΔN50	931/769	Nde1/Pst1	OU492 trcCnYpd1 ΔN50	OU797 (DH5α)	OU797 (DH5α)
Cn	Ypd1-ΔN60	1033/769	Nde1/Pst1	OU518 trcCnYpd1 ΔN60	OU834 (DH5α)	OU834 (DH5α)
Cn	Ypd1-ΔN70	1034/769	Nde1/Pst1	OU519 trcCnYpd1 ΔN70	OU835 (DH5α)	OU835 (DH5α)
Cn	CnYpd-E48A-E54A	1073/1074	Nde1/Pst1	OU521 trcCnYpd-E48A-E54A	OU837 (DH5α)	OU837 (DH5α)

Cn	CnYpd1-D60A-E67A	1075/1076	Nde1/Pst1	OU522 trcCnYpd1-D60A-E67A	OU838 (DH5α)	OU838 (DH5α)
Cn	CnYpd1-E58A	1077/1078	Nde1/Pst1	OU523 trcCnYpd1-E58A	OU839 (DH5α)	OU839 (DH5α)
Cn	Ssk1-Rec	903/908	Nde1/Xho1	OU463	OU758 (Dh5α)	OU758 (Dh5α)
Cn	Skn7-Rec	711/712	Nde1/Sma1	OU437	OU694 (DH5α)	OU694 (DH5α)
Sc	Ypd1-T12C-S69V	848/849	Nde1/Xho1	OU440 Ypd1-T12C-S69V	OU700 (Star)	OU705 (DH5α)
Sc	Ypd1-T12C-S70V	850/851	Nde1/Xho1	OU441 Ypd1-T12C-S70V	OU701 (Star)	OU706 (DH5α)
Sc	Ypd1-T12C-S73V	852/853	Nde1/Xho1	OU442 Ypd1-T12C-S73V	OU703 (Star)	OU708 (DH5α)
Sc	Ypd1-T12C-F27Y	817/818	Nde1/Xho1	OU443 Ypd1-T12C-F27Y	OU702 (Star)	OU707 (DH5α)
Sc	Ypd1-T12C-K67A	821/822	Nde1/Xho1	OU444 Ypd1-T12C-K67A	OU699 (Star)	OU704 (DH5α)
Sc	Ypd1-T12C-E16A	881/882	Nde1/Xho1	OU450 Ypd1-T12C-E16A	OU728 (Star)	OU723 (DH5α)
Sc	Ypd1-T12C-D21E	883/884	Nde1/Xho1	OU451 Ypd1-T12C-D21E	OU729 (Star)	OU724 (DH5α)
Sc	Ypd1-T12C-D23E	885/886	Nde1/Xho1	OU452 Ypd1-T12C-D23E	OU730 (Star)	OU725 (DH5α)
Sc	Ypd1-T12C-Q76L	891/892	Nde1/Xho1	OU453 Ypd1-T12C-Q67L	OU731 (Star)	OU726 (DH5α)
Sc	Ypd1-T12C-L31A	888/889	Nde1/Xho1	OU454 Ypd1-T12C-L31A	OU732 (Star)	OU727 (DH5α)
Sc	Ypd1-G68A	1047/1048	Nde1/Pst1	OU501 Ypd1-G68A	OU810 (DH5α)	OU810 (DH5α)
Sc	Ypd1-G68S	956/957	Nde1/Pst1	OU502 Ypd1-G68S	OU811 (DH5α)	OU811 (DH5α)
Sc	Ypd1-G68V	945/946	Nde1/Pst1	OU503 Ypd1-G68V	OU812 (DH5α)	OU812 (DH5α)
Sc	Ypd1-G68L	943/944	Nde1/Pst1	OU504 Ypd1-G68L	OU813 (DH5α)	OU813 (DH5α)
Sc	Ypd1-G68E	1018/1019	Nde1/Pst1	OU505 Ypd1-G68E	OU814 (DH5α)	OU814 (DH5α)
Sc	Ypd1-G68N	1045/1046	Nde1/Pst1	OU506 Ypd1-G68N	OU815 (DH5α)	OU815 (DH5α)
Sc	Ypd1-T12C-G68A	1047/1048	Nde1/Xho1	OU507 Ypd1-T12C-G68A	OU816 (DH5α)	OU822 (Star)
Sc	Ypd1-T12C-G68S	956/957	Nde1/Xho1	OU508 Ypd1-T12C-G68S	OU817 (DH5α)	OU823 (Star)

Sc	Ypd1-T12C-G68V	945/946	Nde1/Xho1	OU509 Ypd1-T12C-G68V	OU818 (DH5α)	OU824 (Star)
Sc	Ypd1-T12C-G68L	943/944	Nde1/Xho1	OU510 Ypd1-T12C-G68L	OU819 (DH5α)	OU825 (Star)
Sc	Ypd1-T12C-G68E	1018/1019	Nde1/Xho1	OU511 Ypd1-T12C-G68E	OU820 (DH5α)	OU826 (Star)
Sc	Ypd1-T12C-G68N	1045/1046	Nde1/Xho1	OU512 Ypd1-T12C-G68N	OU821 (DH5α)	OU827 (Star)

Table 12. Oligo names, OU numbers, and Sequences

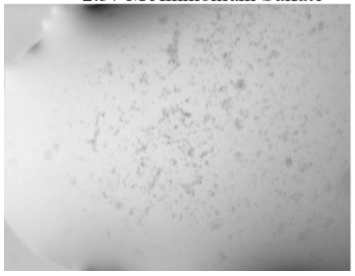
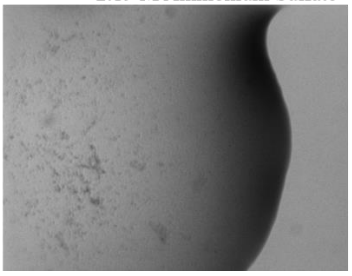
Oligo	OU Number	Sequence
trcCnYpd1 Forward	768	5'-GAATTCCATATGCCAGACCAGGCC-3'
trcCnYpd1 Reverse	769	5'-CTGCAGTTACTTGAGATCATCGTACAT-3'
pTrcHis Forward	774	5'-GAGGTATATATTAATGTATCG-3'
pTrcHis Reverse	775	5'-GATTTAATCTGTATCAGG-3'
Xpress pTrcHis Forward	773	5'-TATGGCTAGCATGACTGGT-3'
CnYpd1-H138Q Forward	721	5'-CCAACTCTCCTCTCTCGGCCAATTTCTCAAAGGCTCGTC-3'
CnYpd1-H138Q Reverse	722	5'-GACGAGCCTTTGAGAAATTGGCCGAGAGAGGAGAGTTTG-3'
Trc-TEV Forward	809	5'-CAGCAAATGGGTCGGGAAAACCTGTATTTTCAGGGGGATCCAACCCTTGGCCAT-3'
Trc-TEV Reverse	810	5'-ATGGCCAAGGGTTGGATCCCCCTGAAAATACAGGTTTTCCCGACCCATTGGCTG-3'
CnYpd1 Δ5 Forward	928	5'-GAATTCCATATGGCCAGATCGCCGTCAGCCCC–3'
CnYpd1 Δ15 Forward	930	5'-GAATTCCATATGTCGAACATCAGCACCGCCAACAT-3'
CnYpd1 Δ19 Forward	897	5'-GAATTCCATATGGACCGCCAACATACGCAG-3'
CnYpd1 Δ43 Forward	898	5'-GGATCCACATATGTCAAGTCGGGAGCAGAGT-3'
CnYpd1 Δ50 Forward	931	5'-GAATTCCATATGCAGGTCGAGGAGGAGGCTG-3'
CnYpd1 Δ60 Forward	1033	5'-GAATTCCATATGGACGACGAGTCGGACGAC-3'
CnYpd1 Δ70 Forward	1034	5'-GAATTCCATATGACCGGCGATGGAATCATC-3'
CnYpd1 Δ77 Forward	899	5'-GAATTCCATATGGAAACGTTCCAGCAA-3'
CnYpd1 Δ84 Forward	900	5'-GAATTCCATATGGACATGGACGAGGAA-3'
CnYpd1 Δ100 Forward	901	5'-GAATTCCATATGTCATTCTCAAAGGGTATC-3'
CnYpd1-H21A Forward	939	5'-ACTACCTCGAACATCAGCGACCGCCAAGCGACGCAGCCG-3'
CnYpd1-H21A Reverse	940	5'-ATCTTTAGCGGGTTGCGGCTGCGTCGCTTGGCGGTCGCT-3'
CnYpd-E48A-E54A Forward	1073	5'-GCAGCGGCCGCGGCGGCGGCTGCGGCCGAAGCG-3'
CnYpd-E48A-E54A Reverse	1074	5'-CGCCGCCGCGGCCGCTGCACTCTGCTCCCGACTTGACTC-3'

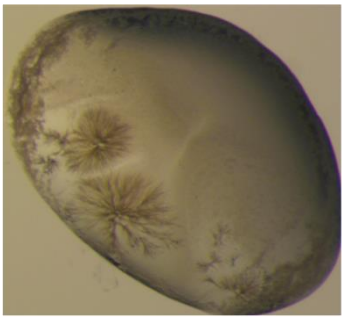
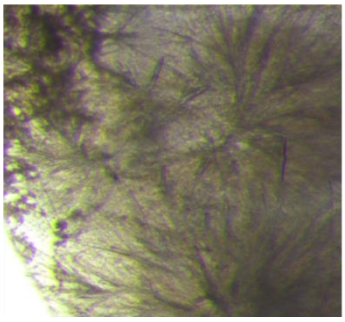
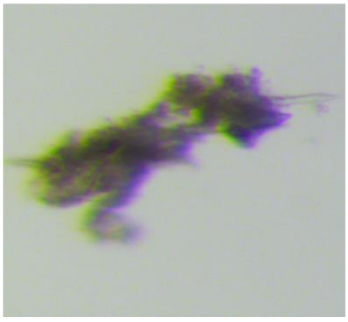
CnYpd1-D60A-E67A Forward	1075	5’-GCAGCGGCCGCGGCGGCGGCAGCACCAGAGACCGGCGATGAAATC-3’
CnYpd1-D60A-E67A Reverse	1076	5’-TGCTGCCGCCGCCGCGGCCGCTGCCGCTTCGGCCGCAGCCTCCTC-3’
CnYpd1-E58A Forward	1077	5’-CAGAGTGAACAGGTCGAGGAGGAGGCTGCGGCCGCAGCGGACGAC-3’
CnYpd1-E58A Reverse	1078	5’-CTCCTCGTCGTCCGACTCGTCGTCCGCTGCGGCCGCAGCCTC-3’
CnYpd1-D75A Forward	1079	5’-ACCGGCGATGAAATCATCGCAATGGAAACGTTC-3’
CnYpd1-D75A Reverse	1080	5’-GTCCATGTCCATGATTTGCTGGAACGTTTCCATTGCGATGATTTC-3’
ScYpd1-E16A Forward	1006	5’-CCCTCAGAAATCATCAATTGGACCATCTTAAATGCAATTATATCT-3’
ScYpd1-E16A Forward	1007	5’-ATCATCGTCATCCATAGATATAATTGCATTTAAGATACA-3’
ScYpd1-S19A Forward	788	5’-GAAATTATATCTATGGATGAC-3’
ScYpd1-S19A Reverse	789	5’-GTCATCCATGAGTATAATTTC-3’
ScYpd1-S19V Forward	792	5’-GAAATTATAGTTATGGATGAC-3’
ScYpd1-S19V Reverse	793	5’-GTCATCCATAACTATAATTTC-3’
ScYpd1-M20A Forward	790	5’-GAAATTATATCTGCGGATGAC-3’
ScYpd1-M20A Reverse	791	5’-GTCATCCGCAGATATAATTTC-3’
ScYpd1-D21A Forward	990	5’-AATGAAATTATATCTATGGCAGACGATGATTCC-3’
ScYpd1-D21A Reverse	991	5’-AGAAAAATCGGAATCATCGTCTGCCATAGATATAAT-3’
ScYpd1-D21E Forward	883	5’-ATCTTAAATGAAATTATATCTATGGAGGACGATGATTCC-3’
ScYpd1-D21E Reverse	884	5’-AGAAAAATCGGAATCATCGTCCTCCATAGATATAAT-3’
ScYpd1-D22A Forward	992	5’-ATCTTAAATGAAATTATATCTATGGATGCAGATGATTCC-3’
ScYpd1-D22A Reverse	993	5’-AGAAAAATCGGAATCATCTGCATCCATAGATATAAT-3’
ScYpd1-D23A Forward	994	5’-AATGAAATTATATCTATGGATGACGCAGATTCCGATTTT-3’
ScYpd1-D23A Reverse	995	5’-AATTAGACCTTTAGAAAAATCGGAATCTGCGTCATCCAT-3’
ScYpd1-D23E Forward	885	5’-ATCTTAAATGAAATTATATCTATGGATGACGAGGATTCCGATTTT-3’
ScYpd1-D23E Reverse	886	5’-AATTAGACCTTTAGAAAAATCGGAATCCTCGTCATCCAT-3’
ScYpd1-D24A Forward	996	5’-ATCTTAAATGAAATTATATCTATGGATGACGATGCATCCGATTTT-3’
ScYpd1-D24A Reverse	997	5’-AATTAGACCTTTAGAAAAATCGGATGCATCGTCATCCAT-3’
ScYpd1-S25A Forward	998	5’-ATATCTATGGATGACGATGATGCAGATTTTTCTAAA -3’
ScYpd1-S25A Reverse	999	5’-AATTAGACCTTTAGAAAAATCTGCATCATCGTCATCCAT-3’
ScYpd1-D26A Forward	1000	5’-ATATCTATGGATGACGATGATTCCGCATTTTCTAAA-3’
ScYpd1-D26A Reverse	1001	5’-TTGAATAATTAGACCTTTAGAAAATGCGGAATCATC-3’
ScYpd1-F27A Forward	1002	5’-ATTATATCTATGGATGACGATGATTCCGATGCATCTAAAGGT-3’
ScYpd1-F27A Reverse	1003	5’-GATAAATTGAATAATTAGACCTTTAGATGCATCGGAATC-3’
ScYpd1-F27Y Forward	817	5’-AATGAAATTATATCTATGGATGACGATGATTCCGATTATTCTAAAGGT-3’

ScYpd1-F27Y Reverse	818	5’-CTGGTCGATAAATTGAATAATTAGACCTTTAGAATAATCGGAATC-3’
ScYpd1-L31A Forward	887	5’-GACGATGATTCCGATTTTTCTAAAGGTGCAATTATTCAATTT-3’
ScYpd1-L31A Reverse	888	5’-TGCCTGGTCGATAAATTGAATAATTGCACCTTTAGA-3’
ScYpd1-E58A Forward	1004	5’-GACGGTGAAAAAAATCTTACCGCATTAGACAATCTG-3’
ScYpd1-E58A Reverse	1005	5’-TAAAAAATGGCCCAGATTGTCTAATGCGGTAAGATT-3’
ScYpd1-K67A Forward	821	5’-ACCGAATTAGACAATCTGGGCCATTTTTTAGCGGGTTCTTCTGCTGCA-3’
ScYpd1-K67A Reverse	822	5’-TTGTAAGCCTAATGCAGCAGAAGAACCCGCTAAAAAATGGCC-3’
ScYpd1-G68A Forward	1047	5’-CATTTTTTAAAGGCTTCTTCTGCTGCATTAGGC-3’
ScYpd1-G68A Reverse	1048	5’-AGCAGAAGAAGCCTTTAAAAAATGGCCCAGATT-3’
ScYpd1-G68S Forward	956	5’-GACAATCTGGGCCATTTTTTAAAGTCTTCTTCTGCT-3’
ScYpd1-G68S Reverse	957	5’-TAAGCCTAATGCAGCAGAAGAAGACTTTAAAAA-3’
ScYpd1-G68V Forward	945	5’-GACAATCTGGGCCATTTTTTAAAGGTTTCTTCTGCT-3’
ScYpd1-G68V Reverse	946	5’-TAAGCCTAATGCAGCAGAAGAAACCTTTAAAAA-3’
ScYpd1-G68L Forward	943	5’-GACAATCTGGGCCATTTTTTAAAGCTTTCTTCTGCT-3’
ScYpd1-G68L Reverse	944	5’-TAAGCCTAATGCAGCAGAAGAAAGCTTTAAAAA-3’
ScYpd1-G68E Forward	1018	5’-AATCTGGGCCATTTTTTAAAGGAATCTTCTGCT-3’
ScYpd1-G68E Reverse	1019	5’-GCCTAATGCAGCAGAAGATTCCTTTAAAAA-3’
ScYpd1-G68Q Forward	1016	5’-AATCTGGGCCATTTTTTAAAGCAATCTTCTGCT-3’
ScYpd1-G68Q Reverse	1017	5’-GCCTAATGCAGCAGAAGATTGCTTTAAAAA-3’
ScYpd1-G68N Forward	1045	5’-TTTTTAAAGAATTCTTCTGCTGCATTAGGC-3’
ScYpd1-G68N Reverse	1046	5’-GCCTAATCGAGCAGAAGAATTCTTTAAAAA-3’
ScYpd1-S69V Forward	848	5’-TTAGACAATCTGGGCCATTTTTTAAAGGGTGTTTCTGCTGCATTAGGC-3’
ScYpd1-S69V Reverse	849	5’-AACCCAGGCAATTCTTTGTAAGCCTAATGCAGCAGAAACACCCTTTAAAAA-3’
ScYpd1-S70V Forward	850	5’-TTAGACAATCTGGGCCATTTTTTAAAGGGTTCTGTTGCTGCATTAGGC-3’
ScYpd1-S70V Reverse	851	5’-AACCCAGGCAATTCTTTGTAAGCCTAATGCAGCAACAGAACCCTTTAAAAA-3’
ScYpd1-S73V Forward	852	5’-GGCCATTTTTTAAAGGGTTCTTCTGCTGCAGTAGGCTTACAAAGA-3’
ScYpd1-S73V Reverse	853	5’-TTCACAAACCCAGGCAATTCTTTGTAAGCCTACTGCAGCAGAAGA-3’
ScYpd1-Q76L Forward	891	5’-ATTGCCTGGGTTTGTGAAAGAATTCTAAACTTGGGAAGA-3’
ScYpd1-G76L Reverse	892	5’-AATTCTTTCACAAACCCAGGCAATTCTTAGTAAGCC-3’

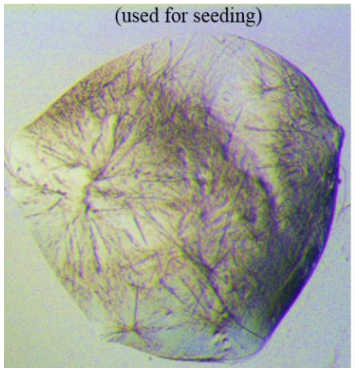
Appendix B: Crystallography attempts for CnYpd1

Table 13. Crystallography attempts for CnYpd1 constructs

Date	Protein	Conc. (mg/mL)	Buffer Condition	Broad Screen	Drop Ratio	Custom Screen
12/7/2012	$CnYpd1_{tag}$	10	10mM Bis-tris pH 6.5, 400 mM NaCl	Index JCSG PACT WizardI/II CSHT	1:1	
12/17/2012	$CnYpd1_{tag}$	3	10mM Bis-tris pH 6.5, 400 mM NaCl	Index JCSG PACT WizardI/II CSHT	1:1	
2/7/13	$CnYpd1_{tag}$	20	10mM Bis-tris pH 6.5, 400 mM NaCl	Index JCSG WizardI/II CSHT	1:1	
2/8/15	$CnYpd1_{tag}$	20	10mM Bis-tris pH 6.5, 400 mM NaCl	-------	1:1	ScYpd1 Optimization Screen **(Table 14)**
4/5/13	$CnYpd1_{tag}$	18	20 mM Tris pH 7.0, 50 mM NaCl	-------	2:1	• ScYpd1 Optimization Screen (**Table 14**) +/- Reducing agent • ScYpd1 Optimization Screen (**Table 14**) + Silver Bullet
6/14/13	$CnYpd1_{tag}$	10	50 mM Tris pH 7.0, 50 mM KCl	CSHT MCSG II MCSG III	1:1	
7/18/13	$CnYpd1_{tag}$	10	50 mM Tris pH 7.0, 50 mM KCl	-------	1:1	• MCSGII B1 Optimization Screen 1 (**Table 15**) • MCSGII B1 Optimization Screen 2 (**Table 16**)
7/18/13	$CnYpd1_{tag}$	10	50 mM Tris pH 7.0, 50 mM KCl	-------	1:1	• MCSG III E5 Optimization Screen (**Table 17**)
C3: 0.1 M Sodium Citrate pH 5 2.37 M Ammonium Sulfate  C6: 0.1 M Sodium Citrate pH 5 2.93 M Ammonium Sulfate  D2: 0.1 M Sodium Citrate pH 5 2.19 M Ammonium Sulfate  Optimization of precipitation seen in well E5of the MCSG III screen yielded similar small crystalline precipitant.						
7/24/13	$CnYpd1\text{-}H138Q_{tag}$	27	20 mM Tris pH 7, 300 mM NaCl	Wizard I&II CSHT Index PACT	1:1	

7/24/13	CnYpd1-H138Q_{tag} 4°C	27	20 mM Tris pH 7, 300 mM NaCl	Wizard I&II CSHT Index PACT	1:1	
7/30/13	CnYpd1-H138Q_{tag}	27	20 mM Tris pH 7.5, 300 mM NaCl	Wizard I&II CSHT Index PACT	1:1	
	CnYpd1-H138Q_{tag} 4°C	27	20 mM Tris pH 7.5	Sigma Additive Screen		
Day 7 0.5 M 1,2,3- octanetriol isomer H  Day 11 0.5 M 1,2,3- octanetriol isomer H  Day 12 0.5 M 1,2,3- octanetriol isomer H 						
	CnYpd1-H138Q_{tag} 4°C/RT	27	20 mM Tris pH 7.5	-------	1:1	Octanetriol Opt. 1 (**Table 18**)
Higher concentration of protein produced larger more needle-like crystals than the hair-like crystals seen at 13.5 mg/mL (see below)						
	CnYpd1-H138Q_{tag} 4°C/RT	13.5	20 mM Tris pH 7.5	-------	1:1	Octanetriol Opt. 2 (**Table 20**)

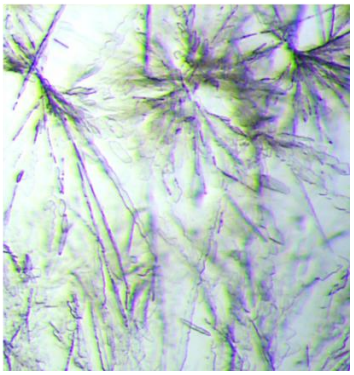
CnYpd1 H138Q 27 mg/ml
Room Temp
(used for seeding)



CnYpd1 H138Q 13.5 mg/ml
Room temp

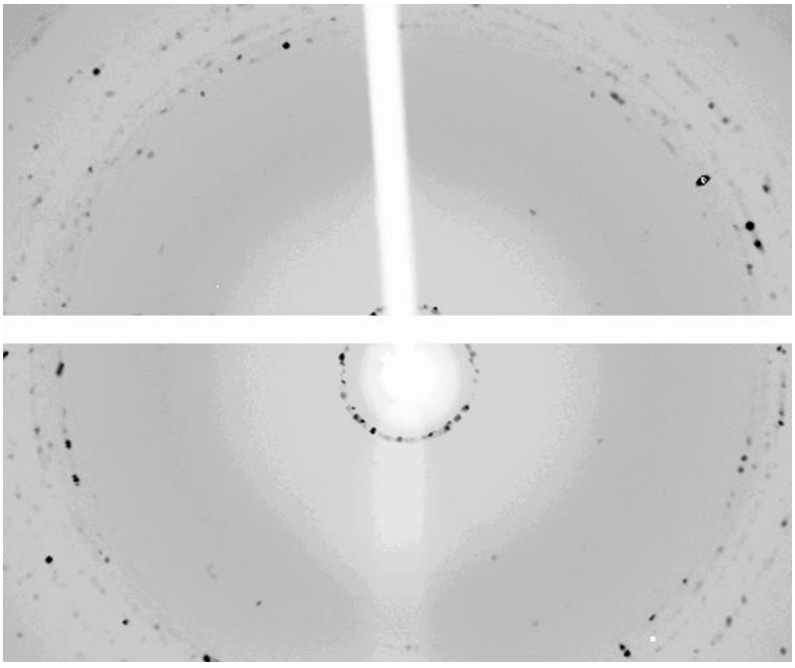


CnYpd1H138Q 27 mg/mL
+seed stock
Room Temp



Needle like crystals observed with the additive 1,2,3-octanetriol isomer H, however diffraction pattern was inconclusive.

Seed stock was obtained from Sigma additive screen day 11.



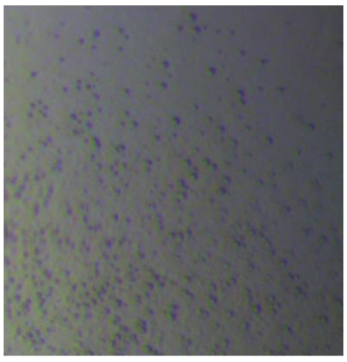
	$CnYpd1_{tag}$ 4°C/RT	9	20 mM Tris pH 7.5	-------	1:1	Octanetriol Opt. 1 (**Table 19**)

10/18/13	CnYpd1$_{tagless}$	10	20 mM Bis-tris pH 6.5, 50 mM NaCl	MCSG 1-4 PACT Wizard I&II CSHT	1:1	

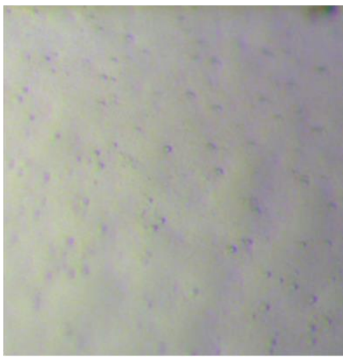
MCSG I A12:
20% PEG 8000
0.1 M HEPES pH 7.4



MCSG I C7:
20% PEG 8000
0.1 M Tris pH 8.5
0.2 M Calcium Chloride

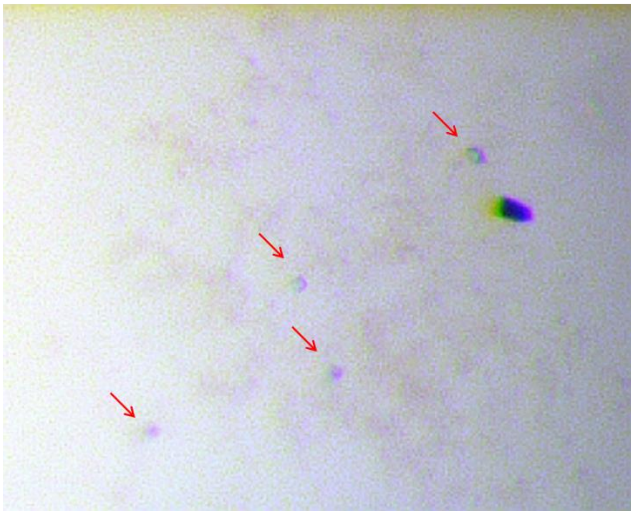


MCSG I E9:
20% PEG 3350
0.2 M Calcium Chloride



Spherulite crystals were observed from the MCSG I Screen. Small crystals were also seen from the CSHT Screen. Optimization screens were created around the CSHT D3 condition (Table 22). Further optimization did not reproduce crystals.

CSHT D3:
0.1 M HEPES sodium pH 7.5
2% v/v Polyethylene glycol 400
2.0 M Ammonium sulfate



10/30/13	CnYpd1$_{tagless}$	10	20 mM Bis-tris pH 6.5, 50 mM NaCl	-------		CSHT D3 Optimization (**Table 21**)
2/25/14	CnYpd1$_{tagless}$	9		MemGold CSHT PACT		
7/3/14	CnYpd1-H138Q$_{tagless}$	7	PBS	MCSG 1-4 PACT Wizard I&II CSHT Index JCSG+ SaltRx	1:1 1:3	

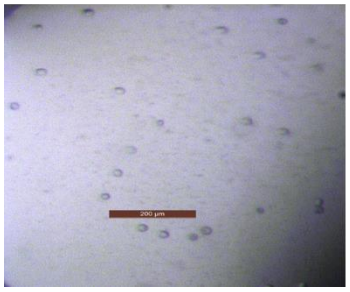
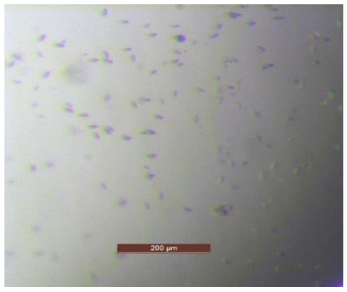
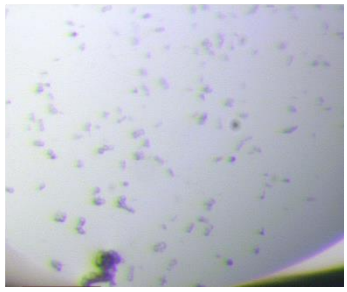
				Ammonium Sulfate Suite		
MCSG I C9 0.8 M Lithium Chloride 32% PEG 4000 0.1 M Tris pH 8.5		MCSG II D11 1.5 M Lithium Sulfate 0.1 M Tris pH 8.5		JCSG D7 0.2 M Lithium Sulfate 40% PEG 400 0.1 M Tris pH 8.5		
						
Small seed-like crystals were seen for several conditions containing lithium salts. Optimization plates set up around these conditions. Diffracted as salt crystals.						
7/3/14	CnYpd1-H138Q$_{tagless}$	7	PBS	-------	1:1	• CSHT H5 Opt. (**Table 22**) • Index G11 Opt. (Error! Reference ource not found.) • JCSG D7 Opt. (**Table 23**) • MCSG 1 C5 Opt. (**Table 24**)
Optimizations of spherulite crystals did not yield crystals that diffracted						
7/3/14	CnYpd1-H138Q$_{tagless}$ 4°C	7	PBS	CSHT Wizard I&II	1:1 1:3	
10/17/14	CnYpd1$_{tagless}$ 4°C	12	PBS	PACT JCSG Midas	1:1	
9/23/15	CnYpd1 ΔN60	10	20 mM Tris pH 8.0, 150 mM NaCl, 0.06% Tween 20	MCSG 1-4		
4/26/16	CnYpd1	10	20 mM Tris pH 8.0, 150 mM NaCl, 10 mM $CaCl_2$	MCSG 1-2, JSCG+	1:1	Seeded with ScYpd1 crystals

Table 14. ScYpd1 Optimization Screen

25% PEG 4000 0.1 M Ammonium Acetate	27.5% PEG 4000 0.1 M Ammonium Acetate	30% PEG 4000 0.1 M Ammonium Acetate	32.8% PEG 4000 0.1 M Ammonium Acetate	35.4% PEG 4000 0.1 M Ammonium Acetate	38% PEG 4000 0.1 M Ammonium Acetate
25% PEG 4000 0.2 M Ammonium Acetate	27.5% PEG 4000 0.2 M Ammonium Acetate	30% PEG 4000 0.2 M Ammonium Acetate	32.8% PEG 4000 0.2 M Ammonium Acetate	35.4% PEG 4000 0.2 M Ammonium Acetate	38% PEG 4000 0.2 M Ammonium Acetate
25% PEG 4000 0.3 M Ammonium Acetate	27.5% PEG 4000 0.3 M Ammonium Acetate	30% PEG 4000 0.3 M Ammonium Acetate	32.8% PEG 400 0.3 M Ammonium Acetate	35.4% PEG 4000 0.3 M Ammonium Acetate	38% PEG 4000 0.3 M Ammonium Acetate
25% PEG 4000 0.4 M Ammonium Acetate	27.5% PEG 4000 0.4 M Ammonium Acetate	30% PEG 4000 0.4 M Ammonium Acetate	32.8% PEG 4000 0.4 M Ammonium Acetate	35.4% PEG 4000 0.4 M Ammonium Acetate	38% PEG 4000 0.4 M Ammonium Acetate

Table 15. MSCG II B1 Optimization Screen 1

.1 M MES pH 6.5 6% PEG 20000	0.1 M MES pH 6.5 7.09% PEG 20000	0.1 M MES pH 6.5 8.18% PEG 20000	0.1 M MES pH 6.5 9.27% PEG 20000	0.1 M MES pH 6.5 10.36% PEG 20000	0.1 M MES pH 6.5 11.45% PEG 20000	0.1 M MES pH 6.5 12.55% PEG 20000	0.1 M MES pH 6.5 13.64% PEG 20000	0.1 M MES pH 6.5 11.45% PEG 20000	0.1 M MES pH 6.5 15.82% PEG 20000	0.1 M MES pH 6.5 16.91% PEG 20000	0.1 M MES pH 6.5 18% PEG 20000
0.1 M MES pH 6.5 6% PEG 20000	0.1 M MES pH 6.5 7.09% PEG 20000	0.1 M MES pH 6.5 8.18% PEG 20000	0.1 M MES pH 6.5 9.27% PEG 20000	0.1 M MES pH 6.5 10.36% PEG 20000	0.1 M MES pH 6.5 11.45% PEG 20000	0.1 M MES pH 6.5 12.55% PEG 20000	0.1 M MES pH 6.5 13.64% PEG 20000	0.1 M MES pH 6.5 11.45% PEG 20000	0.1 M MES pH 6.5 15.82% PEG 20000	0.1 M MES pH 6.5 16.91% PEG 20000	0.1 M MES pH 6.5 18% PEG 20000
0.1 M MES pH 6.5 6% PEG 20000	0.1 M MES pH 6.5 7.09% PEG 20000	0.1 M MES pH 6.5 8.18% PEG 20000	0.1 M MES pH 6.5 9.27% PEG 20000	0.1 M MES pH 6.5 10.36% PEG 20000	0.1 M MES pH 6.5 11.45% PEG 20000	0.1 M MES pH 6.5 12.55% PEG 20000	0.1 M MES pH 6.5 13.64% PEG 20000	0.1 M MES pH 6.5 11.45% PEG 20000	0.1 M MES pH 6.5 15.82% PEG 20000	0.1 M MES pH 6.5 16.91% PEG 20000	0.1 M MES pH 6.5 18% PEG 20000
0.1 M MES pH 6.5 6% PEG 20000	0.1 M MES pH 6.5 7.09% PEG 20000	0.1 M MES pH 6.5 8.18% PEG 20000	0.1 M MES pH 6.5 9.27% PEG 20000	0.1 M MES pH 6.5 10.36% PEG 20000	0.1 M MES pH 6.5 11.45% PEG 20000	0.1 M MES pH 6.5 12.55% PEG 20000	0.1 M MES pH 6.5 13.64% PEG 20000	0.1 M MES pH 6.5 11.45% PEG 20000	0.1 M MES pH 6.5 15.82% PEG 20000	0.1 M MES pH 6.5 16.91% PEG 20000	0.1 M MES pH 6.5 18% PEG 20000
0.1 M MES pH 6.5 6% PEG 20000	0.1 M MES pH 6.5 7.09% PEG 20000	0.1 M MES pH 6.5 8.18% PEG 20000	0.1 M MES pH 6.5 9.27% PEG 20000	0.1 M MES pH 6.5 10.36% PEG 20000	0.1 M MES pH 6.5 11.45% PEG 20000	0.1 M MES pH 6.5 12.55% PEG 20000	0.1 M MES pH 6.5 13.64% PEG 20000	0.1 M MES pH 6.5 11.45% PEG 20000	0.1 M MES pH 6.5 15.82% PEG 20000	0.1 M MES pH 6.5 16.91% PEG 20000	0.1 M MES pH 6.5 18% PEG 20000
0.1 M MES pH 6.5 6% PEG 20000	0.1 M MES pH 6.5 7.09% PEG 20000	0.1 M MES pH 6.5 8.18% PEG 20000	0.1 M MES pH 6.5 9.27% PEG 20000	0.1 M MES pH 6.5 10.36% PEG 20000	0.1 M MES pH 6.5 11.45% PEG 20000	0.1 M MES pH 6.5 12.55% PEG 20000	0.1 M MES pH 6.5 13.64% PEG 20000	0.1 M MES pH 6.5 11.45% PEG 20000	0.1 M MES pH 6.5 15.82% PEG 20000	0.1 M MES pH 6.5 16.91% PEG 20000	0.1 M MES pH 6.5 18% PEG 20000
0.1 M MES pH 6.5 6% PEG 20000	0.1 M MES pH 6.5 7.09 % PEG 20000	0.1 M MES pH 6.5 8.18% PEG 20000	0.1 M MES pH 6.5 9.27% PEG 20000	0.1 M MES pH 6.5 10.36% PEG 20000	0.1 M MES pH 6.5 11.45% PEG 20000	0.1 M MES pH 6.5 12.55% PEG 20000	0.1 M MES pH 6.5 13.64% PEG 20000	0.1 M MES pH 6.5 11.45% PEG 20000	0.1 M MES pH 6.5 15.82% PEG 20000	0.1 M MES pH 6.5 16.91% PEG 20000	0.1 M MES pH 6.5 18% PEG 20000
0.1 M MES pH 6.5 6% PEG 20000	0.1 M MES pH 6.5 7.09% PEG 20000	0.1 M MES pH 6.5 8.18% PEG 20000	0.1 M MES pH 6.5 9.27% PEG 20000	0.1 M MES pH 6.5 10.36% PEG 20000	0.1 M MES pH 6.5 11.45% PEG 20000	0.1 M MES pH 6.5 12.55% PEG 20000	0.1 M MES pH 6.5 13.64% PEG 20000	0.1 M MES pH 6.5 11.45% PEG 20000	0.1 M MES pH 6.5 15.82% PEG 20000	0.1 M MES pH 6.5 16.91% PEG 20000	0.1 M MES pH 6.5 18% PEG 20000
0.1 M MES pH 6.5 6% PEG 20000	0.1 M MES pH 6.5 7.09% PEG 20000	0.1 M MES pH 6.5 8.18% PEG 20000	0.1 M MES pH 6.5 9.27% PEG 20000	0.1 M MES pH 6.5 10.36% PEG 20000	0.1 M MES pH 6.5 11.45% PEG 20000	0.1 M MES pH 6.5 12.55% PEG 20000	0.1 M MES pH 6.5 13.64% PEG 20000	0.1 M MES pH 6.5 11.45% PEG 20000	0.1 M MES pH 6.5 15.82% PEG 20000	0.1 M MES pH 6.5 16.91% PEG 20000	0.1 M MES pH 6.5 18% PEG 20000

Table 16. MSCG II B1 Optimization Screen 2

0.1 M MES pH 6.0 12% PEG 20000	0.1 M MES pH 6.09 12% PEG 20000	1 M MES pH 60.18 12% PEG 20000	1 M MES pH 6.27 12% PEG 20000	1 M MES pH 6.36 12% PEG 20000	1 M MES pH 6.45 12% PEG 20000	1 M MES pH 6.55 12% PEG 20000	1 M MES pH 6.64 12% PEG 20000	1 M MES pH 6.73 12% PEG 20000	1 M MES pH 6.82 12% PEG 20000	1 M MES pH 6.91 12% PEG 20000	1 M MES pH 7.0 12% PEG 20000
0.1 M MES pH 6.0 12% PEG 20000	1 M MES pH 6.09 12% PEG 20000	1 M MES pH 60.18 12% PEG 20000	1 M MES pH 6.27 12% PEG 20000	1 M MES pH 6.36 12% PEG 20000	1 M MES pH 6.45 12% PEG 20000	1 M MES pH 6.55 12% PEG 20000	1 M MES pH 6.64 12% PEG 20000	1 M MES pH 6.73 12% PEG 20000	1 M MES pH 6.82 12% PEG 20000	1 M MES pH 6.91 12% PEG 20000	1 M MES pH 7.0 12% PEG 20000
0.1 M MES pH 6.0 12% PEG 20000	1 M MES pH 6.09 12% PEG 20000	1 M MES pH 60.18 12% PEG 20000	1 M MES pH 6.27 12% PEG 20000	1 M MES pH 6.36 12% PEG 20000	1 M MES pH 6.45 12% PEG 20000	1 M MES pH 6.55 12% PEG 20000	1 M MES pH 6.64 12% PEG 20000	1 M MES pH 6.73 12% PEG 20000	1 M MES pH 6.82 12% PEG 20000	1 M MES pH 6.91 12% PEG 20000	1 M MES pH 7.0 12% PEG 20000
0.1 M MES pH 6.0 12% PEG 20000	1 M MES pH 6.09 12% PEG 20000	1 M MES pH 60.18 12% PEG 20000	1 M MES pH 6.27 12% PEG 20000	1 M MES pH 6.36 12% PEG 20000	1 M MES pH 6.45 12% PEG 20000	1 M MES pH 6.55 12% PEG 20000	1 M MES pH 6.64 12% PEG 20000	1 M MES pH 6.73 12% PEG 20000	1 M MES pH 6.82 12% PEG 20000	1 M MES pH 6.91 12% PEG 20000	1 M MES pH 7.0 12% PEG 20000
.0.1 M MES pH 6.0 12% PEG 20000	1 M MES pH 6.09 12% PEG 20000	1 M MES pH 60.18 12% PEG 20000	1 M MES pH 6.27 12% PEG 20000	1 M MES pH 6.36 12% PEG 20000	1 M MES pH 6.45 12% PEG 20000	1 M MES pH 6.55 12% PEG 20000	1 M MES pH 6.64 12% PEG 20000	1 M MES pH 6.73 12% PEG 20000	1 M MES pH 6.82 12% PEG 20000	1 M MES pH 6.91 12% PEG 20000	1 M MES pH 7.0 12% PEG 20000
0.1 M MES pH 6.0 12% PEG 20000	1 M MES pH 6.09 12% PEG 20000	1 M MES pH 60.18 12% PEG 20000	1 M MES pH 6.27 12% PEG 20000	1 M MES pH 6.36 12% PEG 20000	1 M MES pH 6.45 12% PEG 20000	1 M MES pH 6.55 12% PEG 20000	1 M MES pH 6.64 12% PEG 20000	1 M MES pH 6.73 12% PEG 20000	1 M MES pH 6.82 12% PEG 20000	1 M MES pH 6.91 12% PEG 20000	1 M MES pH 7.0 12% PEG 20000
0.1 M MES pH 6.0 12% PEG 20000	1 M MES pH 6.09 12% PEG 20000	1 M MES pH 60.18 12% PEG 20000	1 M MES pH 6.27 12% PEG 20000	1 M MES pH 6.36 12% PEG 20000	1 M MES pH 6.45 12% PEG 20000	1 M MES pH 6.55 12% PEG 20000	1 M MES pH 6.64 12% PEG 20000	1 M MES pH 6.73 12% PEG 20000	1 M MES pH 6.82 12% PEG 20000	1 M MES pH 6.91 12% PEG 20000	1 M MES pH 7.0 12% PEG 20000
0.1 M MES pH 6.0 12% PEG 20000	1 M MES pH 6.09 12% PEG 20000	1 M MES pH 60.18 12% PEG 20000	1 M MES pH 6.27 12% PEG 20000	1 M MES pH 6.36 12% PEG 20000	1 M MES pH 6.45 12% PEG 20000	1 M MES pH 6.55 12% PEG 20000	1 M MES pH 6.64 12% PEG 20000	1 M MES pH 6.73 12% PEG 20000	1 M MES pH 6.82 12% PEG 20000	1 M MES pH 6.91 12% PEG 20000	1 M MES pH 7.0 12% PEG 20000

Table 17. MCSG III E5 Optimization Screen 1

0.1 M Sodium Citrate pH 5 2 M Ammonium Sulfate	0.1 M Sodium Citrate pH 5 2.19 M Ammonium Sulfate	0.1 M Sodium Citrate pH 5 2.37 M Ammonium Sulfate	0.1 M Sodium Citrate pH 5 2.56 M Ammonium Sulfate	0.1 M Sodium Citrate pH 5 2.74 M Ammonium Sulfate	0.1 M Sodium Citrate pH 5 2.93 M Ammonium Sulfate	0.1 M Sodium Citrate pH 5 3.11 M Ammonium Sulfate	0.1 M Sodium Citrate pH 5 3.3 M Ammonium Sulfate
0.1 M Sodium Citrate pH 5 2 M Ammonium Sulfate	0.1 M Sodium Citrate pH 5 2.19 M Ammonium Sulfate	0.1 M Sodium Citrate pH 5 2.37 M Ammonium Sulfate	0.1 M Sodium Citrate pH 5 2.56 M Ammonium Sulfate	0.1 M Sodium Citrate pH 5 2.74 M Ammonium Sulfate	0.1 M Sodium Citrate pH 5 2.93 M Ammonium Sulfate	0.1 M Sodium Citrate pH 5 3.11 M Ammonium Sulfate	0.1 M Sodium Citrate pH 5 3.3 M Ammonium Sulfate
0.1 M Sodium Citrate pH 5 2 M Ammonium Sulfate	0.1 M Sodium Citrate pH 5 2.19 M Ammonium Sulfate	0.1 M Sodium Citrate pH 5 2.37 M Ammonium Sulfate	0.1 M Sodium Citrate pH 5 2.56 M Ammonium Sulfate	0.1 M Sodium Citrate pH 5 2.74 M Ammonium Sulfate	0.1 M Sodium Citrate pH 5 2.93 M Ammonium Sulfate	0.1 M Sodium Citrate pH 5 3.11 M Ammonium Sulfate	0.1 M Sodium Citrate pH 5 3.3 M Ammonium Sulfate
0.1 M Sodium Citrate pH 5 2 M Ammonium Sulfate	0.1 M Sodium Citrate pH 5 2.19 M Ammonium Sulfate	0.1 M Sodium Citrate pH 5 2.37 M Ammonium Sulfate	0.1 M Sodium Citrate pH 5 2.56 M Ammonium Sulfate	0.1 M Sodium Citrate pH 5 2.74 M Ammonium Sulfate	0.1 M Sodium Citrate pH 5 2.93 M Ammonium Sulfate	0.1 M Sodium Citrate pH 5 3.11 M Ammonium Sulfate	0.1 M Sodium Citrate pH 5 3.3 M Ammonium Sulfate

Table 18. CnYpd1-H138Q Optimization 1 + 0.5 M 1,2,3-octanetriol isomer H

						[Protein]
2.2 M Ammonium Sulfate 0.5 M Sodium Citrate pH 4.7	2.4 M Ammonium Sulfate 0.5 M Sodium Citrate pH 4.7	2.6 M Ammonium Sulfate 0.5 M Sodium Citrate pH 4.7	2.8 M Ammonium Sulfate 0.5 M Sodium Citrate pH 4.7	3.0 M Ammonium Sulfate 0.5 M Sodium Citrate pH 4.7	3.2 M Ammonium Sulfate 0.5 M Sodium Citrate pH 4.7	27 mg/mL
1.1 M Ammonium Sulfate 0.5 M Sodium Citrate pH 4.7	1.2 M Ammonium Sulfate 0.5 M Sodium Citrate pH 4.7	1.3 M Ammonium Sulfate 0.5 M Sodium Citrate pH 4.7	1.4 M Ammonium Sulfate 0.5 M Sodium Citrate pH 4.7	1.5 M Ammonium Sulfate 0.5 M Sodium Citrate pH 4.7	1.6 M Ammonium Sulfate 0.5 M Sodium Citrate pH 4.7	19 mg/mL
1.1 M Ammonium Sulfate 0.5 M Sodium Citrate pH 4.7	1.2 M Ammonium Sulfate 0.5 M Sodium Citrate pH 4.7	1.3 M Ammonium Sulfate 0.5 M Sodium Citrate pH 4.7	1.4 M Ammonium Sulfate 0.5 M Sodium Citrate pH 4.7	1.5 M Ammonium Sulfate 0.5 M Sodium Citrate pH 4.7	1.6 M Ammonium Sulfate 0.5 M Sodium Citrate pH 4.7	15 mg/mL
1.1 M Ammonium Sulfate 0.5 M Sodium Citrate pH 4.7	1.2 M Ammonium Sulfate 0.5 M Sodium Citrate pH 4.7	1.3 M Ammonium Sulfate 0.5 M Sodium Citrate pH 4.7	1.4 M Ammonium Sulfate 0.5 M Sodium Citrate pH 4.7	1.5 M Ammonium Sulfate 0.5 M Sodium Citrate pH 4.7	1.6 M Ammonium Sulfate 0.5 M Sodium Citrate pH 4.7	13.5 mg/mL

Table 19. Octanetriol Optimization 1

2.2 M Ammonium Sulfate 0.5 M Sodium Citrate pH 4.7	2.4 M Ammonium Sulfate 0.5 M Sodium Citrate pH 4.7	2.6 M Ammonium Sulfate 0.5 M Sodium Citrate pH 4.7	2.8 M Ammonium Sulfate 0.5 M Sodium Citrate pH 4.7	3.0 M Ammonium Sulfate 0.5 M Sodium Citrate pH 4.7	3.2 M Ammonium Sulfate 0.5 M Sodium Citrate pH 4.7	0.3 M 1,2,3-octanetriol isomer H
1.1 M Ammonium Sulfate 0.5 M Sodium Citrate pH 4.7	1.2 M Ammonium Sulfate 0.5 M Sodium Citrate pH 4.7	1.3 M Ammonium Sulfate 0.5 M Sodium Citrate pH 4.7	1.4 M Ammonium Sulfate 0.5 M Sodium Citrate pH 4.7	1.5 M Ammonium Sulfate 0.5 M Sodium Citrate pH 4.7	1.6 M Ammonium Sulfate 0.5 M Sodium Citrate pH 4.7	0.4 M 1,2,3-octanetriol isomer H
1.1 M Ammonium Sulfate 0.5 M Sodium Citrate pH 4.7	1.2 M Ammonium Sulfate 0.5 M Sodium Citrate pH 4.7	1.3 M Ammonium Sulfate 0.5 M Sodium Citrate pH 4.7	1.4 M Ammonium Sulfate 0.5 M Sodium Citrate pH 4.7	1.5 M Ammonium Sulfate 0.5 M Sodium Citrate pH 4.7	1.6 M Ammonium Sulfate 0.5 M Sodium Citrate pH 4.7	0.5 M 1,2,3-octanetriol isomer H
1.1 M Ammonium Sulfate 0.5 M Sodium Citrate pH 4.7	1.2 M Ammonium Sulfate 0.5 M Sodium Citrate pH 4.7	1.3 M Ammonium Sulfate 0.5 M Sodium Citrate pH 4.7	1.4 M Ammonium Sulfate 0.5 M Sodium Citrate pH 4.7	1.5 M Ammonium Sulfate 0.5 M Sodium Citrate pH 4.7	1.6 M Ammonium Sulfate 0.5 M Sodium Citrate pH 4.7	0.6 M 1,2,3-octanetriol isomer H

Table 20. Octanetriol Optimization 2

						Additive	Seed
1.1 M Ammonium Sulfate 0.5 M Sodium Citrate pH 4.7	1.2 M Ammonium Sulfate 0.5 M Sodium Citrate pH 4.7	1.3 M Ammonium Sulfate 0.5 M Sodium Citrate pH 4.7	1.4 M Ammonium Sulfate 0.5 M Sodium Citrate pH 4.7	1.5 M Ammonium Sulfate 0.5 M Sodium Citrate pH 4.7	1.6 M Ammonium Sulfate 0.5 M Sodium Citrate pH 4.7	0.3 M 1,2,3-Octanetriol isomer H	10^{-6}
1.1 M Ammonium Sulfate 0.5 M Sodium Citrate pH 4.7	1.2 M Ammonium Sulfate 0.5 M Sodium Citrate pH 4.7	1.3 M Ammonium Sulfate 0.5 M Sodium Citrate pH 4.7	1.4 M Ammonium Sulfate 0.5 M Sodium Citrate pH 4.7	1.5 M Ammonium Sulfate 0.5 M Sodium Citrate pH 4.7	1.6 M Ammonium Sulfate 0.5 M Sodium Citrate pH 4.7	0.4 M 1,2,3-Octanetriol isomer H	10^{-5}
1.1 M Ammonium Sulfate 0.5 M Sodium Citrate pH 4.7	1.2 M Ammonium Sulfate 0.5 M Sodium Citrate pH 4.7	1.3 M Ammonium Sulfate 0.5 M Sodium Citrate pH 4.7	1.4 M Ammonium Sulfate 0.5 M Sodium Citrate pH 4.7	1.5 M Ammonium Sulfate 0.5 M Sodium Citrate pH 4.7	1.6 M Ammonium Sulfate 0.5 M Sodium Citrate pH 4.7	0.5 M 1,2,3-Octanetriol isomer H	10^{-4}
1.1 M Ammonium Sulfate 0.5 M Sodium Citrate pH 4.7	1.2 M Ammonium Sulfate 0.5 M Sodium Citrate pH 4.7	1.3 M Ammonium Sulfate 0.5 M Sodium Citrate pH 4.7	1.4 M Ammonium Sulfate 0.5 M Sodium Citrate pH 4.7	1.5 M Ammonium Sulfate 0.5 M Sodium Citrate pH 4.7	1.6 M Ammonium Sulfate 0.5 M Sodium Citrate pH 4.7	0.6 M 1,2,3-Octanetriol isomer H	10^{-6}

Table 21. CSHT D3 Optimization

						Seed
0.1 M HEPES sodium pH 7.5 1.6 M Ammonium Sulfate 1.6% PEG 400	0.1 M HEPES sodium pH 7.5 1.8 M Ammonium Sulfate 1.6% PEG 400	0.1 M HEPES sodium pH 7.5 2.0 M Ammonium Sulfate 1.6% PEG 400	0.1 M HEPES sodium pH 7.5 2.2 M Ammonium Sulfate 1.6% PEG 400	0.1 M HEPES sodium pH 7.5 2.4 M Ammonium Sulfate 1.6% PEG 400	0.1 M HEPES sodium pH 7.5 2.6 M Ammonium Sulfate 1.6% PEG 400	10^{-6}
0.1 M HEPES sodium pH 7.5 1.6 M Ammonium Sulfate 1.8% PEG 400	0.1 M HEPES sodium pH 7.5 1.6 M Ammonium Sulfate 1.6% PEG 400	0.1 M HEPES sodium pH 7.5 1.6 M Ammonium Sulfate 2.0% PEG 400	0.1 M HEPES sodium pH 7.5 1.6 M Ammonium Sulfate 2.2% PEG 400	0.1 M HEPES sodium pH 7.5 1.6 M Ammonium Sulfate 2.4% PEG 400	0.1 M HEPES sodium pH 7.5 1.6 M Ammonium Sulfate 2.6% PEG 400	10^{-6}
0.1 M HEPES sodium pH 7.5 1.6 M Ammonium Sulfate 1.6% PEG 400	0.1 M HEPES sodium pH 7.5 1.8 M Ammonium Sulfate 1.6% PEG 400	0.1 M HEPES sodium pH 7.5 2.0 M Ammonium Sulfate 1.6% PEG 400	0.1 M HEPES sodium pH 7.5 2.2 M Ammonium Sulfate 1.6% PEG 400	0.1 M HEPES sodium pH 7.5 2.4 M Ammonium Sulfate 1.6% PEG 400	0.1 M HEPES sodium pH 7.5 2.6 M Ammonium Sulfate 1.6% PEG 400	10^{-3}
0.1 M HEPES sodium pH 7.5 1.6 M Ammonium Sulfate 1.8% PEG 400	0.1 M HEPES sodium pH 7.5 1.6 M Ammonium Sulfate 1.6% PEG 400	0.1 M HEPES sodium pH 7.5 1.6 M Ammonium Sulfate 2.0% PEG 400	0.1 M HEPES sodium pH 7.5 1.6 M Ammonium Sulfate 2.2% PEG 400	0.1 M HEPES sodium pH 7.5 1.6 M Ammonium Sulfate 2.4% PEG 400	0.1 M HEPES sodium pH 7.5 1.6 M Ammonium Sulfate 2.6% PEG 400	10^{-3}

Table 22. CSHT H5 Optimization

0.1 M Tris pH 8.5 0.6 M Lithium Sulfate 0.01 M Nickel Chloride	0.1 M Tris pH 8.5 0.8 M Lithium Sulfate 0.02 M Nickel Chloride	0.1 M Tris pH 8.5 1.0 M Lithium Sulfate 0.03 M Nickel Chloride	0.1 M Tris pH 8.5 1.2 M Lithium Sulfate 0.04 M Nickel Chloride	0.1 M Tris pH 8.5 1.4 M Lithium Sulfate 0.05 M Nickel Chloride	0.1 M Tris pH 8.5 1.6 M Lithium Sulfate 0.06 M Nickel Chloride
0.1 M Tris pH 8.5 0.6 M Lithium Sulfate 0.01 M Nickel Chloride	0.1 M Tris pH 8.5 0.8 M Lithium Sulfate 0.02 M Nickel Chloride	0.1 M Tris pH 8.5 1.0 M Lithium Sulfate 0.03 M Nickel Chloride	0.1 M Tris pH 8.5 1.2 M Lithium Sulfate 0.04 M Nickel Chloride	0.1 M Tris pH 8.5 1.4 M Lithium Sulfate 0.05 M Nickel Chloride	0.1 M Tris pH 8.5 1.6 M Lithium Sulfate 0.06 M Nickel Chloride
0.1 M Tris pH 8.5 0.6 M Lithium Sulfate 0.01 M Nickel Chloride	0.1 M Tris pH 8.5 0.8 M Lithium Sulfate 0.02 M Nickel Chloride	0.1 M Tris pH 8.5 1.0 M Lithium Sulfate 0.03 M Nickel Chloride	0.1 M Tris pH 8.5 1.2 M Lithium Sulfate 0.04 M Nickel Chloride	0.1 M Tris pH 8.5 1.4 M Lithium Sulfate 0.05 M Nickel Chloride	0.1 M Tris pH 8.5 1.6 M Lithium Sulfate 0.06 M Nickel Chloride
0.1 M Tris pH 8.5 0.6 M Lithium Sulfate 0.01 M Nickel Chloride	0.1 M Tris pH 8.5 0.8 M Lithium Sulfate 0.02 M Nickel Chloride	0.1 M Tris pH 8.5 1.0 M Lithium Sulfate 0.03 M Nickel Chloride	0.1 M Tris pH 8.5 1.2 M Lithium Sulfate 0.04 M Nickel Chloride	0.1 M Tris pH 8.5 1.4 M Lithium Sulfate 0.05 M Nickel Chloride	0.1 M Tris pH 8.5 1.6 M Lithium Sulfate 0.06 M Nickel Chloride

Table 23. JCSG D7 Optimization

0.1 M Tris pH 8.5 0.1 M Lithium Sulfate 32% PEG 400	0.1 M Tris pH 8.5 0.1 M Lithium Sulfate 34% PEG 400	0.1 M Tris pH 8.5 0.1 M Lithium Sulfate 36% PEG 400	0.1 M Tris pH 8.5 0.1 M Lithium Sulfate 38% PEG 400	0.1 M Tris pH 8.5 0.1 M Lithium Sulfate 40% PEG 400	0.1 M Tris pH 8.5 0.1 M Lithium Sulfate 42% PEG 400
0.1 M Tris pH 8.5 0.05 M Lithium Sulfate 32% PEG 400	0.1 M Tris pH 8.5 0.05 M Lithium Sulfate 34% PEG 400	0.1 M Tris pH 8.5 0.05 M Lithium Sulfate 36% PEG 400	0.1 M Tris pH 8.5 0.05 M Lithium Sulfate 38% PEG 400	0.1 M Tris pH 8.5 0.05 M Lithium Sulfate 40% PEG 400	0.1 M Tris pH 8.5 0.05 M Lithium Sulfate 42% PEG 400
0.1 M Tris pH 8.5 0.2 M Lithium Sulfate 32% PEG 400	0.1 M Tris pH 8.5 0.2 M Lithium Sulfate 34% PEG 400	0.1 M Tris pH 8.5 0.2 M Lithium Sulfate 36% PEG 400	0.1 M Tris pH 8.5 0.2 M Lithium Sulfate 38% PEG 400	0.1 M Tris pH 8.5 0.2 M Lithium Sulfate 40% PEG 400	0.1 M Tris pH 8.5 0.2 M Lithium Sulfate 42% PEG 400
0.1 M Tris pH 8.5 0.3 M Lithium Sulfate 32% PEG 400	0.1 M Tris pH 8.5 0.3 M Lithium Sulfate 34% PEG 400	0.1 M Tris pH 8.5 0.3 M Lithium Sulfate 36% PEG 400	0.1 M Tris pH 8.5 0.3 M Lithium Sulfate 38% PEG 400	0.1 M Tris pH 8.5 0.3 M Lithium Sulfate 40% PEG 400	0.1 M Tris pH 8.5 0.3 M Lithium Sulfate 42% PEG 400

Table 24. MCSG I C5 Optimization

14% PEG 3350 0.1 M Magnesium Acetate	16% PEG 3350 0.1 M Magnesium Acetate	18% PEG 3350 0.1 M Magnesium Acetate	20% PEG 3350 0.1 M Magnesium Acetate	22% PEG 3350 0.1 M Magnesium Acetate	24% PEG 3350 0.1 M Magnesium Acetate
14% PEG 3350 0.2 M Magnesium Acetate	16% PEG 3350 0.2 M Magnesium Acetate	18% PEG 3350 0.2 M Magnesium Acetate	20% PEG 3350 0.2 M Magnesium Acetate	22% PEG 3350 0.2 M Magnesium Acetate	24% PEG 3350 0.2 M Magnesium Acetate
14% PEG 3350 0.3 M Magnesium Acetate	16% PEG 3350 0.3 M Magnesium Acetate	18% PEG 3350 0.3 M Magnesium Acetate	20% PEG 3350 0.3 M Magnesium Acetate	22% PEG 3350 0.3 M Magnesium Acetate	24% PEG 3350 0.3 M Magnesium Acetate
14% PEG 3350 0.4 M Magnesium Acetate	16% PEG 3350 0.4 M Magnesium Acetate	18% PEG 3350 0.4 M Magnesium Acetate	20% PEG 3350 0.4 M Magnesium Acetate	22% PEG 3350 0.4 M Magnesium Acetate	24% PEG 3350 0.4 M Magnesium Acetate

Table 25. MCSG I C5 Optimization

14% PEG 3350 0.1 M Magnesium Acetate	16% PEG 3350 0.1 M Magnesium Acetate	18% PEG 3350 0.1 M Magnesium Acetate	20% PEG 3350 0.1 M Magnesium Acetate	22% PEG 3350 0.1 M Magnesium Acetate	24% PEG 3350 0.1 M Magnesium Acetate
14% PEG 3350 0.2 M Magnesium Acetate	16% PEG 3350 0.2 M Magnesium Acetate	18% PEG 3350 0.2 M Magnesium Acetate	20% PEG 3350 0.2 M Magnesium Acetate	22% PEG 3350 0.2 M Magnesium Acetate	24% PEG 3350 0.2 M Magnesium Acetate
14% PEG 3350 0.3 M Magnesium Acetate	16% PEG 3350 0.3 M Magnesium Acetate	18% PEG 3350 0.3 M Magnesium Acetate	20% PEG 3350 0.3 M Magnesium Acetate	22% PEG 3350 0.3 M Magnesium Acetate	24% PEG 3350 0.3 M Magnesium Acetate
14% PEG 3350 0.4 M Magnesium Acetate	16% PEG 3350 0.4 M Magnesium Acetate	18% PEG 3350 0.4 M Magnesium Acetate	20% PEG 3350 0.4 M Magnesium Acetate	22% PEG 3350 0.4 M Magnesium Acetate	24% PEG 3350 0.4 M Magnesium Acetate

,

Appendix C: Table of Abbreviations

5-IAF: 5-iodoacetamidofluorescein
ATP: Adenosine triphosphate
CA: Catalytic and ATP binding domain
CBD: Chitin binding domain
Cn: *Cryptococcus neoformans*
CoV: Coefficient of variance
CV: Column volume
DHp: Dimerization and Histidine phosphotransfer
EK: Enterokinase
GBAP: gelatinase biosynthesis-activating pheromone
GST: Glutathione S-transferase
HHK: Hybrid histidine kinase
His-to-Asp**:** Histidine-to-Aspartate
HK: Histidine kinase
HOG: High Osmolarity Glycerol
HPt: Histidine-phosphotransfer protein
ICP-MS: Inductively coupled plasma mass spec
IPTG - Isopropyl β-D-1-thiogalactopyranoside
LB: Luria Broth
MAPK: Mitogen Activated Protein Kinase
Ni-NTA resin: Nickel Nitrilotriacetic acid resin
OMRF: Oklahoma Medical Research Foundation
P2CS: Prokaryotic 2-Component Systems
PCR: Polymerase chain reaction
PDB: Protein Data bank
PPC: Protein Production Core
Rec: Receiver domain
RR: Response regulator
R1: Receiver domain of Sln1
R2: Receiver domain of Ssk1
R3: Receiver domain of Skn7
Sc: *Saccharomyces cerevisiae*
SEC: Size exclusion chromatography
SEC-MALS: Size exclusion chromatography with multi-angle light scattering
SDS-PAGE: sodium dodecyl sulfate polyacrylamide gel electrophoresis
TEV: Tobacco etch virus protease
WT: Wild type